12-5-2019 2:00 PM

The Secretory Pathway Calcium ATPase 2C promotes increased cytosolic calcium levels

Melissa Fenech
The University of Western Ontario

Supervisor
Pin, Christopher L.
The University of Western Ontario Co-Supervisor
Stathopulos, Peter B.
The University of Western Ontario

Graduate Program in Physiology and Pharmacology
A thesis submitted in partial fulfillment of the requirements for the degree in Doctor of Philosophy

Abstract

Pancreatic acinar cell exocytosis requires precise calcium (Ca^{2+}) signals. When cytosolic Ca^{2+} levels remain high, cellular functions are disrupted, which is associated with initiation of pancreatitis. Ca^{2+} signals are achieved through regulating endoplasmic reticulum (ER) stores, Ca^{2+}ATPases, and store-operated Ca^{2+} entry (SOCE). However, how these pathways interact to create precise signals is not well understood. In a pancreatic model of dysregulated Ca^{2+} homeostasis, secretory pathway Ca^{2+}ATPase 2 (SPCA2) expression is significantly decreased. In the pancreas, only a C-terminally truncated form of SPCA2 (termed SPAC2C) exists. Recent studies indicate a role for SPCA2 in increasing Ca^{2+} influx involving Orai1 in breast cancer. The goal of this study was to determine the effects of SPCA2C on Ca^{2+} homeostasis.

Here, epitope-tagged SPCA2C was expressed in HEK293A cells. Co-immunofluorescence (Co-IF) determined subcellular localization. Using Fura2 imaging, cytosolic Ca^{2+} concentration [Ca^{2+}] was examined during rest, SOCE and secretagogue-stimulated signaling. Effects of SPCA2C over-expression were also examined in 266.6 pancreatic acinar cells. In pancreatic cancer-derived cells, the abundance of the SPCA2C gene transcript (*ATP2C2C*) was assessed. Effects of SPCA2C over-expression was examined in cancer-derived cells to understand the functional role of SPCA2C in pancreatic pathology. Finally, an unbiased protein proximity assay was used to evaluate the SPCA2C interactome and broaden the understanding of SPCA2C function.

In HEK293A cells, exogenous SPCA2C expression localized to ER and Golgi compartments and increased resting cytosolic [Ca^{2+}], Ca^{2+} release in response to carbachol, ER Ca^{2+} stores, and

Ca^{2+} influx. Co-immunoprecipitation (co-IP) detected Orai1-SPCA2C interactions. However, SPCA2C's effect on cytosolic and ER Ca^{2+} levels are Orai1-independent. In pancreatic cancer, cell lines with increased endogenous *ATP2C2* expression had increased ER Ca^{2+} stores and increased constitutive Ca^{2+} influx, while exogenous over-expression of SPCA2C increased resting Ca^{2+} levels. Examination of identified putative protein interactors using Gene Ontology (GO) and Reactome analysis predicted endoplasmic reticulum cellular compartment localization and Ca^{2+} ion homeostasis as a pathway SPCA2C may be involved. These findings indicate SPCA2C influences Ca^{2+} homeostasis through multiple mechanisms. By delineating the *Atp2c2c* sequence and functionally characterizing SPCA2C's role in Ca^{2+} regulation, I have uncovered a novel mechanism that pancreatic acinar cells use to regulate cytosolic and ER Ca^{2+} levels.

Keywords

calcium homeostasis, calcium signaling, secretory pathway calcium ATPase 2C, Orai1, store operated calcium entry, store independent calcium entry, STIM1

Summary for Lay Audiences

The pancreas is important for the regulation of blood glucose and the production and delivery of substances necessary for digestion. A specific cell type, called the pancreatic acinar cell, has the primary function of producing and secreting substances called enzymes, that digest the food particles you ingest. Enzymes are released from these cells when you eat, which requires a specific signal that can be transmitted to the inside of the cell. Calcium (Ca^{2+}) is required to transmit this signal inside of the cell. Pancreatitis can develop if the Ca^{2+} signal is not transmitted properly. The regulation of Ca^{2+} in pancreatic acinar cells is not fully understood. A novel pancreas-specific protein isoform, termed secretory pathway Ca^{2+} ATPase 2 C (SPCA2C) has been found by my lab. Previous research in breast cancer indicates a role for a related protein SPCA2, to increase Ca^{2+} levels inside cells, leading to disease. The goal of this thesis was to determine the effects of SPCA2C on cellular Ca^{2+} homeostasis.

In this study, the protein sequence of SPCA2C was determined and expressed in cells to determine the effect it has on Ca^{2+} levels within the cell. Cellular Ca^{2+} levels were measured and Ca^{2+} signals were analyzed during stimulation for enzyme exocytosis. In cells isolated from pancreatic cancer patients, the expression level of *ATP2C2,* transcript from which the SPCA2 protein is made, was analyzed. The level of expression was compared to cellular Ca^{2+} levels to understand how SPCA2C influences Ca^{2+} homeostasis in pancreatic disease. Finally, proteins that might interact with SPCA2C were determined to broaden our understanding how SPCA2C functions in cells.

I found that expressing SPCA2C in cells increased cellular Ca^{2+} levels and increased the amount of Ca^{2+} signal after stimulation for enzyme release. In pancreatic cancer cells, increased expression of *ATP2C2* increase the amount of Ca^{2+} that was being brought into the cell. Finally, SPCA2C was predicted to interact with ~263 other proteins within cells. These findings indicate that SPCA2C influences Ca^{2+} homeostasis through multiple mechanisms. Through this research I have uncovered a novel mechanism that pancreatic acinar cells use to regulate Ca^{2+} levels.

Co-Authorship Statement

Chapter 2 is a published body of work. RT-qPCR of *Atp2c2c* was carried out by C. Johnson. Chapter 3 is a published body of work and contains immunofluorescence that was performed by M. Carter. Chapter 4 contains BioID western blots experiments that were carried out by M. Carter. All other experimental work presented here was carried out by M.A. Fenech.

Acknowledgements

In the middle of every difficulty lies opportunity - Albert Einstein

The past five years would not have been possible without help from a number of people. I would like to thank my supervisor Dr. Christopher Pin, for his guidance, encouragement and abundant amount of patience throughout my degree. You provided me with an environment of many opportunities and learning experiences, which have made me a better scientist and collaborator. I would also like to thank the members of the Pin Laboratory who were always willing to help. Thank you to Charis Johnson, for helping me to get me started in the lab and to Kurt for continuing to answer all of my questions. Thank you to Claire and Jelena, the years we worked together will never be forgotten.

I would like to thank Dr. Peter Stathopulos, for his encouragement and guidance over the past five years. I would also like to thank past and present members of the Stathopulos, Sims, and Dixon labs for all of their help and making my work on campus more enjoyable.

I would also like to thank my advisory committee, Drs. Peter Stathopulos, John Di Guglielmo and Tom Drysdale for always being interested in helping me and providing me with valuable advice.

I would like to acknowledge my fellow graduate students and friends for their support. Claire, Lisa and Victoria thank you for patiently listening to all my trials and tribulations and

encouraging me to follow my dreams. Anish, being a part of the phys/pharm department wouldn't have been the same without you. I am so grateful for all of the friendships I have made; you guys are truly amazing people and your support means so much.

Finally, I would like to show my appreciation for my parents, Teresa and Sam Fenech, for their constant support and enthusiasm in everything I do. Thank you for always believing in me, I wouldn't be where I am today without the two of you.

Table of Contents

List of Abbreviations

- / -	Knockout
Ach	Acetyl choline
ADP	Adenosine diphosphate
ATP	Adenosine Triphosphate
BSA	Bovine serum albumin
Ca^{2+}	Calcium
CICR	Calcium induced calcium release
CRAC	Calcium release activated calcium
CCK	Cholecystokinin
CCKR	Cholecystokinin receptors
CIP	Cerulein induced pancreatitis
cAMP	Cyclic adenosine monophosphate
cADPR	Cyclic adenosine diphosphate receptor
DAPI	4',6-diamidoino-2-phenylindole
DMEM	Dulbecco's modified eagle medium
DNA	Deoxyribose nucleic acid
EGTA	Ethylene glycol-bis(β-aminoethyl ether)-N, N, N',N'-tetraacetic acid
ER	Endoplasmic reticulum
FITC	Fluorescein isothiocyanate
GFP	Green fluorescent protein
GPCR	G-protein coupled receptor
HEK	Human embryonic kidney

HRP	Horseradish peroxidase
SPCA	Secretory pathway calcium ATPase
IF	Immunofluorescence
IP	Immunoprecipitation
IP_3	Inositol 1,4,5-trisphosphate
IP_3R	Inositol trisphosphate receptor
kDa	Kilodalton
RyR	Ryanodine receptor
MICU	Mitochondrial calcium uptake
MPTP	Mitochondrial permeability transition pore
mRFP	Monomeric red fluorescent protein
Munc	Mammalian uncoordinated
NAADP	Nicotinic acid adenine dinucleotide phosphate
OCT	Optimal cutting temperature
ORF	Open reading frame
PBS	Phosphate buffered saline
PIP_2	Phosphoinositide bisphosphate
PVDF	Polyvinylidene fluoride
PMCA	Plasma membrane calcium ATPase
PKA	Protein kinase A
PKC	Protein kinase C
qRT-PCR	Quantitative real time-polymerase chain reaction
RGS	Regulator of G protein signalling

RNA	Ribonucleic acid
SEM	Standard error of the mean
SERCA	Sarcoendoplasmic reticulum ATPase
SK3	Small conductance calcium activated K^+ channel
SNAREs	Soluble N-ethylalmide-sensitive fusion protein attachment protein receptors
SICE	Store-independent calcium entry
SOCE	Store-operated calcium entry
STIM	Stromal interactor molecule
SNAPs	Synaptosomal associated proteins
Syn	Syntaxins
TBS	Tris-buffered saline
TG	Thapsigargin
TRITC	Tetramethylrhodamine
TRPML	Transient receptor potential ML
TRPC	Transient recptor potential channel
TSS	Transcriptional start site
TPC	Two-pore channel
VAMPs	Vesicle associated membrane proteins
WT	Wild type
YFP	Yellow fluorescent protein
ZG	Zymogen granules

List of Tables

List of Figures

List of Appendices

Chapter 1

1.0 Introduction

Calcium (Ca^{2+}) is a critical messenger in cells, particularly in pancreatic acinar cells, which depend on specific spatiotemporal signals for their primary function of regulated exocytosis. Disruptions in Ca^{2+} regulation affect cellular function and survival. Therefore, cells depend on the expression of specific protein sensors, buffers, exchangers, pumps and channels to regulate Ca^{2+} signaling and homeostasis. In pancreatic acinar cells, extracellular stimuli cause global oscillatory Ca^{2+} signals, released from the endoplasmic reticulum (ER). Ca^{2+} oscillations promote the movement of vesicles containing proenzymes to the apical plasma membrane and exocytosis of their contents. In pancreatic acinar cells, the regulation of intracellular Ca^{2+} signaling patterns is complex. The type of Ca^{2+} signal depends on stimulus type, concentration and duration and each pattern requires a different combination of regulatory proteins, some of which are still yet to be determined. Mitochondria and Ca^{2+} buffering proteins modulate Ca^{2+} signals, while membrane pumps and channels promote Ca^{2+} movement within the cell and surrounding environment. Upon release of Ca^{2+} from the ER, Ca^{2+} influx across the plasma membrane is also activated. This extracellular Ca^{2+} influx allows for the refilling of ER stores. Ca^{2+}ATPases promote rapid removal of Ca^{2+} from the cytosol, refilling ER stores or extruding Ca^{2+} across the plasma membrane, to maintain cytosolic Ca^{2+} homeostasis.

Our laboratory has identified a pancreas-specific isoform of secretory pathway Ca^{2+}ATPase 2 (SPCA2), termed SPCA2C that has not been characterized to date. Contrary to traditional roles of Ca^{2+} ATPases, SPCA2 increases cytosolic Ca^{2+} levels independent of an ATPase function, by

regulating Ca^{2+} channels on the plasma membrane. The goal of this thesis is to assess the function of the pancreas-specific SPCA2C isoform in Ca^{2+} homeostasis.

1.1 Calcium as a critical second messenger

Ca^{2+} is critical to multicompartment cells, where it aids in communication between compartments and provides information of the extracellular environment. Ca^{2+} is also an important second messenger affecting cellular proliferation, apoptosis, and general cell function (Berridge et al., 2000). Intracellular Ca^{2+} signals depend on the existence of Ca^{2+} concentration gradients. Basal or resting Ca^{2+} concentrations of free cytoplasmic Ca^{2+} are ~75-150 nM (Yule, 2015), while the extracellular Ca^{2+} is typically ~1.8 mM. The ER has the largest intracellular Ca^{2+} store with free concentrations reaching ~1 mM (Burdakov et al., 2005). These concentration gradients created between the cytoplasm and ER stores or across the plasma membrane allow Ca^{2+} to be used as a messenger. In pancreatic acinar cells signals are generated by stimulation on the basal membrane (see below). Upon stimulation, Ca^{2+} is released from the ER to the cytosol, where it will regulate Ca^{2+}-dependent effector proteins, such as kinases or phosphatases, or Ca^{2+}-dependent functions, such as regulated exocytosis. The ER makes close connections with other organelles that also control Ca^{2+} homeostasis. Mitochondrial Ca^{2+} uptake shapes cytosolic Ca^{2+} dynamics (Rizzuto et al., 2012) and lysosomes have been suggested to participate in the regulation of Ca^{2+} homeostasis by acting as Ca^{2+} stores (Gerasimenko et al., 2003, 2006). Therefore, pathways exist to move Ca^{2+} into and out of these organelles.

In the exocrine pancreas, acinar cells must strictly regulate Ca^{2+} levels to allow for proper secretion of digestive enzymes. Acinar cells control Ca^{2+} through multiple pathways [reviewed

in (Wen et al., 2016; Yule, 2015)], with the ER acting as a critical Ca^{2+} store within these cells. This thesis provides insight into how SPCA2C may affect acinar cell function and Ca^{2+} homeostasis.

1.1.1 Relationship between calcium homeostasis and pancreatic pathologies

Understanding how Ca^{2+} is regulated in pancreatic acinar cells is critical since aberrant Ca^{2+} regulation is associated with increased susceptibility and severity of pancreatic disease (Tepikin et al., 1992). Stable increases in cytosolic Ca^{2+} above resting level are proposed to initiate acinar cell injury by inducing premature activation of intracellular enzymes (Criddle et al., 2006), mitochondrial dysfunction (Niederau & Grendell, 1988), vacuolization and necrosis (Shalbueva et al., 2013). Cellular damage promotes an inflammatory response, inducing pancreatitis (Kang, et al., 2014). Pancreatitis is a debilitating disease involving tissue digestion, inflammation and fibrosis. Chronic or recurrent forms of pancreatitis are a leading cause of pancreatic ductal adenocarcinoma, the most common and deadliest form of pancreatic cancer. Pancreatitis and pancreatic ductal adenocarcinoma severely reduce quality of life and life expectancy and insight into their potential mechanisms is crucial for improving outcomes (Anderson et al., 2009). Therefore, it is important that intracellular Ca^{2+} levels be controlled both temporally and spatially. Although potential treatments targets cytosolic Ca^{2+} using Ca^{2+} influx channel inhibitors (Wen et al., 2015), there is currently no treatment available for people suffering from pancreatitis.

1.2 Pancreas

The pancreas is a glandular organ that consists of two major functional compartments: endocrine and exocrine. The endocrine pancreas is comprised of islets of Langerhans and accounts for 1-2% of total pancreatic mass. Five primary cell types are found within islets: insulin-producing β-cells, glucagon-secreting α-cells, somatostatin-secreting δ-cells, pancreatic polypeptide-secreting F-cells, and ghrelin-secreting ε-cells. The levels of glucose in the blood are rapidly and precisely regulated by hormone production from islets. The exocrine pancreas constitutes almost 98% of total pancreatic mass and is comprised of acinar cells, centroacinar cells and duct cells. Centroacinar cells lie at the interface between the acinar cells and duct cells and resemble a hybrid between those two cell types. Centroacinar cells secrete aqueous bicarbonate solution when stimulated by the hormone secretin. They also secrete mucin (Longnecker, 2014). Along with providing a structural function, duct cells also secrete bicarbonate, which is carried along with pancreatic enzymes and microbials to the duodenum. Bicarbonate neutralizes the acidic contents emptying from the stomach. This thesis focuses on acinar cells as this is the primary site of SPCA2C expression.

1.2.1 Acinar cell structure and function

Acinar cells are polarized and form small clusters called acini. Acinar cells produce proteases, lipases and amylases, the materials required for digestion and absorption of nutrients in the small intestine. In most cases, acinar cells store these pancreatic enzymes as proenzymes in zymogen granules near the apical membrane. When stimulated, acinar cells empty their contents into the lumen of intralobular ducts (Figure 1.1). Acinar cells also secrete antimicrobials, including cathelicidin-related peptide, which inhibit intestinal bacterial overgrowth (Ahuja et al., 2017). To

regulate exocytosis, acinar cells have established a network of signaling pathways that can promote different spatial and temporal Ca^{2+} signals within the cell.

1.2.2 Types of calcium release

Global Ca^{2+} signals, including oscillations, are established from basic elementary Ca^{2+} signalling events. Almost all global Ca^{2+} signals are produced by the release of Ca^{2+} from the ER (Berridge, 2007). A single elementary event can be used to perform a highly localized signalling function. For example, the release of a neurotransmitter from a neuron, which requires a brief localized pulse of Ca^{2+} delivered directly to the docked vesicle by a Ca^{2+} channel associated with the exocytosis machinery. Such an event is called a *sparklet* and it is formed as a result of the brief opening of voltage operated Ca^{2+} channels (Berridge, 2007). A *spark* however, is formed by the opening of a group of ryanodine receptors (RyRs). Sparks can be used to activate a Ca^{2+} wave. These Ca^{2+} waves spread throughout the cell, through calcium induced calcium release (CICR; Berridge, 2007). A *puff*, similar to a spark, is formed by the release of Ca^{2+} from a small group of inositol 1,4,5-trisphosphate receptors (IP_3Rs). They are also the building blocks of Ca^{2+} waves, resulting in global Ca^{2+} signals. Intercellular Ca^{2+} waves are thought to be spread through gap junctions by the passage of Ca^{2+} or IP_3, which result in the propagation of waves into neighbouring cells (Berridge, 2007).

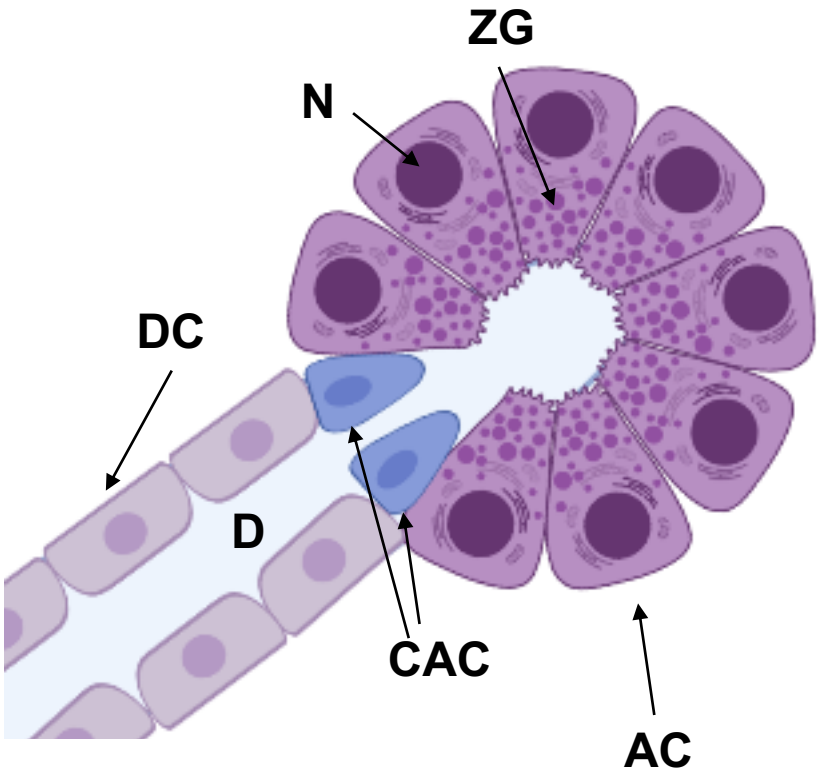
ZG
N
DC
D
CAC
AC

Figure 1.1 Pancreatic tissue with acinar, centroacinar and ductal cells.

The acinar cells (AC) are arranged into acini and contain apically localized zymogen granules (ZG). The nuclei (N) are located in the basal portion of the acinar cell. Centroacinar cells (CAC) contain no ZG. The apical poles of acinar cells face the duct (D) and ductal cells (DC) surround the duct lumen.

1.2.3 Acinar cell organization related to calcium homeostasis

The intracellular organization of pancreatic acini is essential for proper function. The lateral aspects of acinar cells are connected to each other via tight and adherens junctions, and communication occurs through gap junctions. The basal poles are associated with a basal lamina and often endothelial cells of the vasculature (Longnecker, 2014). The basal membrane contains muscarinic or cholecystokinin receptors (CCKR) that receive signals from the nervous system via acetylcholine (Ach; Dormer & Williams 1981) or cholecystokinin (CCK; Matozaki et al., 1991; Streb et al., 1985), respectively, for exocytosis of enzymes.

More than 90% of newly synthesized proteins in pancreatic acinar cells are targeted to the secretory pathway and packed into large secretory granules, called zymogen granules (ZG). These granules are relatively large (*i.e.* ~1 μm in diameter) and are responsible for transport, storage and secretion of digestive enzymes. The ZGs reside in the apical pole of the cell until it is stimulated for enzyme release (Longnecker, 2014). Individual acini are extensively coupled by gap junctions that allow the passage of ions and small molecules (*i.e.* 1-2 kDa) and provide electrical coupling between cells, to facilitate exocytosis (Meda et al., 1983).

The highly organized intracellular compartments are also important for healthy pancreatic function. The ER is predominantly located within the basal aspect of the cell with projections of the ER that extend to the apical portion of the acinus. Acinar cells are the highest protein producing cell in the body, and the ER plays a pivotal role as the site of translation, folding and covalent modification of proteins either destined for secretion or expressed on the surface of

organelles or the plasma membrane. The ER is also the major site of intracellular Ca^{2+} storage, which is essential for regulated exocytosis, the main function of acinar cells.

1.2.4 Role of mitochondria in Ca^{2+} homeostasis

Mitochondria accumulate in three distinct locations within acinar cells. Mitochondria are concentrated in a peri granular belt basal to the zymogen granules, with further sub-populations surrounding the nucleus and immediately adjacent the basolateral membrane. Mitochondria in the peri granular belt play a critical role in limiting the spread of Ca^{2+} signals upon stimulation with agonist (Park et al., 2001; Rizzuto et al., 1998). Mitochondria are able to quickly uptake Ca^{2+} to help modulate a Ca^{2+} signal (Gonzalez et al., 2000). In mitochondria, large capacity Ca^{2+} uptake occurs through the mitochondria Ca^{2+} uniporter (MCU), a highly selective Ca^{2+} channel on the inner mitochondrial membrane (Baughman et al., 2011). MCU is primarily regulated by mitochondrial Ca^{2+} uptake 1 (MICU1), MICU2 and essential MCU regulator (EMRE). EMRE is a 10 kDa protein that mediates the interaction between MCU and regulator subunits MICU1/2, without EMRE, MCU does not allow Ca^{2+} influx (Sancak et al., 2013). MICU1/2 functions as "gate keepers", permitting and inhibiting Ca^{2+} flux at high and resting cytosolic/intermembrane space Ca^{2+} levels, respectively (Csordas et al., 2013; Mallilankaraman et al., 2012; Plovanich et al., 2013). The mitochondria are also able to exchange Ca^{2+} with the ER at sites of ER-mitochondrial contacts (Rizzuto et al., 2012). Experimentally, high doses of CCK or bile acids cause the release of Ca^{2+} from the ER and a stable broad increase in cytosolic Ca^{2+} (Murphy et al., 2008; Voronina et al., 2005). With the mitochondrial membrane tightly localized to the ER, the continual release of Ca^{2+} leads to Ca^{2+} overload in the mitochondrial matrix, initiating the opening of the mitochondrial permeability transition pore (MPTP). The MPTP is a non-specific

channel that forms in the inner mitochondrial membrane. Opening of the MPTP causes a loss of the inner mitochondrial membrane potential and a halt in ATP production (Halangk et al., 2000). Without adequate ATP, Ca^{2+}ATPases cannot function to decrease cytosolic Ca^{2+} and Ca^{2+} continues to accumulate in the cytosol reaching pathogenic levels (Mukherjee et al., 2016). Furthermore, MPP opening results in the release of pro-apoptotic factors, which can mediate cell death independent of the cytoplasmic Ca^{2+} increases (Tait & Green, 2013).

Molecular pathways ensure proper Ca^{2+} movement within the cell and between stores. Some pathways, such as IP_3 mediated Ca^{2+} release from the ER, are very well established, while the receptors and proteins involved in mediating other pathways and responses, such as store operated Ca^{2+} entry and Ca^{2+} oscillations, are still not fully understood within pancreatic acinar cells. Understanding the molecules and mechanisms underlying these pathways is essential for understanding the fundamental basis for regulated exocytosis.

1.3 Regulated Exocytosis

The release of enzymes from pancreatic acinar cells involves stimulus-secretion coupling, where the primary stimulant for secretion occurs at the basal membrane and causes local increases of Ca^{2+} at the apical border. The continual release of Ca^{2+} from the ER and subsequent removal of Ca^{2+} from the cytosol cause transient Ca^{2+} signals. The cyclic pattern of Ca^{2+} signals is associated with the fusion of ZGs to the apical membrane and release of their contents into ducts (Tepikin et al., 1992). ZG fusion to the plasma membrane is mediated through soluble N-ethylmaleimide-sensitive fusion protein attachment protein receptors (SNAREs; Dolai e al., 2012).

1.3.1 SNARE hypothesis for membrane fusion

Membrane fusion events between cellular compartments within a cell is directed by strict compartmentalized targeting of different SNARE isoforms. Vesicle-associated membrane proteins (VAMPs or vSNAREs), specifically VAMP2, are found on ZG membranes (Gaisano et al., 1996). Syntaxins (Syn) and synaptosomal associated proteins (SNAPs), specifically Syn2, are found on the apical plasma membrane (Gaisano et al., 1996). VAMPs and SNAPs form trans-SNARE complexes that are activated by other regulatory proteins, Ca^{2+} sensors and proteins coupled to second messengers including Ca^{2+}, cAMP, protein kinases C (PKC) and protein kinase A (PKA). These trans-snare complexes organize and activate membrane fusion by functioning as either fusion clamps and/or Ca^{2+} sensors capable of responding to a particular Ca^{2+} release event such as oscillatory Ca^{2+} spikes (Sudhof & Rothman, 2009).

Experimental evidence shows that supramaximal stimulation of acinar cells causes phosphorylation of Munc18c by PKC-α, which induces its assembly and activation of the trans-SNARE complex syn-4/VAMP-8/SNAP-23, mediating pathological basolateral exocytosis. Basolateral exocytosis events are usually preceded by dysregulated Ca^{2+} levels, stimulated by pathological extracellular signals (Dolai et al., 2012; Gaisano et al., 2001).

1.3.2 Secretagogue influence on cellular Ca^{2+}

The spatiotemporal pattern of Ca^{2+} signals elicited in pancreatic acinar cells is dependent on the concentration of agonists such as CCK, Ach, bombesin or secretin (Pralong et al., 1988; Stuenkel et al., 1989). For example, physiological concentrations of agonist (*i.e.* ~1-50 pM CCK or 50-

300 nM Ach) result in the initiation of Ca^{2+} oscillations characterized by repetitive, regular cycles of elevated and subsequently decreasing Ca^{2+} levels (Osipchuk et al., 1990). Maximal stimulation with agonist causes peak increases of Ca^{2+} to ~1 μM and an elevated plateau after the peak at ~100 nM above basal Ca^{2+} concentrations. This elevated cytosoplasmic Ca^{2+} plateau is maintained as long as the agonist is present and is dependent on extracellular Ca^{2+}, while the peak is not dependent on extracellular Ca^{2+}.

Each agonist binds a specific, cognate, 7-transmembrane domain G-protein couple receptor (GPCR) on the plasma membrane that couples to the heterotrimeric G protein, $G_{\alpha q}$. Activation of $G_{\alpha q}$ results in the activation of phospholipases that catalyze the hydrolysis of phosphoinositide bisphosphate (PIP_2) in the plasma membrane, generating the second messenger IP_3 (Yule, 2015). Binding of IP_3 to IP_3R on the apical ER causes Ca^{2+} flux through the receptor, with Ca^{2+} moving out of the ER and into the apical aspect of the cytosol (Straube al., 2002; Thorne al., 1993). Increased Ca^{2+} in the cytoplasm activates RyRs, which are also located on the ER membrane, further enhancing Ca^{2+} release from the ER into the cytoplasm (Kasai et al., 1993). The mechanism by which oscillatory Ca^{2+} signals are controled is not well understood but involves a combination of oscillating IP_3 levels (Straub et al., 2002), regulator of G protein signaling (RGS) control over GTPase activity of G_α subunits (Luo et al., 2005; Xu et al., 1999; Zeng et al., 1996) and IP_3R inactivation (Bezprozvanny et al., 1991). This thesis probes the role of SPCA2C isoform in regulating cytosolic Ca^{2+} levels and oscillations.

1.4 Pathways regulating Ca^{2+} in acinar cells

Stimulus-secretion coupling in acinar cells involves specific spatiotemporal Ca^{2+} signals, which involves both Ca^{2+} release from the ER and removal from the cytosol. Important pathways also exist to replenish ER Ca^{2+} stores and to regulate resting Ca^{2+} homeostasis.

1.4.1 Ca^{2+} Release from the ER

The apical initiation of Ca^{2+} release in pancreatic acini is due to the abundant expression of IP_3R in the extreme apical region of the cell. There are three IP_3R subtypes, including IP_3R1, IP_3R2 and IP_3R3, all of which are expressed in pancreatic acinar cells and accumulate on the ER near the apical and lateral plasma membrane (Lee et al., 1997; Yule et al., 1997). Expression of either IP_3R2 or IP_3R3 is essential for proper enzyme exocytosis. Individual knock out of genes encoding IP_3R2 or IP_3R3 are phenotypically normal, while the compound IP_3R2/IP_3R3 null animal dies soon after weaning due to pancreatic insufficiency. IP_3R1 cannot compensate for the loss of other sub-types as secretagogue-simulated Ca^{2+} signals and secretion of fluid and protein are essentially absent in IP_3R2/IP_3R3 null animals (Futatsugi et al., 2005). Ca^{2+} release through IP_3Rs are influenced by many factors including Ca^{2+} itself. Increases in cytosolic Ca^{2+} between the ranges of 0.5-1 μM increases the steady-state open probability, while higher Ca^{2+} concentrations decrease IP_3R activity (Bezprozvanny et al., 1991; Finch et al., 1991). IP_3Rs are also regulated by interactions with other proteins, adenine nucleotides (Pandol et al., 1987), phosphorylation by cyclic nucleotide dependent kinases (Camello et al, 1996; Giovannucci et al., 2000), PKA (Giovannucci et al., 2000; Tsunoda et al., 1990) and PKC (Patel et al., 1999; Patterson et al., 2004).

RyRs are modulated by similar regulators and share some sequence and structural homology to IP_3Rs. However, RyRs do not depend on specific ligands and only require Ca^{2+} to open, producing CICR (Kasai et al., 1993). Pharmacological blocking of RyRs dampens, but does not block, secretagogue-induced Ca^{2+} signals (Nathanson et al., 1992; Straub et al., 2000). Cellular localization of RyR differs from IP_3R, distributed diffusely through the acinar cell with a higher concentration in the basal aspect of the cell. This expression pattern suggests activation of RyR plays a role in the propagation of Ca^{2+} signals from the initial release of Ca^{2+} at the apical projections of ER to other peripheral regions of the cell (Husain et al., 2005; Leite et al., 1999; Straub et al., 2000).

1.4.2 Maintaining endoplasmic reticulum Ca^{2+} homeostasis

Since not all of the Ca^{2+} that leaves the ER upon stimulation is returned, there is an overall net loss of Ca^{2+} in the ER. To accommodate this, acinar cells have a store-operated Ca^{2+} entry (SOCE) pathway, which is activated when ER stores begin to empty, to maintain ER Ca^{2+} homeostasis (Figure 1.2).

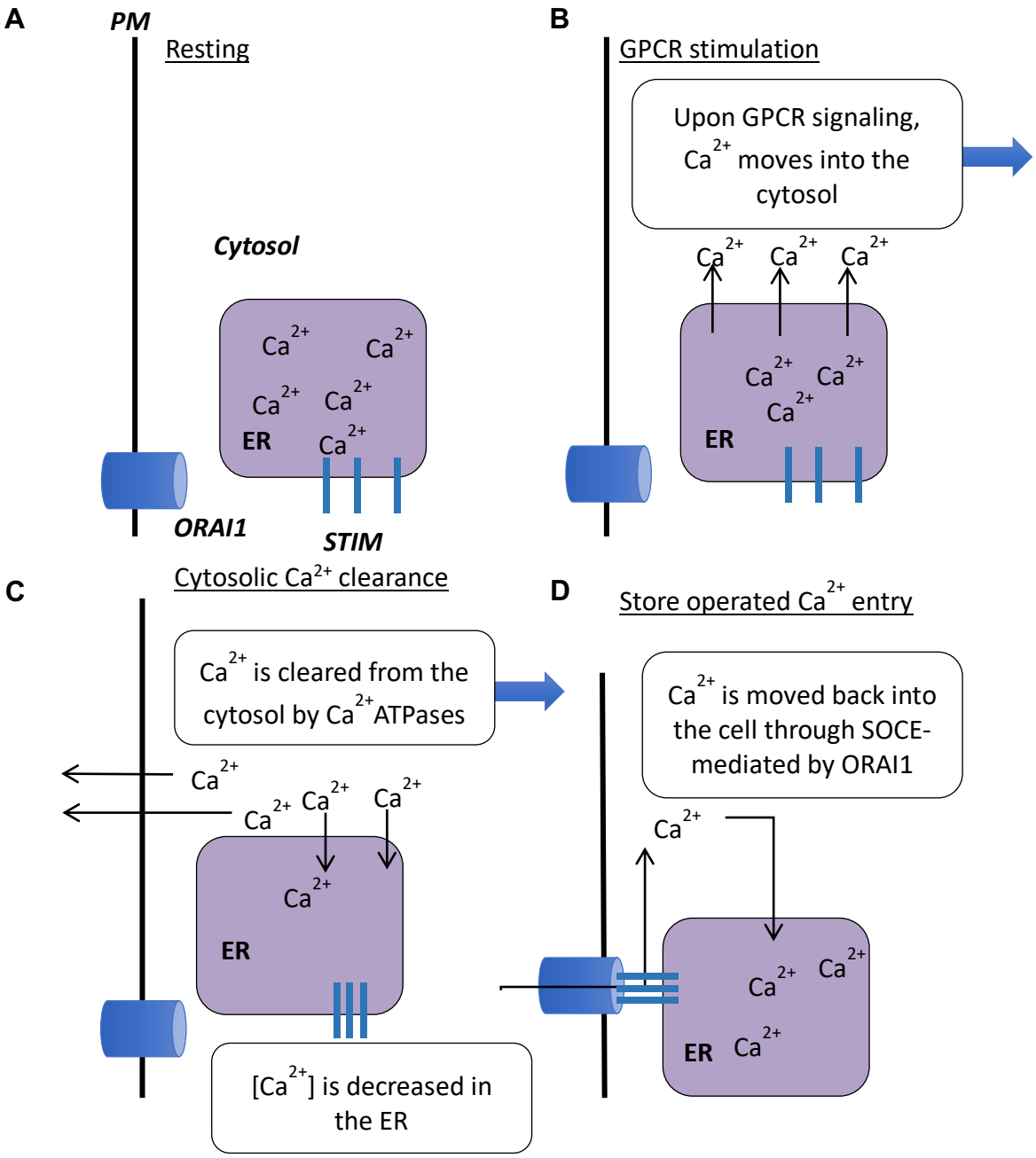
A
PM
Resting
Cytosol
Ca2+
Ca2+
Ca2+
Ca2+
ER
Ca2+
ORAI1
STIM
B
GPCR stimulation
Upon GPCR signaling, Ca2+ moves into the cytosol
Ca2+
Ca2+
Ca2+
Ca2+
Ca2+
Ca2+
ER
C
Cytosolic Ca2+ clearance
Ca2+ is cleared from the cytosol by Ca2+ATPases
Ca2+
Ca2+
Ca2+
Ca2+
Ca2+
ER
[Ca2+] is decreased in the ER
D
Store operated Ca2+ entry
Ca2+ is moved back into the cell through SOCE-mediated by ORAI1
Ca2+
Ca2+
Ca2+
Ca2+
ER
Ca2+

Figure 1.2 Diagram of Ca^{2+} efflux from ER and subsequent activation of SOCE.

A) Unstimulated cells at rest maintain ER and cytoplasmic Ca^{2+} at ~0.1 μM and ~1mM respectively, (**B**) Upon GPCR-mediated IP_3 production, ER Ca^{2+} moves through IP_3Rs down the steep concentration from the lumen to the cytoplasm. (**C**) SERCA and PMCAs, function to clear cytosolic Ca^{2+}; decreased ER Ca^{2+} causes STIMs to cluster and accumulate at ER-plasma membrane junctions. (**D**) Coupling of STIMs to Orai1 at ER-plasma membrane junctions opens these Ca^{2+} channels, causing Ca^{2+} to move down the steep concentration gradient. Ca^{2+} is then pumped back into the ER by SERCAs.

1.4.2.1 SOCE

ER Ca^{2+} stores are replenished through SOCE, which mediates Ca^{2+} uptake by cells from the extracellular stores. This involves movement of Ca^{2+} first into the cytosol down the steep concentration gradient, followed by active uptake into the ER by sarco/endoplasmic reticulum Ca^{2+}ATPases (SERCA) against the concentration gradient. The two vital protein components of the SOCE pathway are the ER resident, Ca^{2+}-sensing protein stromal interaction molecule 1 (STIM1) and the plasma membrane, Ca^{2+}-selective channel forming subunit Orai1(Feske et al., 2006; Hong et al., 2011; Liou et al., 2005; Roos et al., 2005; Vig et al., 2006; Zhang et al., 2006). The Orai1 family of membrane proteins form the conductive pore of Ca^{2+} release-activated Ca^{2+} channels (CRAC; Feske et al., 2006; Hong et al., 2011; Vig et al., 2006). STIM1 consists of a cytoplasmic C-terminal domain, one transmembrane domain that spans the ER membrane, and an N-terminal portion residing in the ER lumen. An EF-hand domain is located within the N-terminal portion of STIM1, which senses ER Ca^{2+} stores decreases through the unbinding of Ca^{2+}, resulting in structural changes that lead to oligomerization and propagate to the C-terminal end of the protein. The STIM1/Orai1 activating region within the cytoplasmic C-terminal end of STIM1 is responsible for moving STIM1 oligomers to ER-plasma membrane junctions, where they interact and activate Orai1(Liou et al., 2005; Wu et al., 2006). Crystal structure analysis shows the Orai1-composed CRAC channel is formed from a hexamer of Orai subunits. Each subunit contains four transmembrane alpha helices (M1-M4) and a helix following M4 termed the M4 extension that extends into the cytosol (Hou et al., 2012). Interactions between STIM1 and both the N- and C-terminal helix extensions of Orai1are involved in opening the channel. Orai1 achieves its high Ca^{2+} selectivity through high-affinity binding of Ca^{2+} to a glutamate ring, which likely acts as the ion selectivity filter. When Orai1 is not bound to STIM1, it is inactive.

In pancreatic acinar cells, SOCE is required for continued cytosolic Ca^{2+} oscillations typical of those that occur to drive enzyme secretion (Yule et al., 1991). If SOCE is inhibited during stimulation of enzyme secretion, Ca^{2+} oscillations will not continue, even if stimulus is present (Yule et al., 1991). Although STIM1 and Orai1 are the key components in SOCE, other proteins can mediate this process. For example, transient receptor potential channel 1/3 (TRPC1/3) can also be part of the SOCE pathway by acting as a Ca^{2+} influx channel when activated by STIM1 in the presence of Orai1 (Hong et al., 2011; Ong et al., 2007).

1.4.2.2 SICE

In addition to the involvement in SOCE, Orai1 plays a key role in other pathways. Orai1 along with Orai3 can be activated by other molecules or proteins, independent of ER Ca^{2+} stores. This pathway is termed the store-independent Ca^{2+} entry (SICE) pathway. SICE is a newly discovered phenomenon with much of the research focusing on the role of this process in cancer. In SICE, Orai1 contributes to Ca^{2+} currents activated by arachidonic acid or the metabolite leukotriene C4, along with Orai3, through ARC/LRC channels (Mignen et al., 2008). Other channels have also been linked to SICE including the small conductance Ca^{2+} activated K^+ channel (SK3). In bone cancer, SK3 controls Ca^{2+} through Orai1 (Chantome et al., 2013) and recently, a functional interaction between $K_v10.1$ and Orai1, which allows constitutive Ca^{2+} influx in a breast cancer cell line has been defined (Badaoui et al., 2018).

1.4.3 cADP and NAADP pathways for Ca^{2+} release from lysosomal stores

In mouse pancreatic acinar cells, the global temporal Ca^{2+} signal stimulated by Ach differs from stimulation by CCK, suggesting different pathways initiate Ca^{2+} release. In mouse pancreatic acinar cells, CCK and ACh stimulate activity of cytosolic ADP-ribosyl cyclase activity resulting in the production of cyclic adenosine diphosphate ribose (cADPR), which then results in Ca^{2+} release from basal aspects of the cell. Physiological levels of CCK result in the production of nicotinic acid adenine dinucleotide phosphate (NAADP). NAADP is a potent Ca^{2+} mobilizer, releasing Ca^{2+} from stores, independent of IP_3 and CICR, suggesting NAADP elicits Ca^{2+} release from different stores (Churchill et al., 2002; Genazzani & Galione, 1996). While the endocytic and hydrolytic functions of the endolysosomal system are well established (reviewed by Luzio, el., 2007), the Ca^{2+} signalling functioning of these organelles remains unclear. A general consensus does exist on a model for functional coupling between the lysosome-ER interface. This model suggests that NAADP mobilizes localized Ca^{2+} signals from lysosome-related Ca^{2+} stores. The Ca^{2+} release from lysosome-related Ca^{2+} stores at the lysosome-ER interface initiates global Ca^{2+} waves through recruitment of Ca^{2+} release from RyR through CICR (Galione, 2015; Penny et al., 2015). The measurement of Ca^{2+} concentrations in the lysosome is difficult, since fluorescent probes for measuring Ca^{2+} are pH sensitive, however, estimates for lysosomal Ca^{2+} concentrations have been made between 400-600 μM (Lloyd-Evans et al., 2008; Ronco et al., 2015). Ca^{2+} enters the lysosome through the H^+/Ca^{2+} exchanger (Luzio et al., 2007). The two-pore channel (TPC) family of proteins, expressed in an endo-lysosomal compartment of the pancreatic acinar cells, has been proposed as the candidate receptor for Ca^{2+} release by NAADP (Hooper & Patel, 2012). TPC2 has been shown to recruit CICR channels (IP3R and RyR) to the ER-lysosomal junctions (Galione, 2011). The family of transient receptor potential cation

channel, mucolipin subfamily (TRPML) channels has also been proposed as a Ca^{2+} release channel on lysosomes; however, TRPML dependence on NAADP for Ca^{2+} release is highly debated (Dong et al., 2010).

Combined, the pathways described above promote increased cytosolic Ca^{2+}. Since high cytosolic levels of Ca^{2+} trigger many unwanted consequences, additional mechanisms are required to clear Ca^{2+} from the cytosol. The key proteins involved in the process are Ca^{2+}ATPases.

1.5 Ca^{2+}ATPase

Stimulated Ca^{2+} release from subcellular stores and Ca^{2+} influx through SOCE is modulated by buffering proteins and mitochondria, while Ca^{2+}ATPases work to return cytosolic levels back to resting levels. There are three families of P-Type Ca^{2+}ATPases; Plasma Membrane Ca^{2+}ATPases (PMCAs), SERCAs and SPCAs, all of which have a primary function in moving Ca^{2+} out of the cytosol against a concentration gradient, using energy from the hydrolysis of ATP. In general, P-Type Ca^{2+}-ATPases contain a cation-binding domain, hydrolase domain and ATPase domain to carry out this process.

1.5.1 Sarco/endoplasmic reticulum Ca^{2+} ATPase

SERCAs are transcribed from the *Atp2a* gene family which include *Atp2a1*, *2a2*, and *2a3* (Wuytack et al., 2002). SERCA2 (*Atp2a2*) is the most widely expressed isoform and exists as four different splice variant isoforms: SERCA2a-d. SERCA2b is ubiquitously expressed. SERCA3 splice variants are always co-expressed with SERCA2b and found in the pancreas, as well as other secretory cells including the trachea, colon, lymphocytes, platelets, mast cells and

thyroid [reviewed in (Altshuler et al. 2012)]. The primary function of SERCAs is to move Ca^{2+} from the cytosol into the lumen of the ER, where the ion can be stored (Mogami et al., 1997). In pancreatic acinar cells, SERCA2a and SERCA2b are expressed in the luminal pole. Inhibiting SERCA pumps hinders physiologically stimulated Ca^{2+} oscillations (Lee et al., 1997). All SERCA pumps are inhibited by thapsagargin (TG), which causes passive ER Ca^{2+} store depletion (Lee et al., 1997). TG is a sesquiterpene lactone (Rogers et al., 1995). Treating cells with TG results increased levels of cytoplasmic Ca^{2+}, as the ion leaks out of the lumen and cannot be pumped back in due to SERCA inactivation. Therefore, the increase in cytoplasmic Ca^{2+} levels after TG treatment of cells is often used as a gauge of ER Ca^{2+} store levels in experiments.

1.5.2 Plasma membrane Ca^{2+} ATPases

There are four different genes encoding PMCAs - *Atp2b1*, *2b2*, *2b3*, and *2b4*. PMCA1, transcribed from *Atp2b1*, is ubiquitously expressed beginning in the earliest stages of embryonic development. PMCA2 is expressed in lactating mammary glands and the nervous system, while PMCA3 is expressed in skeletal muscles and the nervous system. PMCA4 is expressed in the heart, brain and, at high concentrations, in the spermatozoa. Due to alternative splicing, over 30 PMCA isoforms have been identified to date, accounting for tissue-specific cellular localization, Ca^{2+} regulatory abilities and calmodulin affinity [reviewed in (Brini et al. 2013)]. In pancreatic acinar cells, PMCA1 appears to be most abundant, accumulating in the apical and lateral plasma membrane, and correlating with the preferential site of Ca^{2+} extrusion on the apical aspect of the cell (Lee et al., 1997). PMCA1 is active even while the pancreatic acinar cell is at rest, implying that PMCAs are important for maintaining basal cytosolic Ca^{2+} levels (Camello et al., 1996). The

rate of Ca^{2+} pumping by PMCAs has a steep dependence on intracellular Ca^{2+} concentrations and is saturated above 400 nM (Camello et al., 1996). Clearance of Ca^{2+} can be attenuated using PMCA inhibitor (Bruce, 2013); however, no pancreatic phenotype has been reported for *Pmca1*, *Pmca*2 or *Pmca*4 homozygous or heterozygous knockout mice, suggesting there is redundancy in function between PMCA isoforms in the pancreas.

1.5.3 Secretory Pathway Ca^{2+} ATPase

The secretory pathway Ca^{2+} ATPase was first identified in yeast *Saccharomyces cerevisiae* as plasma membrane ATPase-related 1 (Pmr1; Antebi & Fink 1992). Pmr1 is biochemically distinct from the other Ca^{2+}ATPases, as it has an unusual selectivity for Mn^{2+} and plays a prominent role in detoxification (Xiang et al. , 2005).

There are two SPCA isoforms SPCA1 and SPCA2, transcribed from different genes. SPCA1 is ubiquitously expressed in tissues, while SPCA2 shows limited expression to a few tissues/cell types (Pestov et al., 2012). Homozygous loss of *ATP2C1*, the gene encoding SPCA1, results in fetal mortality. Haploinsufficiency causes Hailey-Hailey disease, a debilitating blistering disorder of the skin characterized by disruption of desmosome contacts in keratinocytes (Deng & Xiao, 2017). Although the exon/intron layout is perfectly conserved between *ATP2C1* and *ATP2C2* and the two proteins encoded by the respective genes share a 64% amino acid sequence identity, it is clear that SPCA2 carries out other physiological functions compared to SPCA1 since it is not able to compensate for reductions in SPCA1 expression or activity (Dode et al., 2006). In fact, recent studies suggest a unique role for SPCA2 in SICE (Feng et al., 2010),

though, the existence of this pathway has not yet been confirmed in pancreatic acinar cells. This thesis will investigate a possible physiological role for SPCA2C, an SPCA2 isoform, in the SICE pathway.

1.5.3.1 Secretory Pathway Ca^{2+}ATPase 2

SPCA2 is only expressed in higher eukaryotes. The highest accumulation of SPCA2 is found throughout the gastrointestinal tract (Pestov et al., 2012). Other tissues expressing SPCA2 include the brain, stomach, large and small intestine, prostate, salivary and mammary glands (Pestov et al., 2012). *ATP2C2,* the gene that encodes SPCA2, spans a region of 95.5 kb on human chromosome 16 and consists of 27 exons ranging from 36-393 bp. The SPCA2 protein is 946 amino acids long. Due to the close homology between SPCA2 and SPCA1, Golgi subcellular localization is presumed, similar to SPCA1; however, subcellular localization seems to depend on cell type. In C2C12 cells (Vanoevelen et al., 2005), a mouse myoblast cell line, human HT-29 and CHO cells (Jenkins, Papkovsky, & Dmitriev, 2016), SPCA2 exhibited a Golgi-like localization. However, in the skin of rat there was strong labeling in the perinuclear region, and in the rat duodenum, SPCA2 was strongly associated with the plasma membrane (Pestov et al., 2012). In the MCF7 breast cancer cell line, SPCA2 partially localized to the plasma membrane, showing up to 10% of SPCA2 protein being cell surface biotinylated (Feng et al., 2010).

Immunofluorescence (IF) analysis showed SPCA2 expression in mouse pancreatic acini and subsets of islet cells, but not in duct cells or blood vessels (Garside et al., 2010). Subcellular localization of SPCA2 in pancreatic acinar cells showed expression similar to ER associated

protein calreticulin, rather than Golgi resident proteins such as GM130 (Garside et al., 2010). Interestingly, in pancreatic tissue the *Atp2c2* transcript is significantly smaller than the predicted, full-length sequence. Northern and Western blot analysis both confirmed a shorter transcript and no expression of the full-length *Atp2c2* gene and protein was observed in the pancreas (Garside et al., 2010). Additional analysis suggested this smaller *Atp2c2* transcript and SPCA2, termed SPCA2C, protein was pancreas-specific and that the protein contained at least the carboxy terminus of the full length protein. However, it is unclear if this isoform is the product of a splice variant or is produced through an alternative transcriptional start site. Determination of the exact DNA coding sequence of the isoform is essential for interpretation of its amino acid sequence and to propose a function for SPCA2C through interpretation of its amino acid sequence. The first question that this study addresses is defining the coding sequence of the *Atp2c2* gene expressed in pancreatic tissue.

1.6 Alternative functions of SPCA2

Given the high degree of homology between SPCA1 and SPCA2, it was postulated that their functions complemented each other (Vanoevelen et al., 2005). However, based on recent studies, it is clear that SPCA2 is functionally distinct from SPCA1. Studies show SPCA2 has different subcellular localization patterns, is expressed as unique isoforms, and is involved in SICE, depending on cell type, making SPCA2 an intriguing protein for Ca^{2+} regulation. Given that Ca^{2+} is key to pancreatic acinar cell function and survival and that SPCA2C is the only isoform expressed in pancreatic acinar cells, understanding the role of SPCA2C in this cell type is paramount.

As mentioned, the general function of P-Type Ca^{2+}ATPases is to move Ca^{2+} away from the cytosol. However, in breast cancer cells, 10% of SPCA2 is localized to the plasma membrane, and surface residence of SPCA2 correlates with elevation of basal cytosolic Ca^{2+} concentrations (Feng et al., 2010). Remarkably, the ability of SPCA2 to increase cytosolic Ca^{2+} concentrations was found to be independent of Ca^{2+}ATPase activity. Instead, this function was associated with an interaction of its C-terminal region with the plasma membrane store operated Ca^{2+} channel Orai1 (Feng et al., 2010). This information further distinguished SPCA2 function from SPCA1 and exemplified a potentially important alternate role in specific cell types, such as acinar cells.

Co-localization of endogenous SPCA2 and Orai1 was shown in MCF7 cells, and an interaction was confirmed between these two proteins. Unlike the interaction between STIM1 and Orai1 in SOCE, localization and the ability to activate Orai1 was independent of ER Ca^{2+} store levels and did not require STIM1 or STIM2 (Feng et al., 2010). Furthermore, knock-down of endogenous expression of SPCA2 expression in MCF7 cells significantly decreased resting cytosolic Ca^{2+} concentrations. This supports an alternate function for SPCA2 in increasing cytosolic Ca^{2+} concentrations in a store and STIM-independent manner (Feng et al., 2010).

Interestingly, enhanced expression of endogenous SPCA2 has a physiological role in lactation. Specifically, in mammary epithelia, SPCA2 expression is driven by prolactin, a polypeptide hormone indispensable for the growth and development of mammary glands, synthesis of milk and maintenance of milk secretion. An increase in SPCA2 expression in mammary epithelial cells increased the concentration of Ca^{2+} in the Golgi apparatus. SPCA2 was increased during lactation, while SPCA1 was not (Anantamongkol et al., 2007).

Despite these studies, there is still much that is unknown regarding SPCA2 function. This is particularly true regarding SPCA2C, which is the only isoform expressed in pancreatic cells. Based on the short nature of SPCA2C and seemingly pancreas-specific expression, several questions need to be addressed. Does this short C-terminal isoform SPCA2C have a function; does it perform similar or different functions as SPCA2; and do these functions depend on cell type? The goal of my thesis was to address, in part, some of these questions regarding SPCA2C biology.

1.7 Rational, hypothesis and objectives

The first recognition of SPCA2 in pancreatic tissue originated from a screen comparing gene expression between wild type and *Mist1*$^{-/-}$ mice (Garside et al., 2010), which present phenotypes of cellular disorganization (Pin et al., 2001), an increased susceptibility to pancreatitis (Kowalik et al., 2007) and pancreatic cancer (Zhu et al., 2004) and defects in Ca^{2+} handling (Luo et al., 2005). This comparison identified *Atp2c2* as being the most significantly decreased mRNA in the absence of *Mist1*$^{-/-}$, model of pancreatic pathology. Further characterization of SPCA2 in pancreatic tissue indicated a significantly smaller protein compared to the predicted full length SPCA2, which is 944 amino acids in length. The goal of my study was to understand the function of SPCA2C.

1.7.1 Governing hypothesis

My governing hypothesis is that **SPCA2C influences Ca^{2+} influx and cytosolic Ca^{2+} levels.**

The goals of the first results chapter were to delineate the DNA sequence of *Atp2c2c* and to determine if the transcript generates a protein that functions in Ca^{2+} homeostasis. Mouse pancreatic RNA was analyzed by RNA-seq and the *Atp2c2*sequence mapped to the carboxy terminus of the full length SPCA2. SPCA2C sequence was then expressed in HEK293A cells and Fura2 ratiometric imaging was used to determine the effects of SPCA2C on cytosolic Ca^{2+} levels.

The goals of the second results chapter were to determine subcellular localization of SPCA2C and test the functional role SPCA2C plays in specific Ca^{2+} signaling pathways, including SOCE and SICE. SPCA2C was transiently expressed in HEK293A and in HEK293A cells stably expressing Orai1 fused to yellow fluorescence protein (YFP) (HEK-Orai1^{YFP}). Cells were treated with a physiological agonist (carbachol) and pathological SERCA inhibitor (TG) agonist to promote altered Ca^{2+} signaling. Cytosolic Ca^{2+} concentrations were measured by Fura2 ratiometric imaging to test Ca^{2+} influx rates, organelle Ca^{2+} stores, STIM1-Orai1 mediated SOCE and store independent Ca^{2+} influx.

In the third results chapter, the experiments were extended in cell lines more relevant to the pancreas. Mouse 266.6 cells, a cell line derived from acinar cells, and pancreatic cancer patient-derived cell lines, were examined in a similar fashion as HEK293A cells. As part of this chapter, an unbiased protein-protein interaction assay was used to establish the SPCA2C interactome. Specifically, biotinylating identification (BioID) protein interaction assay was used to identify proteins in close proximity to SPCA2C. The list of interaction candidates identified by BioID was assessed bioinformatically using GO and Kyoto encyclopedia of genes and genomes

(KEGG) pathway analysis to confirm our findings on SPCA2C biology and predict novel roles for SPCA2C.

By delineating the *Atp2c2c* sequence and functionally characterizing the role of SPCA2C in Ca^{2+} homeostasis, I have uncovered a novel mechanism that pancreatic acinar cells use to regulate cytosolic and ER Ca^{2+} levels.

Chapter 2

Atp2c2 is transcribed from a unique transcriptional start site in mouse pancreatic acinar cells

The work in this Chapter was published as "Atp2c2 is transcribed from a unique transcriptional start site in mouse pancreatic acinar cells" Fenech et al (2016) in the *Journal of Cellular Physiology*. The contributing authors on this manuscript includes Caitlin Sullivan, Dr. Lucimar Ferreira, Dr. Rashid Mehmood, Dr. William MacDonald, Dr. Peter Stathopulos and Dr. Christopher Pin. The work performed by those individuals has been omitted with the exception of Figures 5C, which was completed by C. Johnson. The text within this Chapter related to the omitted figures has been removed or references the result as data not shown.

2.1 Introduction

Pancreatic acinar cells are polarized with highly organized intracellular compartments that permit rapid receptor-regulated exocytosis of enzymes. The precise spatial and temporal control of Ca^{2+} release is fundamental for proper exocytosis of enzymes (Lee et al., 1997). The ability of Ca^{2+} to act as a second messenger in enzyme release is provided by the maintenance of cytosolic Ca^{2+} gradient with greater concentrations of Ca^{2+} outside the cell or within intracellular compartments such as the ER, relative to the cytosol. Transient increases in cytosolic Ca^{2+} are coupled to exocytosis of zymogen granules (ZG) containing enzymes (Burnham et al., 1984), while dysregulation of intracellular Ca^{2+} concentration affects gene transcription, cell proliferation, apoptosis, or necrosis and is associated with the initiation of pancreatitis (Kruger et al., 2000; Li et al., 2014; Zhou et al., 1996). The ability to restore the cytosolic Ca^{2+} gradient

after ER release is due, in part, to P-type Ca^{2+}ATPases that remove Ca^{2+} from the cytosol (Lee et al., 1997). There are three families of P-type Ca^{2+}ATPases. Sarco/endoplasmic reticulum Ca^{2+}ATPases (SERCAs: encoded by three *Atp2a* genes) translocate Ca^{2+} into the ER (Arredouani et al., 2002; Beauvois et al., 2004; Zhao et al. , 2001). Plasma membrane Ca^{2+}ATPases (PMCAs; encoded by four *Atp2b* genes) translocate Ca^{2+} out of the cell. The third type of Ca^{2+}ATPase (SPCAs, encoded by two *Atp2c* genes), which translocate Ca^{2+} into the Golgi [reviewed in (He & Hu, 2012; Vanoevelen et al., 2005). SPCA1/*Atp2c1* is a homolog of Pmr1 /*PMRI* first described in *Saccharomyces cervisiae* (Rudolph et al., 1989). SPCA1 is ubiquitously expressed and targeted deletion of *Atp2c1* in mice results in gestational growth retardation and death before embryonic day 10.5 (Okunade et al., 2007). Embryo development occurs normally until the neural tube fails to close at the dorsal end on ED 8.5. Golgi and ER swelling and increased apoptotic death was observed in $SPCA1^{-/-}$ embryos (Okunade et al., 2007). In humans, mutations in the *ATP2C1* gene are found in Hailey-Hailey disease (Sudbrak et al., 2000). A second gene, SPCA2/*Atp2c2* is expressed only in higher organisms (mammals) and is limited to a few tissues, including secretory and absorptive epithelia of the gastrointestinal, genitourinary, mammary, and salivary glands (Vanoevelen et al., 2005). Although SPCA2 expression is limited to a few tissue/cell types, SPCA2 appears to have a broader localization pattern within the cell compared to SPCA1. Unlike SPCA1, which is localized to the Golgi, SPCA2C is found in the Golgi, ER, and secretory vesicles (Feng et al., 2010; Garside et al., 2010; Pestov et al., 2012; Xiang et al., 2005). In lactating gland luminal epithelia, SPCA2 is localized predominantly to vesicles that travel to the plasma membrane rather than the Golgi and has a major role in increasing intracellular Ca^{2+} (Cross et al., 2013). Human breast adenocarcinoma MCF7 cells have higher SPCA2 expression compared to MCF-10A, a non-

malignant human mammary epithelial cell line. Increased SPCA2 expression was also observed in a small group of breast cancer patients suggesting a potential link between SPCA2, cytosolic Ca^{2+}, and metastasis (Feng et al., 2010). Indeed, they found that exogenous expression of SPCA2 in MCF-10A cells increased cytosolic Ca^{2+} levels, while knocking down SPCA2 in MCF7 cells decreased it. They also show that the C-terminus of SPCA2 is required for Ca^{2+} influx, which was via the plasma membrane calcium channel Orai1, a mechanism they called store independent Ca^{2+} entry (SICE; Feng et al., 2010). These studies suggest that truncations of SPCA2 may also be involved in SICE by activating Orai1 protein function (Feng et al., 2010).

SPCA2 is encoded by the *Atp2c2* gene that spans a region of 95.5 kb on human chromosome 16, which contains 27 exons. SPCA2 is 946 amino acids long (Vanoevelen et al., 2005). SPCA2 is expressed in pancreatic acinar cells, but characterization of SPCA2 expression indicated a significantly smaller protein (Garside et al., 2010) than the predicted full length SPCA2 (Vanoevelen et al., 2005). Expression analysis of this smaller SPCA2 isoform suggested a novel function from the full length SPCA2 as it was localized to both the Golgi and ER. Relevant to acinar cell physiology, SPCA2 expression was markedly decreased in *Mist1*$^{-/-}$ mice, which show defects in Ca^{2+} handling (Garside et al., 2010). While it is clear that the pancreatic isoform, termed SPCA2C, contains at least the carboxy terminus of SPCA2, without knowledge of the exact transcriptional start site and exon/intron splicing; it is unclear what functional significance SPCA2C has in Ca^{2+} homeostasis. To appropriately study the function and regulation of SPCA2/*Atp2c2* in the pancreas, it is imperative to determine if *Atpc2c2* is the result of altered splicing or a pancreatic-specific transcriptional start site (TSS).

The goals of this study were to determine the complete *Atp2c2* transcript encoding SPCA2C and determine if SPCA2C affects Ca^{2+} homeostasis. My results show *Atp2c2* is transcribed from a unique TSS in pancreatic acinar tissue, encoding only the carboxy terminal portion of SPCA2. In addition, over expressing SPCA2C is accompanied by persistent elevation in cytosolic Ca^{2+}, revealing a novel role for SPCA2C in regulating acinar cell function.

2.2 Methods

2.2.1 Mouse handling and initiation of cerulein-induced pancreatitis

C57Bl/6 mice were used for all experiments except transgene analysis. Mice were handled according to guidelines approved by the Animal Care and Use Subcommittee at the University of Western Ontario (Protocols 2008-116 and 2008-027). Transgenic mice carrying the -*1181+57Atp2c2* promoter region upstream of *LacZ* reporter gene were generated through pronuclear injection of CBA/C57Bl/6 hybrid zygotes followed by implantation into CD1 pseudo pregnant mice (completed by the London Transgenic Facility, Western University). Founder mice (F0) were mated to C57Bl/6 mice, and 3-4-week-old F1 mice characterized for transgene expression. 2-4-month-old male C57Bl/6 animals were used for gene and RNA-sequencing (RNA-seq) analysis. The targeted deletion of *Mist1* gene has previously been described (Pin et al., 2001). Cerulein-induced pancreatitis (CIP) was initiated as described (Kowalik et al., 2007) with 4-8 hourly intraperitoneal injections of 50 μg/kg cerulein (cholecystokinin analog) and mice sacrificed 4, 8, 32 and 72 hours after initial injection.

2.2.2 RNA isolation, qRT-PCR, and RNA-Seq

RNA was isolated from pancreatic tissue of C57/Bl6 mice or pancreatic tissue of *Mist1*$^{-/-}$ mice as described (Johnson et al., 2009). RNA was isolated from whole tissue using TRIzol (Invitrogen, Burlington, ON), following the manufacturer's instructions. Real-time qRT-PCR was performed on cDNA samples. To make cDNA samples, 1 μg of total RNA was reverse transcribed using Improm-II Reverse Transcriptase and random primers (Promega, Madison, WI). Quantitative real time PCR (qRT-PCR) was performed using the Roche LightCycler 1.5 carousel-based system (Roche Diagnostics, Laval, PQ). Duplicate reactions were performed for each sample using 1μl cDNA in 19 μl SYBR™ Green Master Mix as per manufacturer's instructions. Reactions were started at 94°C for 10 minutes, followed by 45 cycles of 94°C for 10s, 60°C for 48°C for 40s, 72°C for 10s. Relative quantification using the calibrator normalized method with standard curves for efficiency correction was carried out using *Mitochondrial ribosomal protein L1* (*Mrpl1*) was used as a normalization control. ViiA 7 RUO software (Applied Biosystems) was used to calculate the amount of RNA relative to saline treatment for the equivalent time points.

2.2.3 Plasmid construction

The putative promoter region upstream of the ATG codon in exon 24 of the *Atp2c2* gene, which corresponds to +2,580 (RNA sequence) or +54,891 (DNA sequence) in the full length *Atp2c2* genomic sequence was designed based on the UCSC Genome browser identification of *Atp2c2* (uc009nqg.I). Promoter-less pWHERE plasmid was used as a negative control for transfection assays.

To generate a transgene promoter construct, *-1811+57Atp2c2cpGL3* was digested with *Xho1* and *Sma1* and cloned into pWHERE (Invitrogen, San Diego, CA; Figure 2.1) digested with the same enzymes. Finally, a *pcDNA3.1* expression vector containing the exact *Atp2c2c* reading frame was generated by Gene Art (Thermo Fisher Scientific, Waltham, MA) based on sequence information from NCBI (Accession #AC_000030.1). The *Atp2c2c* sequence was followed by a FLAG antigenic tag sequence (5'GATTACAAGGATGACGACGATAAG 3'; *pcDNA-SPCA2*^{FLAG}) and stop codon.

A

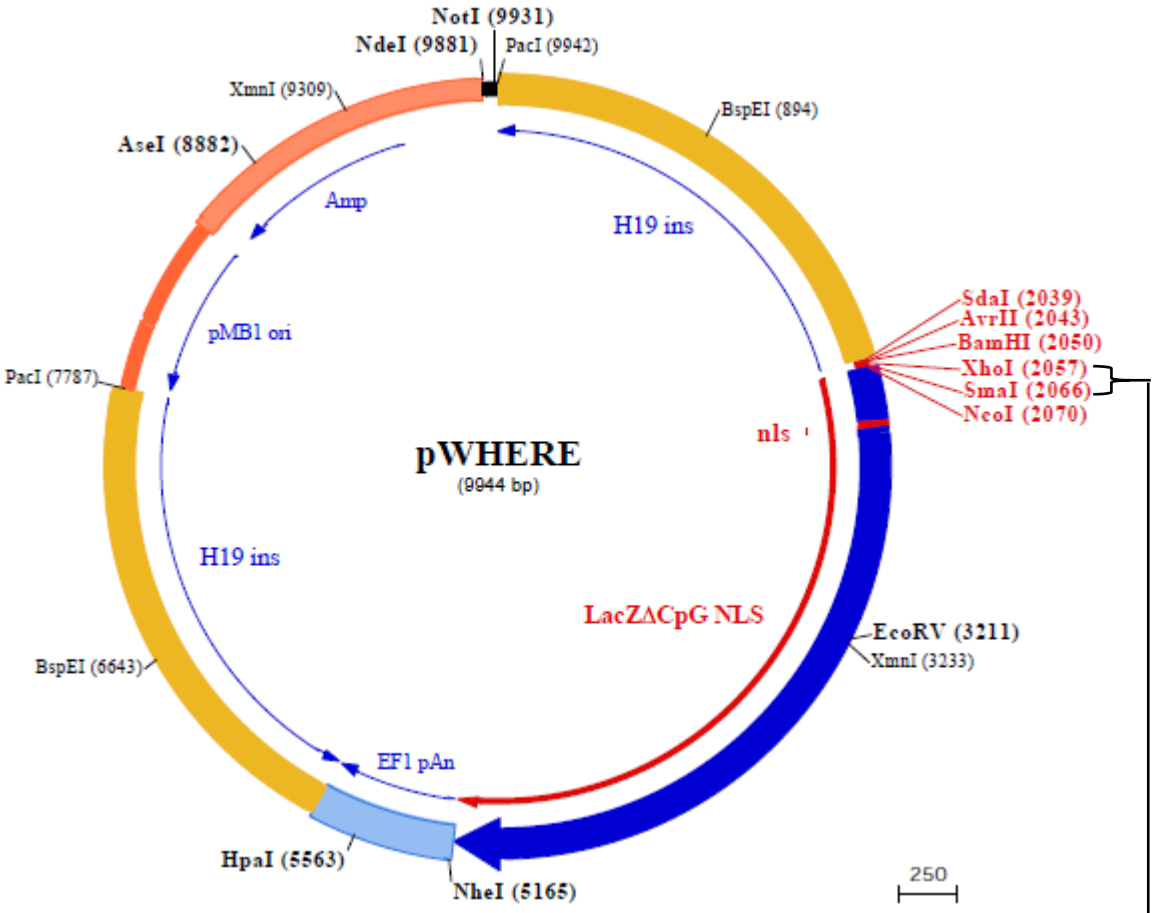

B

-1181+57Atp2c2c

gtgagacggtgggctgcgggcaggaccccgtgggctccctctcagaaaggaatctccgggctgctggagtgtgaacagtgtctagagggg
gcagactggagctccctgggttacattgcactcctggggcccatggctcggtcc**cactg**taaagtcaggccaccgcatccaggcagtcct
ctctgattactctataatggtggcctcatccttgagcctctgccccgcctttcactgatgggaaaatgtcattgttgtgattgattgggt
ccatccccattctagctggttatcatggactagctggttaccaaggactagcttagctggttaccatggacttgatgccccctgaccct
taggatgctgctcgcgtgacatggatgctcactggtgttgcaggaatccatgggaagtgaagtgtgggctagctggagggtacagaaggc
ccgtgtgcccagcagccttggtagctcacacagggaggtgtcattacaaacacactgatgcttctgttagtgtctctatcatcatctgtg
gtccacagaggggagcccagcctgtttccccagagcccagcgggggctgaggtttccataaggctcctgtgagacggcaggtcggctag
ctcccaggtctctaccc**cacatgcatctg**ggctctcctgatgtttctgggtgacagagctgggccctgtttctccaggccccacttaggg
ccccttatggtaataggaacgcatgggggttagaaggctgtgatgtgggaaaggctgaagcccagtgctggcccttgctcggttctttgg
cctctcca**catctg**gatatttggagactgatgagtagagagagctatggctacctgtgggatagttgctcagggacaagagcagcccggc
ttacaggcaacactttggagaacaagtctgagtccatgccaggtatccttttttaaatatttcatttttttttttttgaaagctctcagt
gtgtagtctaggctggcctgggggatttactatgtaacccagactggccttgaacccagagatcctcctgcctccacctcctgaaagctg
gggttacaggctgtgtac**cacctg**ggccagcttc**caagtg**actgttgtcttttctgcacag**CCTTGGGGTGGAGCCTGTGGACAGAGACG**
CCCTGCGGAGGCCTCCACGGAGTGTCGGGGACACGATCCTGAACAGAGCCCTGATCCTGAGGGTCCTC

Figure 2.1 Plasmid construct pWHERE with -1181+57Atp2c2c.

(**A**) Plasmid map. (**B**) Sequence of the *Atp2c2c* promoter region used. Complete sequences of the 5' upstream region from *Atp2c2c* that was used for -*1181+57Atp2c2cpWHERE*. E-box consensus sites highlighted in black represent potential MIST1 binding sites.

2.2.4 Cell culture

HEK293A cells were maintained in Dulbecco's Modified Eagle Medium (DMEM) high glucose media (HyClone, Logan, UT) containing 10% (v/v) FBS and antibiotics (penicillin G 100U.mL, streptomycin 100 μg/mL). When cultures reached 70-80% confluence, cells were transfected using JetPrime transfection kit (PolyPlus, NY) with *Atp2c2c* promoter-*LacZ* plasmids described above, or *pcDNA3.1-SPCA2C*^{FLAG} and or/ *pcDNA3.1-SPCA2*^{MYC}, following manufactures instructions. Promoter-less pWHERE plasmid was used as a control. Forty-eight hours after transfection cells were fixed in 4% (v/v) formalin in PBS.

2.2.5 Immunofluorescence analysis

HEK293A cells were transfected as described above with *pcDNA3.1-SPCA2C*^{FLAG} and/or *pcDNA3.1-SPCA2*^{MYC}. Forty-eight hours after transfection, HEK293A cells were fixed with 4% (v/v) formalin in PBS. Cells were permeabilized with 1% TritonX-100 in PBS and incubated in blocking solution (5% BSA, 1% triton in PBS). Mouse α-FLAG (diluted 1:500, Sigma) or rabbit α-MYC (1:1000, Sigma), was diluted in blocking solution. Fluorescently labelled (TRITC or FITC) secondary goat antibodies were diluted 1:250 in PBS (Jackson Immunoresearch Labs, West Grove, PA or Sigma, Oakville, ON, Canada). Confocal images were acquired using a Leica SP5 Confocal microscope and the colocalization finder plugin for ImageJ (http://I.usa.gov/IPn0ruI) was used to determine overlap of fluorochromes.

2.2.6 β-galactosidase staining

Cells were transfected as stated above with *Atp2c2c* promoter-*LacZ* or empty pWHERE plasmid. 48 hours after transfection cell were fixed in 4% (v/v) formalin in PBS. Pancreata were dissected

from 2-month-old *1181+57Atp2c2* transgenic mice and either fixed in 4% formalin for whole mount β-galactosidase staining or flash frozen in optimal cutting temperature (OCT) compound (Sakura Finetek, CA, USA). OCT-embedded tissue was section at 20 μm using a Shandon cryostat. Whole mount fixed tissues were placed in x-gal solution (4 mM potassium ferricyanide, 2 mM MgCl, 0.08% x-gal in PBS) for up to 12 hours. Tissue sections or cells were fixed in 4% formalin, washed and immersed in x-gal solution for up to one hour. Slides were cover slipped and sealed with Permount mounting medium (Fisher Scientific, NJ). Stained sections were viewed under a Leica microscope DM5500B and whole mount tissues visualized under Leica M205 FA microscope.

2.2.7 Ca^{2+} imaging

HEK293A cells were transfected as described above with *pcDNA3.0-GFP*, *pcDNA3.1-SPCA2C^{FLAG}*, or *pcDNA3.1-SPCA2^{MYC}* (encodes full length SPCA2; kindly provided by R. Rao; Feng et al., 2010). Forty-eight hours after transfection cells were loaded (incubated) with Fura2-AM at 1μM in culture media [Dulbecco's Modified Eagle Medium (DMEM) high glucose media (HyClone) containing 10% (v/v) FBS and antibiotics (penicillin G 100U.mL, streptomycin 100 μg/mL, amphotericin B 0.25 μg/mL; Gibco-BRL, Grand Island, NY)] for 30 minutes at 37 °C and 5% CO_2. After loading, cells were rinsed once in Hank's Buffered Saline Solution (HBSS; 140 mM NaCl, 4.7 mM MgCl, 10 mM HEPES, 1.8 mM CaCl) and then allowed to rest for 10 minutes at room temperature in HBSS before recoding was started. Cells were excited at 340 nm and 380 nm, and Fura2 emissions at 505 nm were measured per individual cell. Changes in the Fura2 fluorescence ratio using excitation wavelengths of 340/380 nm were taken as a measure of changes in intracellular Ca^{2+} levels while individual groups of cells were stimulated with 10 μM

carbachol for 5 minutes at a pressure of 2 Pa by puffing. Five-minute puffing experiments were completed no more than three times per plate, and never on the same group of cells.

2.2.8 Statistics

N values are provided for each study within the figure legends. Data is shown +/- standard error of the mean (SEM) and significance was determined using a one-way ANOVA and Tukey's posthoc test. $p<0.05$ was considered significant.

2.3 Results

2.3.1. The pancreatic isoform of SPCA2 is transcribed from an alternative transcriptional start site in Atp2c2.

The pancreatic isoform of *Atp2c2*/SPCA2 is significantly smaller (Garside et al., 2010) than the published full-length molecule that has been reported in the literature (Vanoevelen et al., 2005). However, it is unclear whether the pancreatic transcript (termed *Atp2c2c*; c for carboxy) is the result of an alternative transcriptional start site (TSS) or alternative splicing of the larger *Atp2c2* transcript. To resolve this question, the *Atp2c2* genomic region was visualized with the UCSC Genome browser (https://genome.ucsc.edu) using RNA-seq data on total pancreatic tissue from 2-month old mice (Figure 2.2A). Examination of the complete *Atp2c2* gene showed no sequence enrichment in exons 1-23, indicating that these exons were not transcribed within the pancreatic genome. Sequence alignment was observed ~41 bp into exon 24 (Figure 2.2B), corresponding to +2403 in the full-length transcript, and including all of the remaining exons (24-27) of the *Atp2c2* gene. Several Expressed Sequence Tags (ESTs) have been identified for *Atp2c2*, but only EST AK007419.1, previously identified in a 10-day-old pancreatic EST library, showed

alignment to *Atp2c2c* (Figure 2.2A, B). Alignment of the AK007419.1 sequence with the full length *Atp2c2* identifies a single missing G nucleotide, which is not missing in our RNA-seq data, indicating that *Atp2c2c* perfectly aligns with the last 702 bp of *Atp2c2*. Based on the RNA-seq and AK007419.1 sequence, I designated the first bp of the *Atp2c2c* transcript as +41 bp into exon 24 of the *Atp2c2* gene. Examination of the *Atp2c2c* sequence identified an open reading frame that initiates from an ATG codon at +57 into *Atp2c2c* and produces a protein that perfectly aligns with the last 136 amino acids of SPCA2 (designated SPCA2C; Figure 2.2C). SPCA2C contains the residues that form the last four transmembrane domains, part of the cation ATPase domain and a cation binding site found within SPCA2 (Figure 2.3).

Examination of other *Atp2* genes showed no unique splicing variants but a potential alternative TSS for *Atp2b1* (Figure 2.4). Examination of RNA-seq data from other regions of the gastrointestinal tract (GEO accession number: GSE36025) showed some enrichment along the entire *Atp2c2* gene with greater sequence enrichment of exons near the 3' end of the *Atp2c2* gene (Figure 2.5), suggesting that other tissues may contain unique isoforms for *Atp2c2* as well as heterogeneity in the *Atp2c2* isoform expressed. However, none of these tissues express only the pancreatic isoform I have identified.

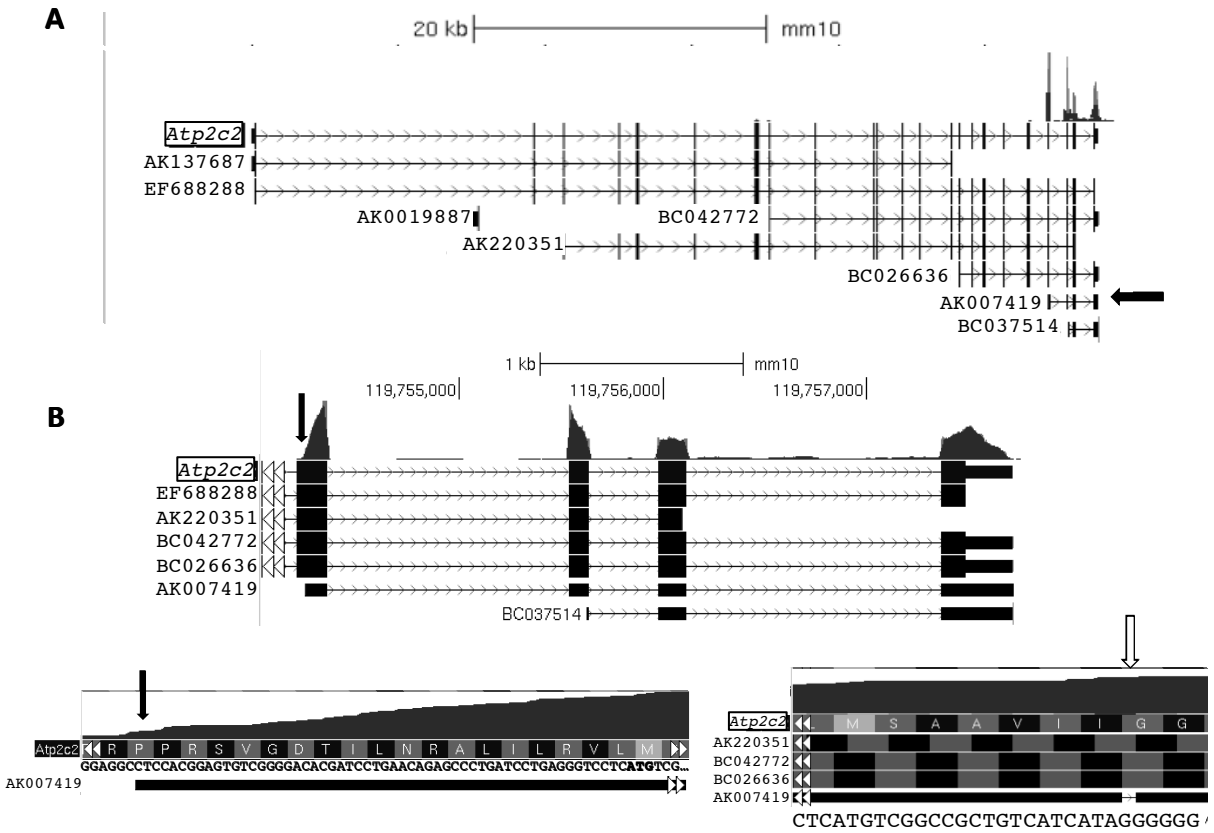

C

```
1       GCTCCACGGAGTGTCGGGGACACGATCCTGAACAGAGCCCTGATCCTGAGGGTCCTCATGTCGGCCGCTGTC
                                                        M  S  A  A  V
73      ATCATAGGGGGGACCCTCTTTATCTTCTGGAGAGAGATCCCAGCGAACGGCACCAGCACCCCACGTACAACC
          I  I  G  G  T  L  F  I  F  W  R  E  I  P  A  N  G  T  S  T  P  R  T  T
145     ACCATGGCCTTCACCTGCTTCGTGTTTTTCGACCTCTTCAATGCCCTGAGCTGTCGCTCTCAGACCAAGCTG
          T  M  A  F  T  C  F  V  F  F  D  L  F  N  A  L  S  C  R  S  Q  T  K  L
217     ATATTTGAGATTGGCTTTTTCCGGAACCGCATGTTCCTGTACTCAGTCCTTGGGTCCCTCCTGGGGCAGCTG
          I  F  E  I  G  F  F  R  N  R  M  F  L  Y  S  V  L  G  S  L  L  G  Q  L
289     GCCGTGATCTATGCCCCGCCCCTACAAAAGGTCTTCCAGACTGAAAACCTGAGCGCGCTCGACCTGCTGCTG
          A  V  I  Y  A  P  P  L  Q  K  V  F  Q  T  E  N  L  S  A  L  D  L  L  L
361     CTGACGGGCCTGGCCTCGTCTGTCTTCATTCTGTCGGAGCTGCTCAAGCTCTGGGAAAAGTTCTTGTCCAGA
          L  T  G  L  A  S  S  V  F  I  L  S  E  L  L  K  L  W  E  K  F  L  S  R
433     GCCAGGCCCACTCAGATGCTCCCGGAAGCTGTGTAACGGAACCAGTGTGTCAAGGCCCTGACTGACCTGTGT
          A  R  P  T  Q  M  L  P  E  A  V  *
505     GCTTGGGTGCCTCTGGCCTGTCCCCATCCATCTGTACTAACCACTCCAAGGGGCAATTCTCAGGACCGTGCA
577     GCATCGGACGCTGGCTCCACCTGTCCTCCTGGCCTGCTGGGCCATGTCCCGCACAGGACAGGGTGGAGCTTA
649     TTATACTGAAACGTGGCGCTATTTATTAAACCACCGTGGTTTTTTTATTTAACTC
```

Figure 2.2 Transcription from the Atp2c2 gene is limited to the last four exons within pancreatic tissue.

(**A**) RNA-seq visualization of the *Atp2c2* gene reveals sequence enrichment only with exons 24 to 27. The only EST that corresponds with this sequence is AK007419 (arrow). (**B**) Higher resolution RNA-seq data indicates that *Atp2c2c* starts within the 4th exon, exactly where the AK007419 EST begins (downward arrow). However, *Atp2c2c* contains the single G nucleotide missing within the published sequence for AK007419 (open arrow). (**C**) The *Atp2c2c* sequence produces an open reading frame that generates a 136 amino acid protein that aligns with the carboxy terminus of SPCA2.

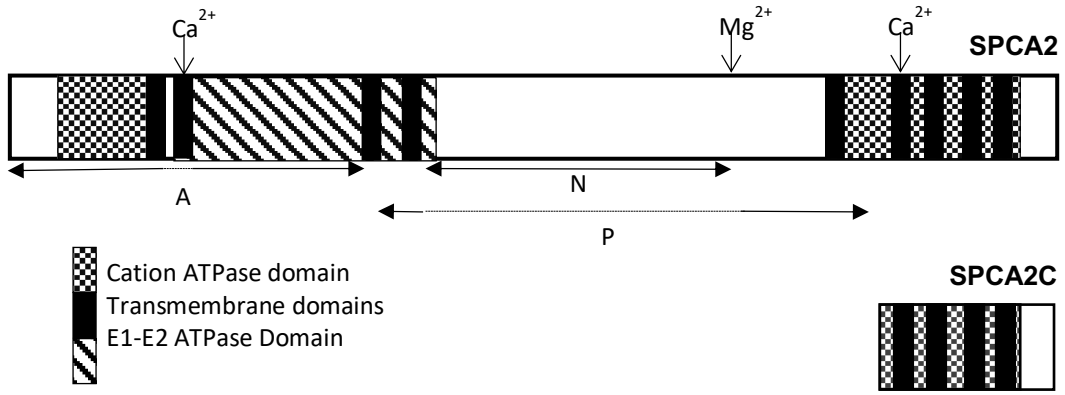
Ca2+
Mg2+
Ca2+
SPCA2
A
N
P
Cation ATPase domain
Transmembrane domains
E1-E2 ATPase Domain
SPCA2C

Figure 2.3 Prediction of SPCA2C protein domains.

Full-length SPCA2 contains cation ATPase, E1-E2 ATPase and nine transmembrane domains. Putative cation binding sites are denoted by arrow heads, which represent multiple closely located residues in three-dimensional space. The putative actuator (A), phosphorylation (P), and nucleotide-binding (N) domain as conserved in many P-type ATPases (Kuhlbrandt, 2004; Vanoevelen et al., 2005) are indicated with dotted sections denoting breaks in protein sequence but not structure. The predicted SPCA2C contains the residues that form the last four transmembrane domains and a portion of the cation ATPase domain.

A

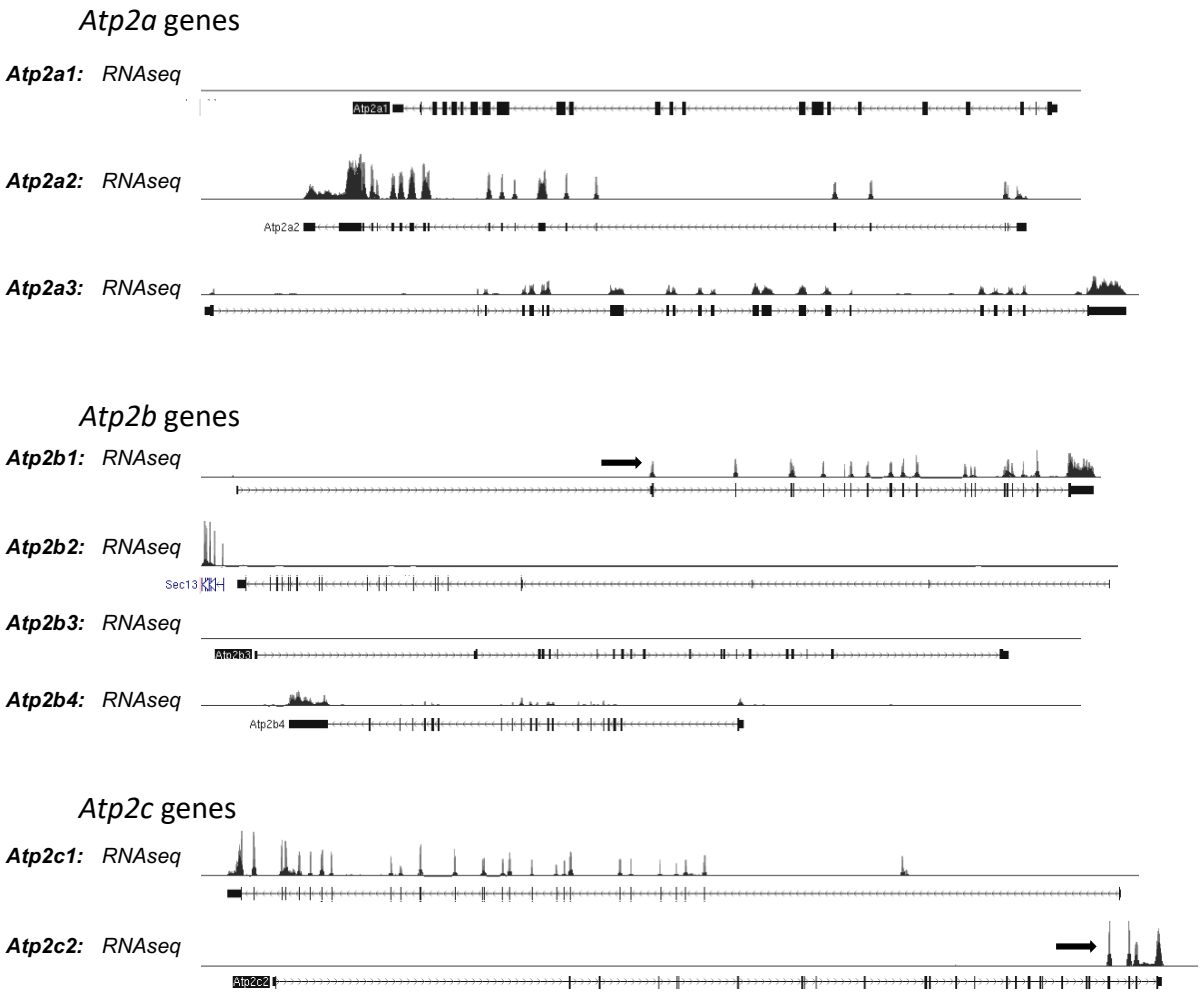
Atp2a genes
Atp2a1: RNAseq
Atp2a1
Atp2a2: RNAseq
Atp2a2
Atp2a3: RNAseq
Atp2b genes
Atp2b1: RNAseq
Atp2b2: RNAseq
Sec13
Atp2b3: RNAseq
Atp2b3
Atp2b4: RNAseq
Atp2b4
Atp2c genes
Atp2c1: RNAseq
Atp2c2: RNAseq
Atp2c2

B

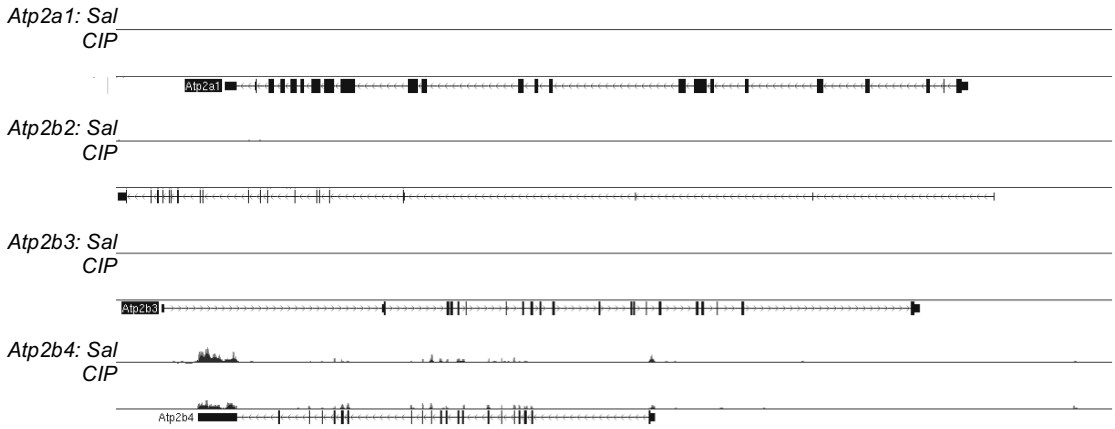
Atp2a1: Sal CIP
Atp2a1
Atp2b2: Sal CIP
Atp2b3: Sal CIP
Atp2b3
Atp2b4: Sal CIP
Atp2b4

Figure 2.4 RNA-seq of other Atp2 genes in mouse pancreatic tissue.

(A) Schematic representation of *Atp2* gene expression based on RNA-seq values and visualized using the UCSC genome browser. Arrows indicate putative TSSs not corresponding to the full-length genes, **(B)** Visualization of RNA-seq for *Atp2* gene not significantly affected during CIP.

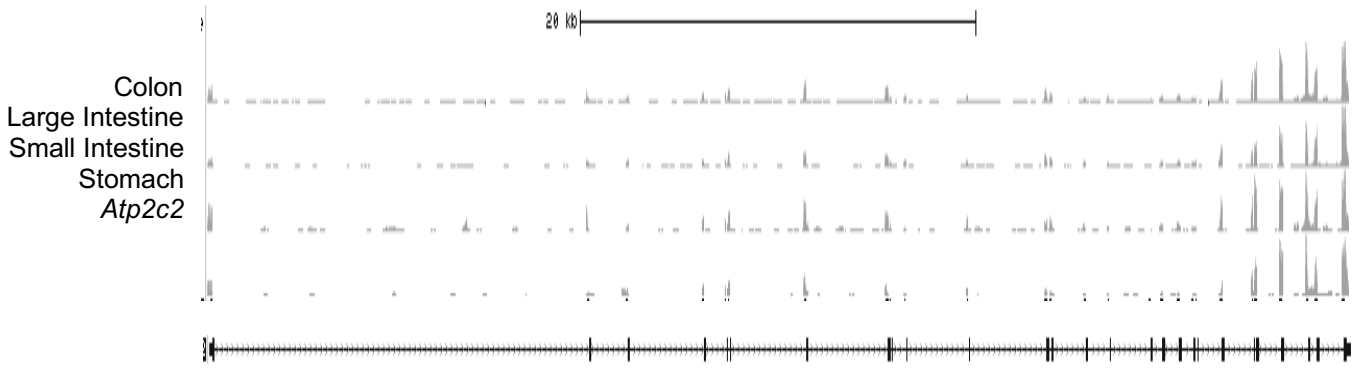
20 kb
Colon
Large Intestine
Small Intestine
Stomach
Atp2c2

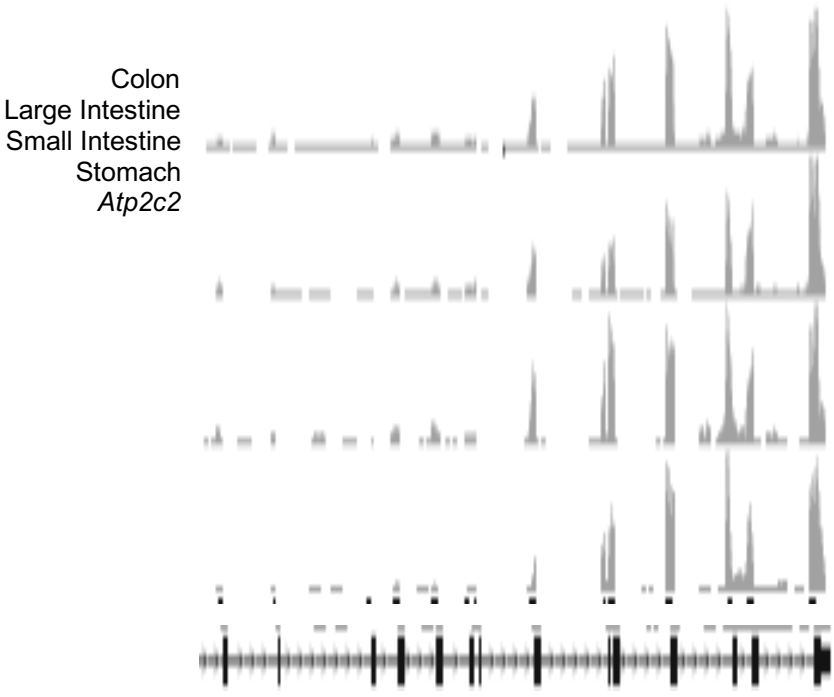
Colon
Large Intestine
Small Intestine
Stomach
Atp2c2

Figure 2.5 Examination of Atp2c2 expression in other regions of the gastrointestinal tract.

(A) Schematic representation of *Atp2c2* gene expression on RNA-seq values of 8-week-old mouse colon, large intestine, small intestine and stomach tissues visualized using the UCSC genome browser. (B) Magnified region focusing on the last half of the *Atp2c2* gene.

2.3.2. The region upstream of Atp2c2c acts as a promoter

The region upstream of the *Atp2c2c* TSS was examined for putative transcription factor binding motifs using the Alibaba-Gene Regulation Data Base and Nsite -- softberry (http://www.softberry.com). Several potential binding motifs were identified including NFκ-β TNFα-K.3 (NF-κB), Sp 1-Ku80 (Sp1), and NF-IL6-CCR1 (NF-IL6) consensus site. However, no consensus TATA box sequence was observed within this region. Therefore, to confirm that the 23rd intron and initial part of the 24th exon of the *Atp2c2* gene drive expression of *Atp2c2c,* the *-1181+57* sequence region was inserted upstream of a nuclear *LacZ* cassette *(-1181+57pWHERE*). Distinct β-galactosidase expression was observed upon transfection in HEK293A cells (Figure 2.6A), confirming promoter activity. To determine if the *-1181+57pWHERE* promoter reporter construct was active *in vivo*, several transgenic lines were generated through pronuclear injection of the *-1181+57Atp2c2cpWHERE* construct (Figure 2.6). In total, nine founder lines were identified. Evaluation of pancreatic tissue using whole mount β-galactosidase analysis revealed no detectable expression above control levels. To perform more sensitive analysis, RT-PCR analysis was performed for *LacZ* mRNA (Figure 2.6C). No detectable *LacZ* expression could be discerned. These findings suggest that the 1181 bp promoter region for *Atp2c2c* does not contain sufficient regulator elements required for pancreatic-specific expression *in vivo*.

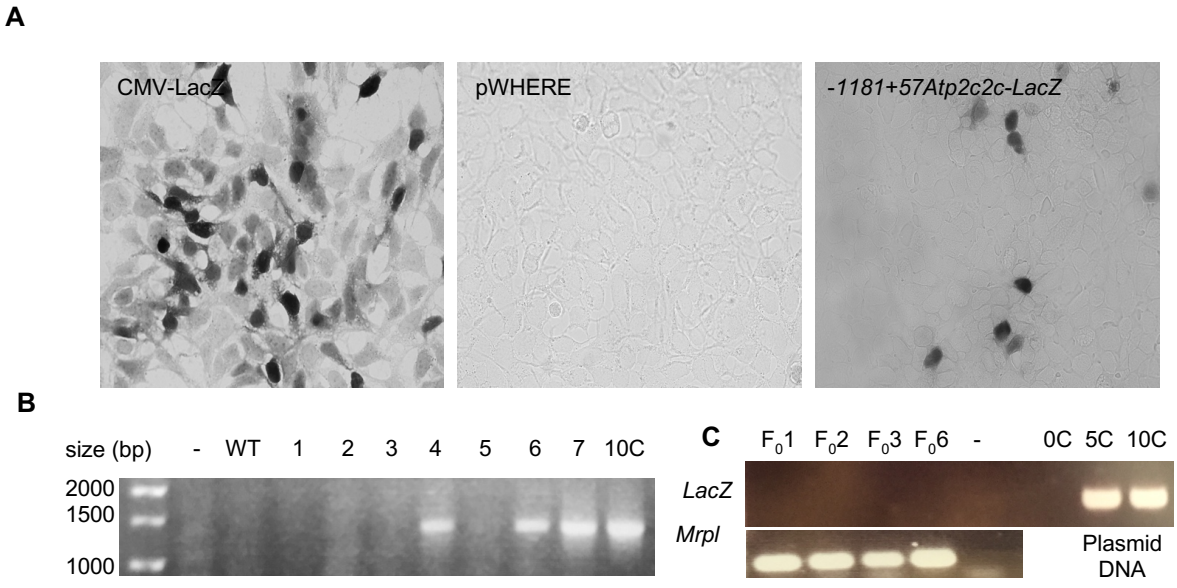
A
CMV-LacZ
pWHERE
-1181+57Atp2c2c-LacZ
B
size (bp)
-
WT
1
2
3
4
5
6
7
10C
2000
1500
1000
C
F0 1
F0 2
F0 3
F0 6
-
0C
5C
10C
LacZ
Mrpl
Plasmid DNA

Figure 2.6 The sequence from the genomic region upstream of the Atp2c2c transcript start site exhibits promoter activity

(**A**) *LacZ* histochemistry of HEK293A cells transiently transfected with *CMV-LacZ*, *pWHERE* with no promoter, or *pWHERE* containing the *+1181-+57Atp2c2c* region in front of *LacZ*. (**B**) Representative PCR for transgene in genomic DNA from one litter of potential founder mice identifying three positive samples. Control is genomic DNA spiked with the equivalent of 10 copies (10C) of the transgenic plasmid. (**C**) RT-PCR for *LacZ* RNA expression in founder mice, *Mrpl* was used as loading control and non-transgenic DNA spiked with 5 or 10 copies (C) of *-1181 + 57Atp2c2cpWHERE* plasmid.

2.3.3. Atp2c2c expression is reduced after inducing pancreatitis in mice.

Atp2c2c expression is significantly reduced in mice lacking the transcription factor MIST1 (Garside et al., 2010), which is a model of increased pancreatitis susceptibility with deficits in Ca^{2+} homeostasis (Luo et al., 2005). Based on this decrease in expression of *Mist1*$^{-/-}$ mice, I predicted *Atp2c2* expression may be altered in response to cerulein-induced pancreatitis (CIP). Cerulein is a CCK analogue that at pharmacological levels (*i.e.* ~50 μg/kg) initiates a pancreatitis response involving premature enzyme activation, altered cell signalling, and initiation of inflammatory genes (Williams, 2008). RNA-seq showed a rapid decrease in *Atp2c2c* expression 4 hours after initiating CIP (Figure 2.7A), which was confirmed by qRT-PCR (Figure 2.7C). *Atp2c2c* expression remained low in CIP treated mice relative to saline-treated mice even as long as 72 hours after initial cerulein injection. *Atp2c2c* expression showed a markedly different response compared to the genes encoding other Ca^{2+} ATPases (Fig 2.7D and Table 2.1). All other *Atp2* genes showed either no difference or increased expression 4 hours into CIP treatment. The increased gene expression for several Ca^{2+} ATPase isoforms suggests acinar cells may upregulate genes that promote a decrease in cytosolic Ca^{2+}. Analysis of the RNA-seq data for genes affecting Ca^{2+} 4 hours into CIP identified expression of 193 out of a possible 254 genes (76%) linked to Ca^{2+} regulation in either saline or cerulein-treated tissue based on Gene Ontology (GO) categorization. Twenty-six genes (10.3% of all known-related Ca^{2+} genes or 13.5% of those Ca^{2+} genes expressed in the pancreas) are significantly up regulated in that time, with an additional 21 genes (8.3% or 10.9% respectively) down-regulated. Therefore, >24% of all genes expressed in the pancreas that affect Ca^{2+} levels are altered within 4 hours of initiated CIP. Using Kyoto Encyclopedia of Genes and Genomes (KEGG) pathway, these genes were mapped to pathways affecting cytosolic Ca^{2+} (Figure 2.8). The effects of altered expression were

predicted for each gene that would affect cytosolic Ca^{2+} based on the published protein function (Table 2.1.). A distinct trend was observed in which genes encoding proteins that elevate cytosolic Ca^{2+}, such as CCKAR and IP_3R3, were significantly reduced. Conversely, several Ca^{2+}ATPase encoding genes, including *Atp2a3* and *Atp2b1*, were significantly increased. *Atp2c2c* fell within the former group suggesting that it may promote increased cytosolic Ca^{2+}.

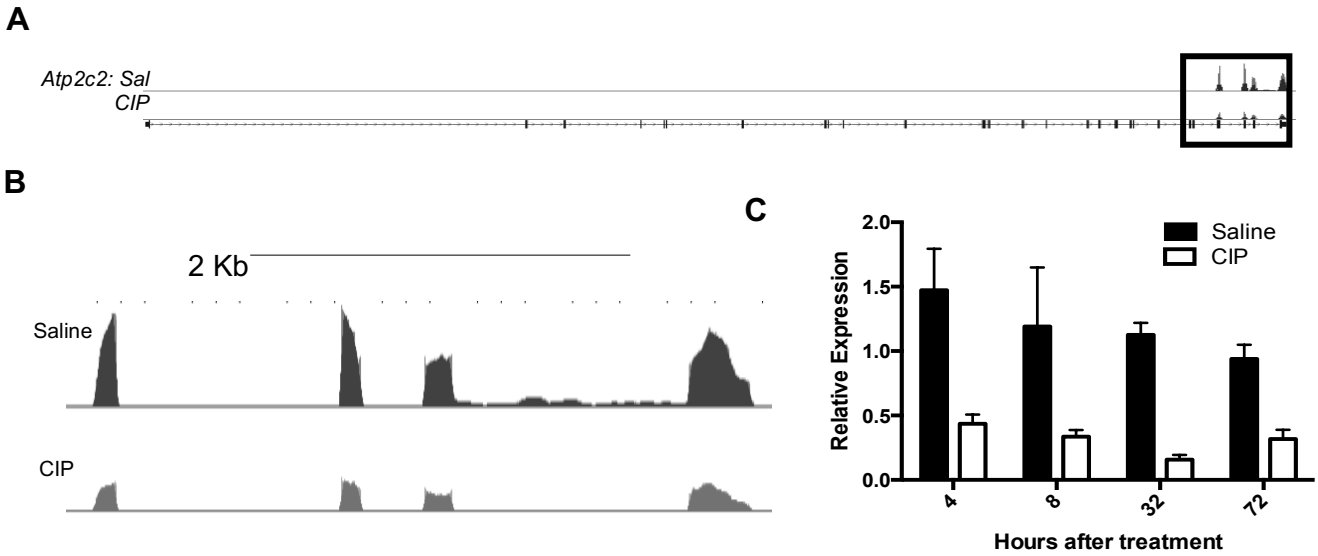
A
Atp2c2: Sal
CIP
B
2 Kb
Saline
CIP
C
Saline
CIP
Relative Expression
2.0
1.5
1.0
0.5
0.0
4
8
32
72
Hours after treatment

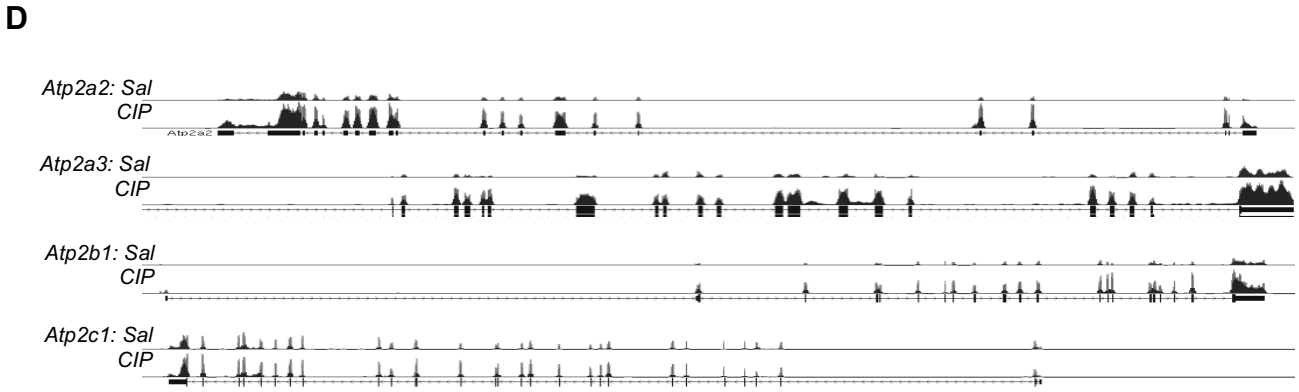
D
Atp2a2: Sal
CIP
Atp2a2
Atp2a3: Sal
CIP
Atp2b1: Sal
CIP
Atp2c1: Sal
CIP

Figure 2.7 Atp2c2c expression is reduced during pancreatitis.

RNA-seq at low (**A**) and high (**B**) resolution for *Atp2c2c* expression 4 hours after initiating CIP. (**C**) qRT-PCR confirms significantly reduced *Atp2c2c* expression until at least 72 hours into CIP. (**D**) Visualization of *Atp2* gene expression using the UCSC genome browser and RNA-seq tracks developed from whole pancreatic RNA obtained 4 hours into cerulein or saline treatment. *Atp2c2c* expression is significantly decreased by CIP treatment, while *Atp2a2*, *Atp2a3*, *Atp2b1*, and *Atp2c1* are all significantly increased.

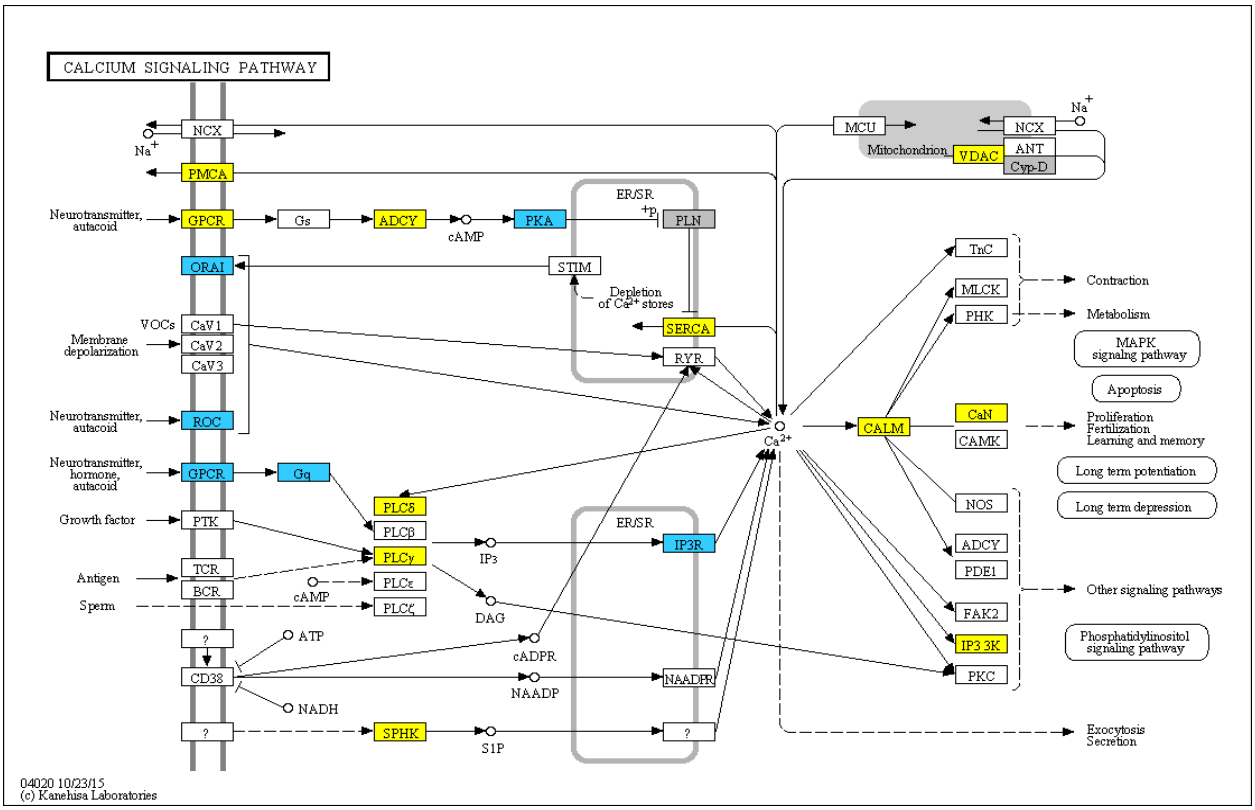
CALCIUM SIGNALING PATHWAY
NCX
PMCA
Neurotransmitter, autacoid
GPCR
Gs
ADCY
cAMP
PKA
ER/SR
PLN
ORAI
STIM
Depletion of Ca2+ stores
VOCs
CaV1
CaV2
CaV3
Membrane depolarization
SERCA
RYR
Neurotransmitter, autacoid
ROC
Neurotransmitter, hormone, autacoid
GPCR
Gq
Growth factor
PTK
PLCβ
PLCγ
PLCε
PLCζ
IP3
DAG
ER/SR
IP3R
Antigen
TCR
BCR
Sperm
cAMP
ATP
cADPR
CD38
NADH
NAADP
NAADPR
SPHK
S1P
MCU
Mitochondrion
VDAC
NCX
ANT
Cyp-D
CALM
TnC
MLCK
PHK
CaN
CAMK
NOS
ADCY
PDE1
FAK2
IP3 3K
PKC
Contraction
Metabolism
MAPK signaling pathway
Apoptosis
Proliferation
Fertilization
Learning and memory
Long term potentiation
Long term depression
Other signaling pathways
Phosphatidylinositol signaling pathway
Exocytosis
Secretion
04020 10/23/15
(c) Kanehisa Laboratories

Figure 2.8 Relative changes in transcript abundance of genes in Ca^{2+} signaling pathways after induced pancreatitis in mice.

Schematic linking the various genes that regulate cytosolic Ca^{2+} (based on GO analysis) into a series of interconnected pathways. Genes in yellow show significantly increased expression during CIP while genes in blue are significantly decreased during CIP.

Table 2.1 Expression of Ca^{2+} regulating genes 4 hours after inducing CIP

Gene	log2 (fold change)	Effect on cytosolic Ca^{2+}	Reference[a]
Itpkc	6.25	Remove	Li et al. (2013)
Sphk1	5.01	---	
Ncs1	4.03	Remove	Nakamura et al. (2011)
Cacnb2	2.68	Add	Breitenkamp et al. (2014)
Trpc1	2.57	Add	Willoughby et al. (2014)
Micu3	1.91	Remove	Plovanich et al. (2013)
Atp2a2	1.69	Remove	Ringpfeil et al., (2001)
Calm2	1.67	---	
Atp2b1	1.38	Remove	Strehler and Treiman (2004)
Atp2a3	1.23	Remove	Bobe et al. (2004)
Adora2b	1.02	---	
Calm1	0.99	---	
Plcg2	0.95	Add	Sreb et al. (1985)
Adcy4	0.90	---	
Adcy9	0.83	---	
Ppp3r1	0.78	Remove	Guerini (1997)
Plcd1	0.77	Add	Jaken and Yuspa (1988); Punnonen et al. (1993)
Chrm3	0.75	Add	Wess et al (2007)
Cherp	0.70	Add	Laplante et al. (2000)
Vdac3	0.68	Remove	Huang et al. (2013)
Orai2	-0.66	Add	Mercer et al. (2006)
Mcu	-0.73	Remove	Patron et al. (2013)
P2rx1	-0.84	Add	North et al. (2002)
Orai3	-1.01	Add	Mercer et al. (2006)
Itpr2	-1.08	Add	Yamamoto-Hino et al. (1994)
Itpka	-1.09	---	
Prkaca	-1.17	---	
Ptger3	-1.36	Add	Morimoto et al. (2014)
Atp2c2	-2.19	?	
Grpr	-2.20	Add	Xiao et al. (2003)
Gna14	-2.89	Add	Hubbard and Hepler (2006)
Chrm1	-3.03	Add	Wess et al. (2007)
Cckar	-4.22	Add	Pandol et al. (1985)

[a]Effect on cytosolic Ca^{2+} was denoted based on function reported in literature

2.3.4. SPCA2C over-expression in HEK293A cells increases cytosolic Ca^{2+} levels.

To test the theory that SPCA2C increases cytosolic Ca^{2+} levels, HEK293A cells were transfected with GFP +/- plasmids encoding a full length MYC-tagged SPCA2 ($SPCA2^{MYC}$), or a FLAG-tagged C-terminal truncated protein that completely mimicked the coding region SPCA2C (*pcDNA3.1-SPCA2C*^{FLAG}). Examination of protein localized by co-IF analysis for $SPCA2C^{FLAG}$ and $SPCA2^{MYC}$ showed overlapping localization of the two proteins (Figure 2.9). However, there were also regions of unique accumulation, indicating different cellular localizations of the full length and SPCA2C isoforms. HEK293A cells expressing $SPCA2C^{FLAG}$ showed a significant increase in resting cytosolic Ca^{2+} relative to GFP or $SPCA2^{MYC}$-expressing cells using Fura2 ratiometric analysis (Figure 2.10A, B). In addition, expression of $SPCA2C^{FLAG}$ resulted in greater increases in cytosolic Ca^{2+} following carbachol stimulation (Figure 2.10A, C) while $SPCA2^{MYC}$ showed only a trend towards significance. These results suggest that SPCA2C elevated basal cytosolic Ca^{2+} levels, opposite to the functional role of other Ca^{2+}ATPases.

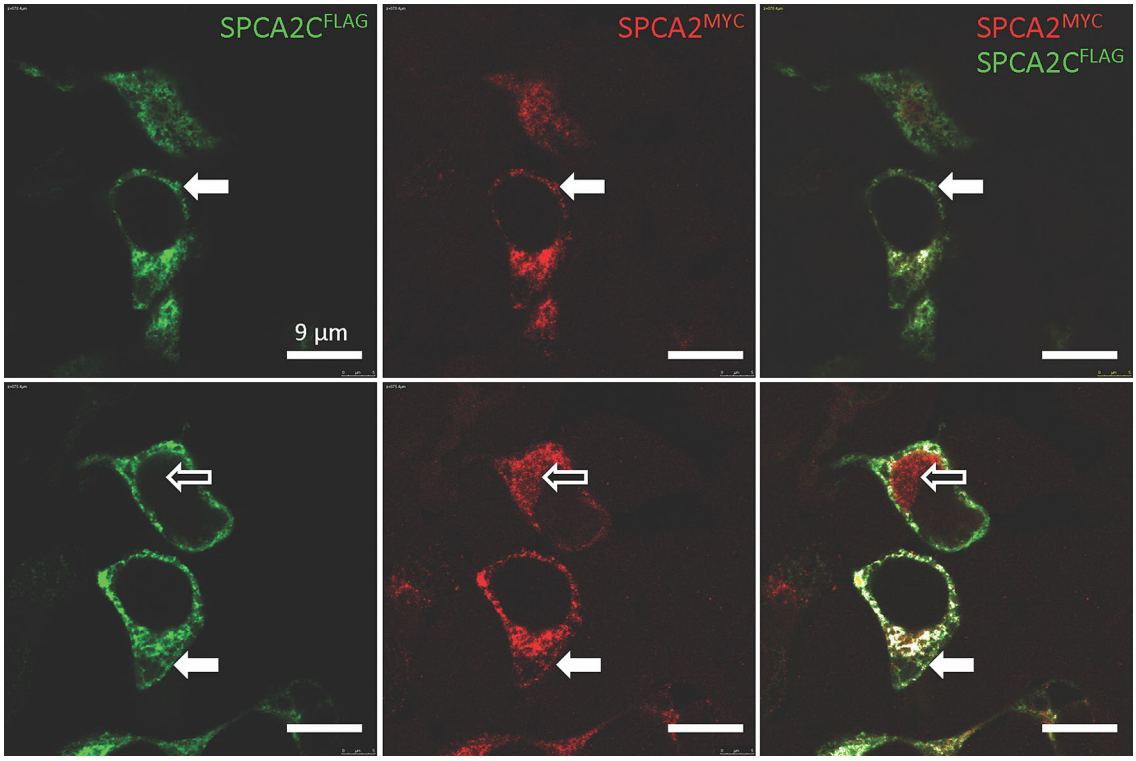
SPCA2C^FLAG
9 µm
SPCA2^MYC
SPCA2^MYC
SPCA2C^FLAG

Figure 2.9 Intracellular protein accumulation of SPCA2^{MYC} and SPCA2C^{FLAG}.

Co-localization of SPCA2C^{FLAG} and SPCA2^{MYC} following transfection of HEK293A cells shows cellular regions that express either SPCA2C^{FLAG} (green; closed arrow) or SPCA2^{MYC} (red; open arrow), or both (white). Top row images represent optical Z-axis slices that are separated by 3 μm from bottom row images. Magnification bar = 9 μm.

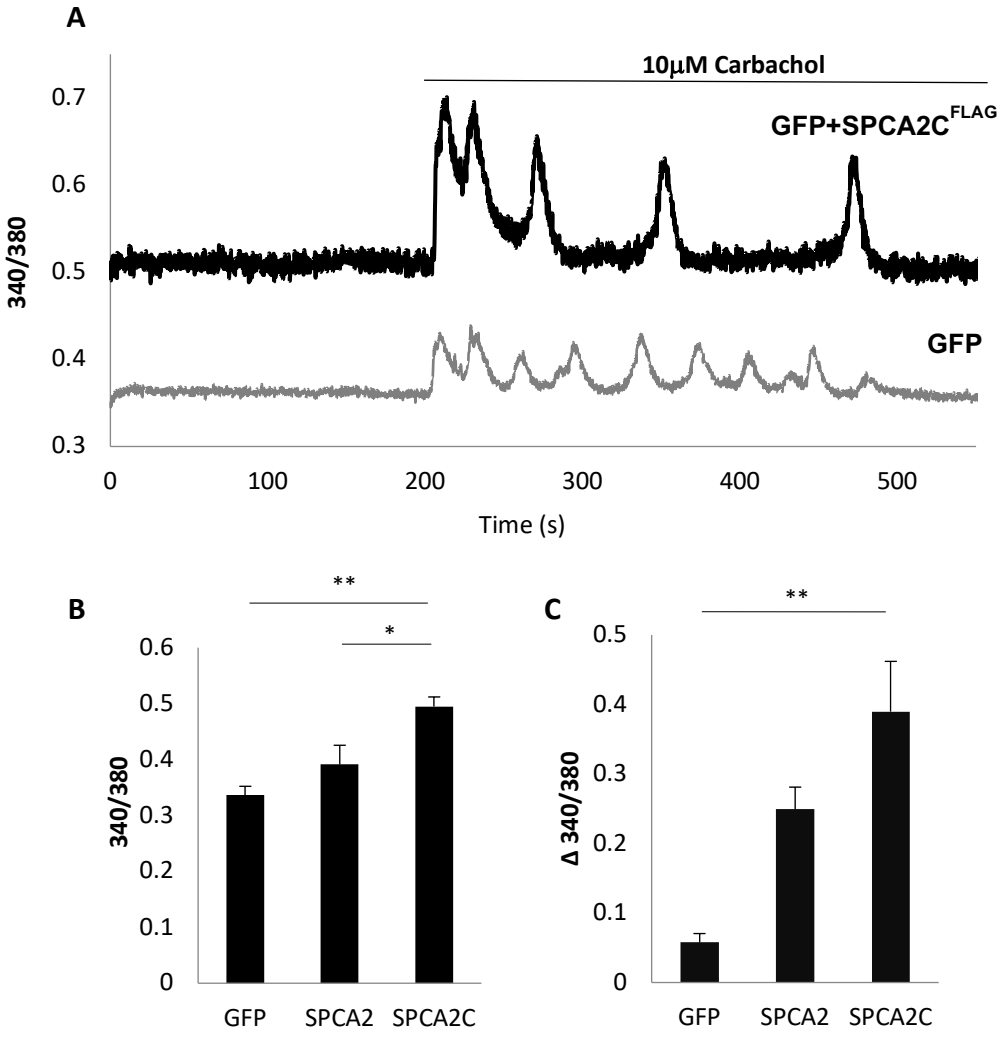
A
10μM Carbachol
GFP+SPCA2C^FLAG
GFP
340/380
0.7
0.6
0.5
0.4
0.3
0
100
200
300
400
500
Time (s)
B
**
*
340/380
0.6
0.5
0.4
0.3
0.2
0.1
0
GFP
SPCA2
SPCA2C
C
**
Δ 340/380
0.5
0.4
0.3
0.2
0.1
0
GFP
SPCA2
SPCA2C

Figure 2.10 SPCA2C exhibits a unique Ca^{2+} signaling function.

(A) Ratiometric Fura2 fluorescence analysis of single cell responses following transfection of GFP or GFP +/- $SPCA2C^{FLAG}$. Lines indicate the duration of 10 μM carbachol stimulation. (**B**) Measurement of resting cytosolic Ca^{2+} levels (before stimulation) in cells expressing GFP (n=34) or GFP+$SPCA2C^{FLAG}$ (n=22), or GFP+$SPCA2^{MYC}$ (n=12) or (**C**) the maximal response to carbachol stimulation show increased cytosolic Ca^{2+} levels and release only in cells transfected with $SPCA2C^{FLAG}$ (n=12) compared to GFP (n=16) and GFP+$SPCA2^{MYC}$ (n=3). Cells transfected with the full length SPCA2 show a trend towards increased maximal Ca^{2+} release. Values expressed as mean +/- SEM; *p<0.05, **<p0.001.

2.4 Discussion

The importance of Ca^{2+} as a second messenger for pancreatic acinar exocytosis and cell function is well established. Ca^{2+} ATPases, including those of the PMCA and SERCA families, have key roles in acinar cell biology (Lee et al., 1997; Prasad et al., 2004). We have previously shown that SPCA2 is expressed to high levels in the pancreas (Garside et al., 2010), but little is known about its function in this tissue. In this study, I show that the novel pancreatic isoform of SPCA2 (SPCA2C) is transcribed from a novel TSS within the *Atp2c2* gene that generates a transcript that includes only the last four exons of the full length *Atp2c2* gene. The SPCA2C protein sequence aligns with the carboxy terminus of SPCA2.

Importantly, SPCA2C shows decreased expression during CIP, and is part of a larger molecular response by the acinar cell to possibly reduce basal and stimulated cytosolic Ca^{2+} levels following acute pancreatic injury. Most of the *Atp2* genes encode several isoforms of Ca^{2+} ATPase proteins, giving rise to extensive cell-specific expression patterns for these genes. In most cases, these isoforms are the result of alternative splicing. In the case of *Atp2c2c*, the alternative isoform expressed within the pancreas is the result of a TSS that exists within the 24th exon of the gene. Our previous reports of a pancreatic specific *Atp2c2c* transcript suggested a size of ~1.2kb (Garside et al., 2010), significantly larger than the 702 bp transcript identified in this study. This is likely due to the different methodologies used. RNA-seq analysis is significantly more accurate than Northern blot analysis, allowing the identification of a TSS within a few base pairs, and does not include the polyA tail that increases the size of the mature transcript. The identification of this TSS is based on high resolution RNA-seq data. We have also published on the characterization of epigenetic modifications that are known to exist specifically

at TSSs. This includes enrichment of histone markers such as H3K4Me3, H3K36Me3, and acetylated H3. Both H3K36Me3 and H3 acetylation extend along the gene corresponding to transcription (Gunderson et al., 2011; Schwartz et al., 2009), which has been observed for the *Atp2c2c* gene. The TSS has also been observed to be enriched for RNA polymerase II (C. Sullivan Thesis).

The 252 bp region upstream of the *Atp2c2c* TSS was sufficient to promote transcription. Surprisingly, this region does not promote expression *in vivo* suggesting additional promoter and enhancer regions are required to recapitulate *Atp2c2c* expression in the pancreas. Indeed lack of MIST1 prevents SPCA2C expression (Garside et al., 2010), which suggests that the sequence used for analysis of the promoter region did not include regions where MIST1 binds. While the -1181+57 *Atp2c2c* region tested includes several putative E boxes (binding sites for basic helix-loop-helix proteins such as MIST1), none of these correspond to the preferred MIST1 binding site, and analysis of the intronic region between exons 24 and 25 identified an E-box with the canonical CATAGTG (Tran et al., 2007) sequence preferentially targeted by MIST1.

Importantly, delineation of the complete transcript of the *Atp2c2c* identified an open reading frame (ORF) within the transcript that encodes a 136 amino acid protein that perfectly aligns with the carboxy terminus of the full length SPCA2, hence the designation of SPCA2C. Previous work had shown that the pancreas-specific isoform contains the C-terminus of the protein (Garside et al., 2010), but had not identified the exact sequence of the protein. Sequence alignment confirms that SPCA2C completely lacks the first five transmembrane domains, the E1-E2 hydrolase domain, a Ca^{2+} binding site, as well as other domains common to P-type

ATPases, suggesting that SPCA2C does not act as a Ca^{2+} ATPase in acinar cells. Nor is it likely to act as a competitor for the full length SPCA2 since RNA-seq data indicate non-detectable amounts of this isoform in pancreatic tissue.

In other cell types, SPCA2 affects both Ca^{2+} accumulation within the Golgi apparatus and store-independent Ca^{2+} entry (Faddy et al., 2008; Feng et al., 2010; Vanoevelen et al., 2005) and truncated versions of SPCA2 affect Orai1 function in cell lines (Cross et al., 2013), suggesting a Ca^{2+} signaling role for SPCA2C. We have now confirmed that SPCA2C has both a cell localization pattern and effect on cytosolic Ca^{2+}, that is unique from the full length SPCA2 protein. Co-localization of epitope tagged SPCA2 and SPCA2C indicates that their localization is not identical. Since RNA-seq suggests that SPCA2C is the only isoform of *Atp2c2* expressed in the pancreas (>99% of total amount), the previous documentation of endogenous SPCA2 accumulation likely indicates only SPCA2C (Garside et al., 2010). Previous studies have shown a direct interaction of SPCA2 with Orai1 channels and the ability of C-terminal regions of SPCA2 to affect SICE (Feng et al., 2010). This study also suggests a global molecular response in acinar cells to reduce cytosolic Ca^{2+} levels. Genes encoding proteins that normally increase cytosolic Ca^{2+} are decreased within four hours of inducing CIP. This includes decreases in *Atp2c2c*, which is unlike the other *Atp2* genes that either do not change expression or increase during CIP. The decreased *Atp2c2c* expression supports a function that is opposite to other Ca^{2+} ATPases and is in line with a role for SPCA2C in increasing cytosolic Ca^{2+}. As mentioned, SPCA2 interacts with Orai1-composed plasma membrane Ca^{2+} channels, promoting SICE and Ca^{2+} influx into the cytosol (Feng et al., 2010).

Importantly, the regulation of SICE by SPCA2 is mediated through the carboxy terminus of SPCA2 (Feng et al., 2010). Our findings support a role in which expression of SPCA2C increases cytosolic Ca^{2+} and Ca^{2+} release following carbachol treatment. Recent studies indicate that inhibition of Orai1 channels during pancreatitis is protective (Wen et al., 2015), and reducing expression observed of *Atp2c2c* during CIP may be protective via decreased Orai1 activation. Ultimately, a more complete analysis of SPCA2C function and how it affects SICE and GPCR-mediated Ca^{2+} release is needed to fully understand its role in pancreatic function. Targeted knockouts of *Atp2c2* have not been reported to date. However, this study suggests that targeting the full length *Atp2c2* gene will not uncover a pancreatic phenotype, since using typical gene trapping strategies will leave the truncated gene and alternate TSS intact. Therefore, our identification of the novel TSS will enable more appropriate strategies for targeting *Atp2c2*.

In conclusion, this study determines that the truncated form of *Atp2c2* is transcribed from a novel TSS within the 24th exon and produces a protein that retains the C-terminus of the full-length protein. Transcription from this TSS appears to be regulated in part by MIST1 and repressed during pancreatic injury. Future studies are required to determine how SPCA2C regulates acinar cell function and how this function relates to the response of the acinar cell during pancreatic injury.

Chapter 3

The Secretory Pathway Calcium ATPase 2C interacts with Orai1 and regulates Ca^{2+} influx through SICE and other mechanisms

The work in this Chapter was published as "The pancreas-specific form of secretory pathway calcium ATPase 2 regulates multiple pathways involved in calcium homeostasis" Fenech et al., (2019) in *BBA-Molecular Cell Biology*. Other authors contributing to this manuscript include M. Carter, P. Stathopulos and C. Pin. M. Fenech performed experiments, contributed to study design, data analysis, preparation and revision of manuscript. M. Carter contributed to IF in Figure 3.6. P. Stathopulos performed protein sequence comparison for SPCA2C in Figure 3.1A, contributed to study design, provided theoretical input and revised the manuscript. C. Pin contributed to study design, revised the manuscript and provided theoretical input.

3.1 Introduction

Cellular calcium (Ca^{2+}) is a critical second messenger required for cellular processes involved in cell function, survival and apoptosis (Kruger et al., 2000; Li et al., 2014; Zhou et al., 1996). Cytosolic Ca^{2+} levels need to be tightly regulated both temporally and spatially as constitutively high levels of cytosolic Ca^{2+} are detrimental to the cell. Therefore, several mechanisms are in place to keep sources of Ca^{2+} available yet sequester Ca^{2+} away from the cytosol, thereby allowing transient Ca^{2+} increases when required.

Proper Ca^{2+} signalling is particularly critical for regulated exocytosis in pancreatic acinar cells. At rest, Ca^{2+}ATPases, buffering proteins and Ca^{2+} channels all work to maintain low cytosolic Ca^{2+} (*i.e.* ~100 nM) relative to the endoplasmic reticulum (ER) lumen (*i.e.* ~1 mM) and

extracellular space (*i.e.* ~2mM; Finch et al., 1991; Futatsugi et al., 2005; Hurwitz, 1996; Pralong et al., 1988). Ca^{2+} exchangers are not expressed in pancreatic acinar cells to high amounts. Exocytosis occurs due to secretagogue binding to cell surface receptors, leading to activation of the inositol 1,4,5-trisphosphate (IP_3) pathway and promotion of Ca^{2+} transients in the apical pole of the cell (Bezprozvanny et al., 1991; Finch et al., 1991; Futatsugi et al., 2005; Straub et al., 2000). IP_3 receptors (IP_3R) and ryanodine receptors (RyR) on the ER facilitate Ca^{2+} efflux from the ER, while plasma membrane Ca^{2+}ATPases (PMCA) and sarco/endoplasmic reticulum Ca^{2+}ATPases (SERCA) quickly clear Ca^{2+} from the cytosol. The combination of IP_3R/RyR and ATPase activity promotes oscillatory Ca^{2+} signals critical for enzyme exocytosis (Ponnappa et al., 1981; Tepikin et al., 1992). As Ca^{2+} is steadily removed from the ER and shuttled out of the cytoplasm by PMCAs, there is a net loss of Ca^{2+} stores in the ER. The depletion of Ca^{2+} within the ER triggers store operated Ca^{2+} entry (SOCE). ER Ca^{2+} is monitored by stromal interaction molecule 1 (STIM1), which senses Ca^{2+} through an EF-hand domain that resides in the ER lumen. When ER Ca^{2+} concentrations decrease, STIM1 undergoes a conformational change involving oligomerization and translocation to ER-Plasma membrane junctions, where it activates Orai1 allowing extracellular Ca^{2+} influx into the cytosol for refilling of ER stores (Liou et al., 2005; Roos et al., 2005; Wu et al., 2006). Orai1 forms Ca^{2+} release-activated channels (CRAC) and is required for SOCE (Prakriya et al., 2006).

Orai1 also directly interacts with secretory pathway Ca^{2+}ATPase 2 (SPCA2), a member of a third family of Ca^{2+}ATPases. The SPCA2-Orai1 interaction occurs independent of ER Ca^{2+} store depletion, constitutively acting to increase cytosolic levels. This pathway has been termed store independent Ca^{2+} entry (SICE), and increased SPCA2 expression correlates with increases in cytosolic Ca^{2+} concentrations. (Feng et al., 2010) This represents a unique dual function for

SPCA proteins, as they may utilize their Ca^{2+}ATPase function to promote Ca^{2+} uptake into the Golgi apparatus or promote SICE independent of primary active transport.

My previous studies showed only a truncated form of SPCA2, termed SPCA2C, is expressed within pancreatic acinar cells (chapter 2). Assessment of the role of SPCA2C in Ca^{2+} homeostasis has been limited, but its expression pattern suggests unique functions in the pancreas. SPCA2C is transcribed from an alternative start site that includes only the last four exons of the SPCA2 coding sequence, thereby eliminating domains required for SPCA2 to function as a Ca^{2+}ATPase (Chapter 2). Acinar cells are highly sensitive to altered Ca^{2+} homeostasis. Improper Ca^{2+} signalling and regulation disrupts exocytosis and promotes cellular damage associated with pancreatitis (Li et al., 2014; Zhou et al., 1996). Inhibition of Orai1 or Ca^{2+} influx mediated by other channels decreased the severity of pancreatitis (M. S. Kim et al., 2011; Vigont et al., 2015; Wen et al., 2015), and decreased accumulation of SPCA2C is observed following initiation of secretagogue-induced pancreatitis (Chapter 2). Since SPCA2C is the only isoform expressed in the pancreas, it is important to determine its involvement in store-operated or store-independent Ca^{2+} entry, Ca^{2+} signaling and Ca^{2+} homeostasis.

The goal of this study was to determine if SPCA2C maintains the non-traditional roles exhibited by the full length SPCA2 in the context of Ca^{2+} movement. In HEK 293A cells, SPCA2C expression localized to the ER and increased ER Ca^{2+} stores and Ca^{2+} influx after ER store depletion. Using HEK293T cells with stable expression of Orai1 and HEK293A, we determined that SPCA2C interacts with Orai1 to mediate SICE. Importantly, this role in Ca^{2+} influx upon store depletion was independent of Orai1, suggesting a novel mechanism for regulating Ca^{2+} influx.

3.2 Methods

3.2.1. Protein sequence comparison

The NCBI reference codes for the *Xenopus tropicalis* (frog), *Notechis scutatus* (snake), *Mus musculus* (mouse), *Homo sapiens* (human), *Sus scrofa* (pig), *Bos taurus* (cow) and *Felis catus* (cat) amino acid sequences used in the alignment are NP 001072524.1, XP 026539825.1, NP_081198.1, NP_055676.3, XP_003126874.1, XP_002694791.2 and XP 023101802.1, respectively. The sequence alignment was performed using Clutal Omega (Sievers et al., 2011) and PSIPRED (McGuffin, Bryson, & Jones, 2000) was used for predicting structure.

3.2.2. Plasmid construction

A *pcDNA3.1-SPCA2C*^{FLAG} expression vector was generated by Gene Art (Thermo Fisher Scientific, Waltham, MA), using the mouse *Atp2c2* sequence (NCBI accession #:AC_000030.1). A FLAG antigenic tag sequence (5' GATTACAAGGATGACGACGATAAG 3') was placed in frame at the 3' end of the *Atp2c2* coding sequence. *pcDNA3.1-SPCA2C*^{mRFP} was generated by inserting PCR-amplified *Atp2c2c* into the *XhoI* and *BamHI* sites, using forward primer sequence 3' CTAGGCGGCCGCGCTCCACGGACT 5' and reverse primer sequence 3' CTAGCTCGAGCACAGCTTCC 5' in *pcDNA3.1-mRFP*. *pcDNA3-mRFP* was acquired from Addgene (Addgene plasmid # 13032; http://n2t.net/addgene:13032; RRID:Addgene_13032; Figure 3.1). All plasmid insert sequences were verified by the London Regional Genomics Facility (Western University, London, ON).

A

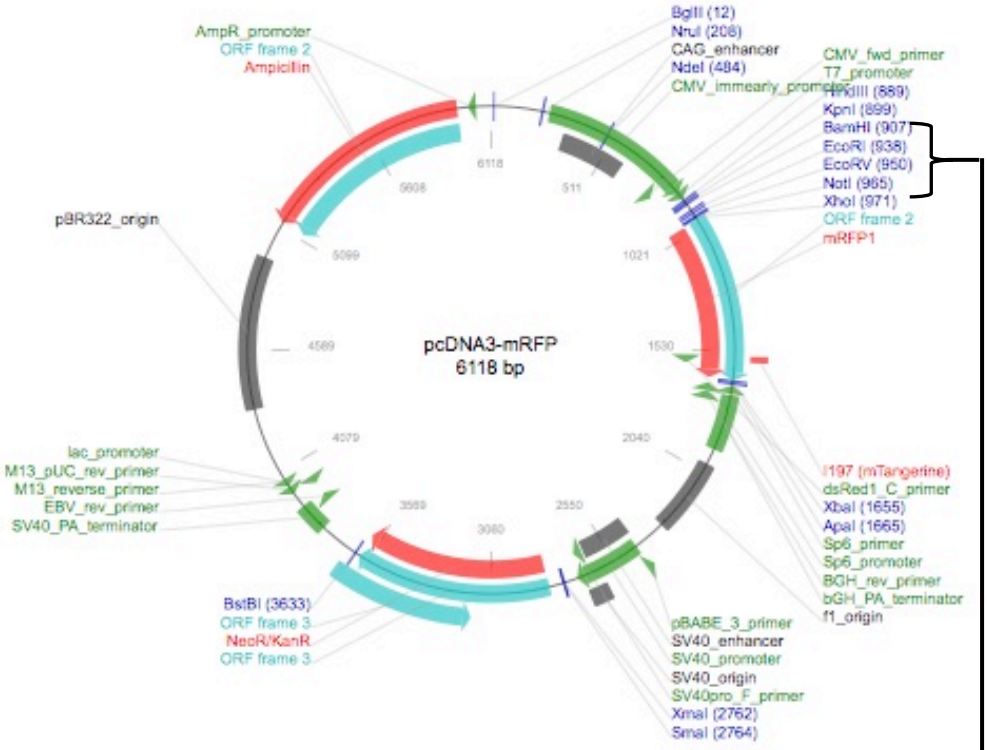

B

```
1       GGATCCGCTCCACGGAGTGTCGGGGACACGATCCTGAACAGAGCCCTGATCCTGAGGGTCCTCATGTCGGCC
         BamHI                                                          M  S  A
73      GCTGTCATCATAGGGGGGACCCTCTTTATCTTCTGGAGAGAGATCCCAGCGAACGGCACCAGCACCCCACGT
          A  V  I  I  G  G  T  L  F  I  F  W  R  E  I  P  A  N  G  T  S  T  P  R
145     ACAACCACCATGGCCTTCACCTGCTTCGTGTTTTTCGACCTCTTCAATGCCCTGAGCTGTCGCTCTCAGACC
         T  T  T  M  A  F  T  C  F  V  F  F  D  L  F  N  A  L  S  C  R  S  Q  T
217     AAGCTGATATTTGAGATTGGCTTTTTCCGGAACCGCATGTTCCTGTACTCAGTCCTTGGGTCCCTCCTGGGG
         T  T  I  F  E  I  G  F  F  R  N  R  M  F  L  Y  S  V  L  G  S  L  L  G
289     CAGCTGGCCGTGATCTATGCCCCGCCCCTACAAAAGGTCTTCCAGACTGAAAACCTGAGCGCGCTCGACCTG
         Q  L  A  V  I  Y  A  P  P  L  Q  K  V  F  Q  T  E  N  L  S  A  L  D  L
361     CTGCTGCTGACGGGCCTGGCCTCGTCTGTCTTCATTCTGTCGGAGCTGCTCAAGCTCTGGGAAAAGTTCTTG
         L  L  L  T  G  L  A  S  S  V  F  I  L  S  E  L  L  K  L  W  E  K  F  L
433     TCCAGAGCCAGGCCCACTCAGATGCTCCCGGAAGCTGTGCTCGAG ATGGCT…
         S  R  A  R  P  T  Q  M  L  P  E  A  V  XhoI  mRFP
```

Figure 3.1 Plasmid map of pcDNA3-SPCA2Cm^{RFP}.

(**A**) pcDNA3-mRFP was aquired from Addgene. (**B**) Sequence amplified by PCR to insert into *pcDNA3*. Both the plasmid and PCR product were digested with *BamHI* and *XhoI* then ligated together.

3.2.3. Cell culture

Human embryonic kidney (HEK)293A cells were maintained in Dulbecco's Modified Eagle Medium (DMEM) with 4.5 g/L D-glucose, L-Glutamine containing 10% (v/v) FBS and antibiotics (penicillin G 100U.mL, streptomycin 100 μg/mL). HEK293T cells stably expressing YFP-tagged Orai1 (HEK-Orai1^{YFP}) were a generous gift from Dr. Monica Vig (Tata Institute of Fundamental Research, India; Vig et al. 2006). HEK-Orai1^{YFP} cells were maintained in DMEM with 4.5 g/L Glucose, L-glutamine and sodium pyruvate; containing 10% (v/v) FBS and antibiotics [penicillin G 100U.mL, streptomycin 100 μg/mL, gentamicin 400 μg/mL (Wisent, St. Bruno, QC)]. When cultures reached 70-80% confluence, cells were transfected using JetPrime transfection kit (Polyplus, NY), with *pcDNA3.1-SPCA2C^{FLAG}*, *pcDNA3.1-SPCA2^{MYC}* (encodes full length SPCA2; kindly provided by R. Rao; Feng et al. 2010). or *pCMV6- Stim1^{mCherry}*, which encodes a monomeric cherry fluorescence protein fused to the N-terminus of STIM1, immediately downstream of the ER signal peptide (Luik, Wu, Buchanan, & Lewis, 2006; J. Zhu, Lu, Feng, & Stathopulos, 2018). For Nuclear factor of activated T-cells (NFAT) experiments, HEK cells were transfected, as described above, with *pcDNA-NFAT-EGFP* and *pcDNA3.1-SPCA2C^{mRFP}* or *pcDNA3.1-SPCA2^{MYC}*. Cells were incubated in transfection mixture for 24 hours before analysis. As a control, HEK293A cells transfected with *pcDNA -NFAT-EGFP* only were treated with 2 μM thapsagargin (TG) in 2 mM Ca^{2+} for 30 minutes at 37°C and 5% CO2, then fixed in 4% formalin for 10 minutes.

3.2.4. Calcium imaging

48 hours after transfection, HEK-Orai1^{YFP} +/- *pcDNA3.0-GFP* and/or *pcDNA3.1-SPCA2C^{FLAG}*, or *pcDNA3.1-SPCA2^{MYC}* cells were loaded with Fura2-AM at 1-3 μM in culture media for 30 minutes at 37°C and 5% CO_2. After loading, cells were rinsed once in Hank's Buffered Saline

Solution (HBSS) supplemented with 1.8 mM Ca^{2+} (unless otherwise stated) and allowed to equilibrate to 37°C for a minimum of 10 minutes. Fura2 emission was measured in individual cells (as described in 2.2.7). To examine the effect of SPCA2C on Ca^{2+} release in response to GPCR signaling, individual groups of cells were stimulated with 10 μM carbachol for 5 minutes at a pressure of 2 Pa by puffing. Five-minute puffing experiments were completed no more than three times per plate and never on the same group of cells. To examine SOCE and intracellular Ca^{2+} stores, cells were treated with 2 μM TG and 2 mM EGTA followed by either ionomycin (1 μM) or Ca^{2+} (2 mM, 4 mM, 6 mM) addition back to HBSS media. To examine SICE, cells were loaded with Fura2 as described above and a resting level of cytosolic Ca^{2+} achieved in 0 mM Ca^{2+} HBSS was determined. Ca^{2+} was added to the media in incremental amounts (1.0 mM or 2.0 mM Ca^{2+}) and intracellular Ca^{2+} recorded for three minutes. Ca^{2+} influx rate was calculated as:

$$R_{\Delta 340/380} = (R_{F340/380} - R_{I340/380})/60$$

where R_F is the final 340/380 ratio. R_I represents the initial 340/380 ratio and 60 is the time in seconds for recording after Ca^{2+} was added to media.

3.2.5. Protein collection, western blotting and co-immunoprecipitation

Cells were transfected as described with 5 μg of *pcDNA3.1-SPCA2C*^{FLAG} + 0 – 5 μg of *pCMV6-Stim1*^{mCherry}. Cells were harvested by trypsinization 72 hours after transfection, washed with cold phosphate buffered saline (PBS) and incubated in a mild lysis buffer (150 mM NaCl, 50 nM HEPES pH 7.4, 25 μg/ml digitonin) for 10 minutes. Samples were centrifuged at 2,000 RCF, and supernatant collected for the cytosolic protein fraction. The remaining insoluble pellet was washed with PBS, resuspended in a second lysis buffer (150 mM NaCl, 50 nM HEPES pH

7.4, 1% NP40), and incubated 40 minutes with mild agitation. Samples were centrifuged at 7,000 RCF, and the supernatant was taken as the membrane protein fraction. All antibodies, sources and dilutions are listed in Table 3.1. Western blot analysis was performed as described (Johnson et al., 2009). Briefly, 15-60 μg of protein was separated by SDS- PAGE and transferred to polyvinylidene diflouride (PVDF) membrane (BioRad, Hercules, CA). Following a 1-hour incubation in blocking solution [5% non-fat skim milk in tris-buffered saline and 0.1% Tween 20 (TBST)], membranes were incubated in primary antibodies diluted in TBS overnight at 4 °C. Following several washes with TBST, membranes were incubated in secondary antibodies diluted in TBS for 1 hour at room temperature. Protein expression was visualized using Bio-Rad Clarity Western ECL substrate on a Bio-Rad VersaDoc Imaging System (BioRad; Hercules, CA).

For co-immunoprecipitation (co-IP) experiments, 400 μg of protein from HEK293A or HEK-Orai1YFP cells transfected with *pcDNA3.1-SPCA2C*^{FLAG} +/- *pCMV6-Stim1*^{mCherry} were incubated with G-Sepharose beads (Invitrogen Dynabeads) and Orai1 antibody (Sigma, Oakville, ON) overnight at 4°C. Samples were washed 4x in second lysis buffer. IP samples were resolved by SDS-PAGE and transferred to PVDF membrane. Western blotting was performed as described above.

3.2.6. Immunofluorescence analysis

HEK293A cells were transfected as described above with *pcDNA3.1-SPCA2C*^{FLAG} and/or *pCMV6-Stim1*^{mCherry}. Forty-eight hours after transfection, HEK293A cells were fixed with 4% (v/v) formalin in PBS. IF was performed as described (section 2.2.5). All antibodies used (Table

3.1) were diluted in blocking solution (PBS, 5% (w/v) bovine serum albumin (BSA), 1% TritonX-100). Fluorescently labelled secondary goat antibodies were diluted 1:250 in PBS (Jackson Immunoresearch Labs, West Grove, PA or Sigma). Images acquired using Leica TCS SP5 II microscope. For nuclear factor of activated T-cells (NFAT) experiments, formalin-fixed cells were stained with DAPI (1:1000 in PBS) for 5 minutes and then visualized for RFP (SPCA2C) or EGFP (NFAT). IF was performed on cells transfected with *pcDNA-SPCA2*^{MYC} as above using a rabbit anti-MYC primary (1:500; SIGMA) and TRITC-conjugated anti-rabbit IgG (1:250).

3.2.7. Statistics

N values are provided within the figure legends for each experiment. Data shown are +/- standard error of the mean (SEM) and significance was determined using unpaired t-tests or two-way ANOVA and Sidak's or Tukey's posthoc test. $p<0.05$ considered statistically significant.

Table 3.1 Antibodies used in this study

Antibody	Reactivity	Dilution	Company	Methodology
STIM1	rabbit, α-mouse, rat, human	1:1000	Sigma	IF
FLAG	mouse, all	1:500	Sigma	IF, IB
Orai1	rabbit, α-human	1:1000	Sigma	IB, IP
Selenoprotein S	mouse, α-human	1:250	Santa Cruz	IF
GM130	mouse, α-human	1:250	Abcam	IF
ATP5f1	mouse α-human	1:250	Santa Cruz	IF
E-catinin	mouse, α-human	1:250	Santa Cruz	IF
RCAS	rabbit, α-mouse, human	1:250	Abcam	IF

IF, immunofluorescence; IB, immunoblotting; IP, immunoprecipitation

3.3. Results

3.3.1. SPCA2C interacts with Orai1 and increases cytosolic Ca^{2+} levels.

Since SPCA2C is the predominant isoform expressed in pancreatic acinar cells, I first investigated whether it served a similar function to the full length SPCA2. Previous work showed SPCA2 interacts with Orai1 to enhance SICE through its C- terminal domain (Feng et al., 2010), which is identical to SPCA2C. To determine if this C-terminal domain function is conserved among phylogeny, we performed *in silico* analysis comparing the C- terminal domain of SPCA2 from different species. At least 8 polar and non-polar residue positions within the 20 residue C-terminal domain, which is downstream of the final transmembrane helix, are fully or partially conserved among different species (Figure 3.2A) suggesting the function of the C-terminal domain is likely retained and important in higher and lower vertebrates. Additionally, PSIPRED (McGuffin et al., 2000) analysis indicated that this C-terminal region of SPCA2 has a propensity to form an α-helix (Figure 3.2A). It is noteworthy that intermolecular α-helix interactions between STIM1 and Orai1 underlie Orai1 channel assembly and gating in SOCE (Stathopulos et al., 2013; Yang et al., 2012).

Given our bioinformatics analysis suggesting the C-terminal domain of SPCA2 may form a structural motif conducive to activation of Orai1 channels, I assessed whether SPCA2C interacts with Orai1. To determine if SPCA2C directly interacted with Orai1, co-IP was performed on membrane-enriched protein fractions following $SPCA2C^{FLAG}$ transfection into HEK293A cells, which do not express Orai1, or HEK 293A cells stably expressing an $Orai1^{YFP}$ fusion protein (HEK-$Orai1^{YFP}$). IF indicated $SPCA2C^{FLAG}$ accumulates throughout HEK-$Orai1^{YFP}$ cells with some overlap with Orai1 (Figure 3.2B). Co-IP showed SPCA2C is readily pulled down by Orai1

IP (Figure 3.2C**)**. Remarkably, co-expression of STIM1 competed away the SPCA2C-Orai1 interaction and reduced accumulation of $SPCA2C^{FLAG}$ in the membrane only when Orai1 was present (Figure 3.2C). IF for $SPCA2C^{FLAG}$ +/- STIM1 protein supported the finding that STIM1 affected SPCA2C membrane localization. Without STIM1, SPCA2C showed co-localization with Orai1 (Figure 3.2D). However, the cellular localization of $SPCA2C^{FLAG}$ became more diffuse and did not overlap with Orai1 when $STIM1^{mCherry}$ was present. Therefore, SPCA2C appears to bind Orai1 through a similar region as STIM1.

We next examined the ability for SPCA2C to increase resting cytosolic Ca^{2+}. Epitope-tagged versions of full length SPCA2 ($SPCA2^{MYC}$) or SPCA2C ($SPCA2C^{FLAG}$) were expressed in HEK-$Orai1^{YFP}$ cells. Similar to HEK293A cells, HEK-$Orai1^{YFP}$ cells do not normally express SPCA2 or SPCA2C (data not shown). Examination of cytosolic Ca^{2+} levels, in 1.8 mM extracellular Ca^{2+}, using Fura2 ratiometric imaging showed both $SPCA2^{MYC}$ (R340/380 = 0.43 ± 0.02) and $SPCA2C^{FLAG}$ ($R_{340/380}$= 0.58 ± 0.03) significantly increased resting cytosolic Ca^{2+} concentrations in HEK-$Orai1^{YFP}$ cells compared to GFP alone ($R_{340/380}$ = 0.26 ± 0.01; Figure 3.2E). The increase in cytosolic Ca^{2+} levels in HEK-$Orai1^{YFP}$ cells was also significantly higher when comparing cells expressing $SPCA2C^{FLAG}$ to $SPCA2^{MYC}$ ($p<0.05$; Figure 3.2E), suggesting SPCA2C may affect additional pathways involved in Ca^{2+} homeostasis that SPCA2 does not.

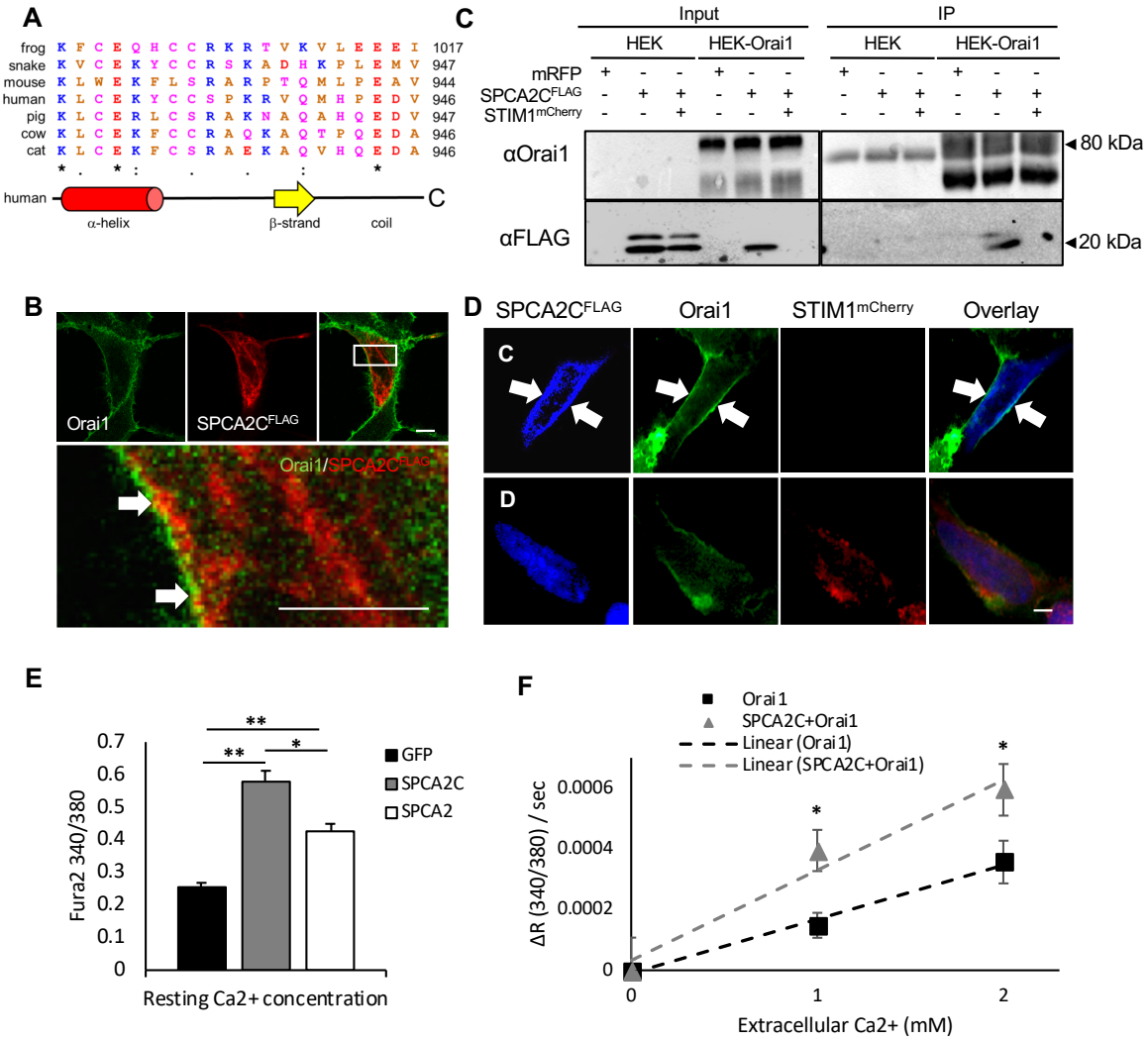
A
frog K F C E Q H C C R K R T V K V L E E E I 1017
snake K V C E K Y C C R S K A D H K P L E M V 947
mouse K L W E K F L S R A R P T Q M L P E A V 944
human K L C E K Y C C S P K R V Q M H P E D V 946
pig K L C E R L C S R A K N A Q A H Q E D V 947
cow K L C E K F C C R A Q K A Q T P Q E D A 946
cat K L C E K F C S R A E K A Q V H Q E D A 946
human
C
α-helix
β-strand
coil
C
Input
IP
HEK
HEK-Orai1
HEK
HEK-Orai1
mRFP
SPCA2C^FLAG
STIM1^mCherry
αOrai1
αFLAG
80 kDa
20 kDa
B
Orai1
SPCA2C^FLAG
Orai1/SPCA2C^FLAG
D
SPCA2C^FLAG
Orai1
STIM1^mCherry
Overlay
C
D
E
Fura2 340/380
0.7
0.6
0.5
0.4
0.3
0.2
0.1
0
**
**
*
GFP
SPCA2C
SPCA2
Resting Ca2+ concentration
F
Orai1
SPCA2C+Orai1
Linear (Orai1)
Linear (SPCA2C+Orai1)
ΔR (340/380) / sec
0.0006
0.0004
0.0002
0
*
*
0
1
2
Extracellular Ca2+ (mM)

Figure 3.2 SPCA2C interacts with Orai1 and increases cytosolic Ca^{2+} levels.

(**A**) Multiple sequence alignment of the C-terminal domain of SPCA2 from higher to lower vertebrates. Basic, acidic, non-polar and polar residues are coloured blue, red, brown and magenta, respectively. Completely (*), highly (:) and partially (.) conserved residues are indicated below the residue position. The carboxyl terminal residue number of each of the sequences is shown at right. The PSPIRE predicted secondary structure composition of the human SPCA2 C-terminal domains is indicated below the alignment. C, carboxyl terminus. **(B)** IF for $SPCA2C^{FLAG}$ following transfection of HEK-$Orai1^{YFP}$ cells shows some co-localization of $Orai1^{YFP}$ and $SPCA2C^{FLAG}$ (arrow). Scale bar = 10 μm. **(C)** Co-IP for Orai1 in HEK293A or HEK-$Orai1^{YFP}$ cells expressing mRFP or $SPCA2C^{FLAG}$ +/- $STIM1^{mCherry}$. Western blot for Orai1 or $SPCA2C^{FLAG}$ (predicted weight 17 kDa) in membrane-enriched fractions (left panels) or following IP for Orai1 (right panels). Black arrow indicates $Orai1^{YFP}$ (predicted weight 59kDa); other bands reflect IgG. **(D)** IF for $SPCA2C^{FLAG}$ in HEK-$Orai1^{YFP}$ cells +/- $STIM1^{mCherry}$. Arrows indicate co-localization of $Orai1^{YFP}$ and $SPCA2C^{FLAG}$. Scale bar = 10 μm. **(E)** Resting cytosolic Ca^{2+} levels recorded in HEK-$Orai1^{YFP}$ cells expressing GFP only (n=12), $SPCA2^{MYC}$ (n=15) or $SPCA2C^{FLAG}$ (n=13). Cytosolic Ca^{2+} measurements were made using Fura2. Values expressed as mean +/- SEM; *$p<0.05$; **$p<0.01$. **(F)** Rates of Ca^{2+} influx in HEK293A cells expressing $Orai1^{YFP}$ (n = 22 [0 mM]), 22 [1.0 mM], and 29 [2.0 mM]) or Orai1+SPCA2 (n = 26 [0 mM Ca^{2+}], 22 [1.0 mM], and 32 [2.0 mM]).

3.3.2. SPCA2C interacts with Orai1 to increase SICE

To determine if SPCA2C's ability to increase cytosolic Ca^{2+} was due to an increased rate of Ca^{2+} influx across the plasma membrane through SICE, GFP was expressed +/- $SPCA2C^{FLAG}$ in HEK-$Orai1^{YFP}$ cells and incubated in nominally Ca^{2+}-free media followed by addition of Ca^{2+} back to the media. Incremental addition of Ca^{2+} to the media resulted in a significant increase in the rate of Ca^{2+} influx in $SPCA2C^{FLAG}$-expressing cells compared to GFP-only expressing cells. At 1 mM Ca^{2+}, $SPCA2C^{FLAG}$-expressing cells showed a 2.7-fold increase in Ca^{2+} influx ($\Delta R_{(340/380)}$/sec = $3.95x10^{-4}\pm 6.79x10^{-5}$) vs. GFP-expressing cells ($\Delta R_{(340/380)}$/sec = $1.48x10^{-4} \pm 4.11x10^{-5}$). At 2 mM extracellular Ca^{2+}, Ca^{2+} influx was still almost 2-fold higher in SPCA2C ($\Delta R_{(340/380)}$/sec = $5.95x10^{-4} \pm 8.5x10^{-5}$) vs. GFP-expressing cells ($\Delta R_{(340/380)}$/sec = $3.57x10^{-4} \pm 7.03x10^{-5}$; Figure 3.2F). These results suggest that SPCA2C enhances Ca^{2+} uptake into the cell through SICE.

3.3.3. SPCA2C localizes to the ER in HEK293A cells

IF showed $SPCA2C^{FLAG}$ is not only co-localized with $Orai1^{YFP}$ but also has an extensive pattern of expression throughout the cell. We previously showed SPCA2C has a different subcellular expression pattern than full length SPCA2 (Garside et al., 2010) suggesting diverse roles for SPCA2C in affecting Ca^{2+} homeostasis. To determine the subcellular localization of SPCA2C, HEK293A cells were transfected with *pcDNA3-*$SPCA2C^{mRFP}$ and IF performed for organelle-specific markers (Figure 3.3). I chose to determine SPCA2C cellular localization in HEK293A cells since the Orai1YFP limited fluorochrome analysis. Co-localization of $SPCA2C^{mRFP}$ with markers for the ER (Figure 3.3A; Selenoprotein S) and Golgi (Figure 3.3B; GM130) was readily observed. More than 75% of cells expressing $SPCA2C^{mRFP}$ showed partial, if not complete,

overlap with ER localized markers, while 50% of the cells showed complete or partial Golgi marker co-localization, indicating the expression pattern was not simply due to over-expression. Quantitative co-localization analysis was not reliable as IF images showed SPCA2C^{mRFP} localization is not limited specifically to the ER or Golgi. Conversely, limited localization of SPCA2C^{mRFP} was observed at the plasma membrane (Figure 3.3C**;** E-catenin).

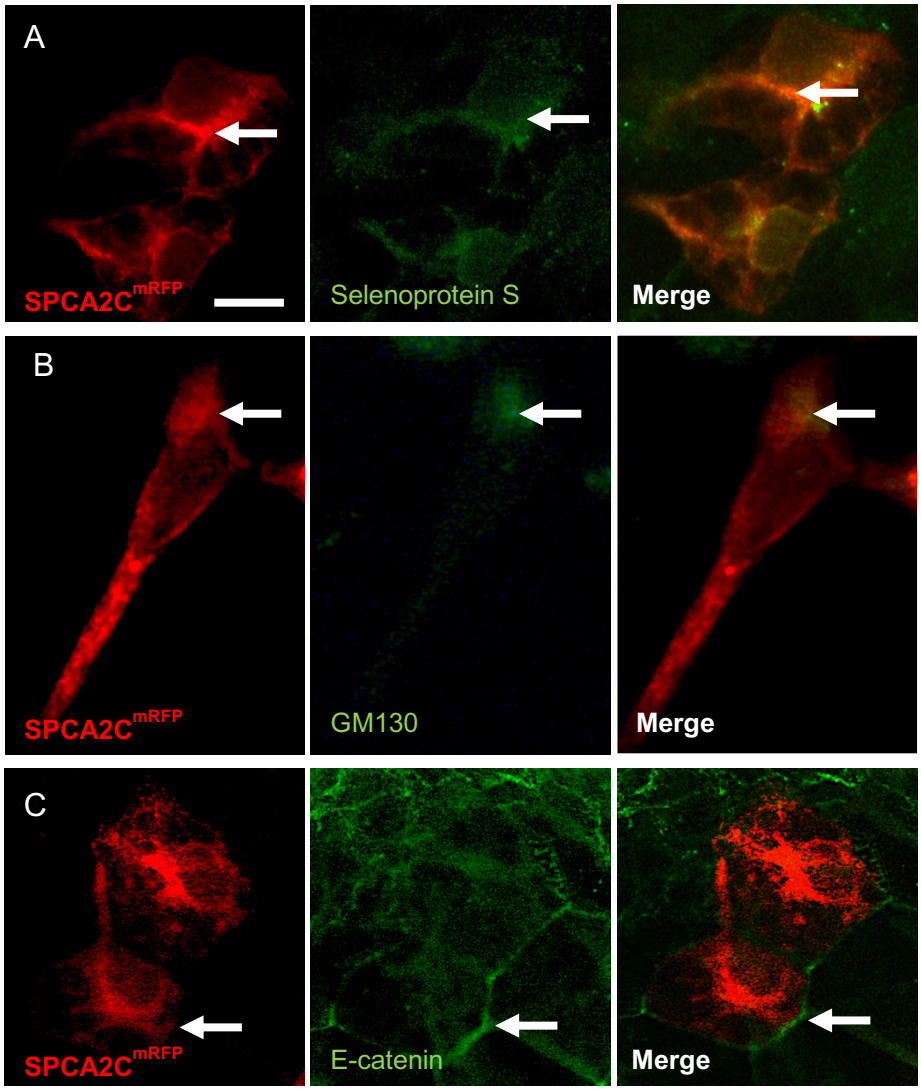
A
SPCA2C^mRFP
Selenoprotein S
Merge
B
SPCA2C^mRFP
GM130
Merge
C
SPCA2C^mRFP
E-catenin
Merge

Figure 3.3 SPCA2C protein localized to the endoplasmic reticulum and Golgi.

Co-localization of SPCA2C^{mRFP} (SPCA2C^{mRFP}; red) with Selenoprotein S (row **A**; green), GM130 (row **B**; green), or E-Catenin (row **C**; green). Arrows indicate areas of co-localization. Scale bar = 10 μm.

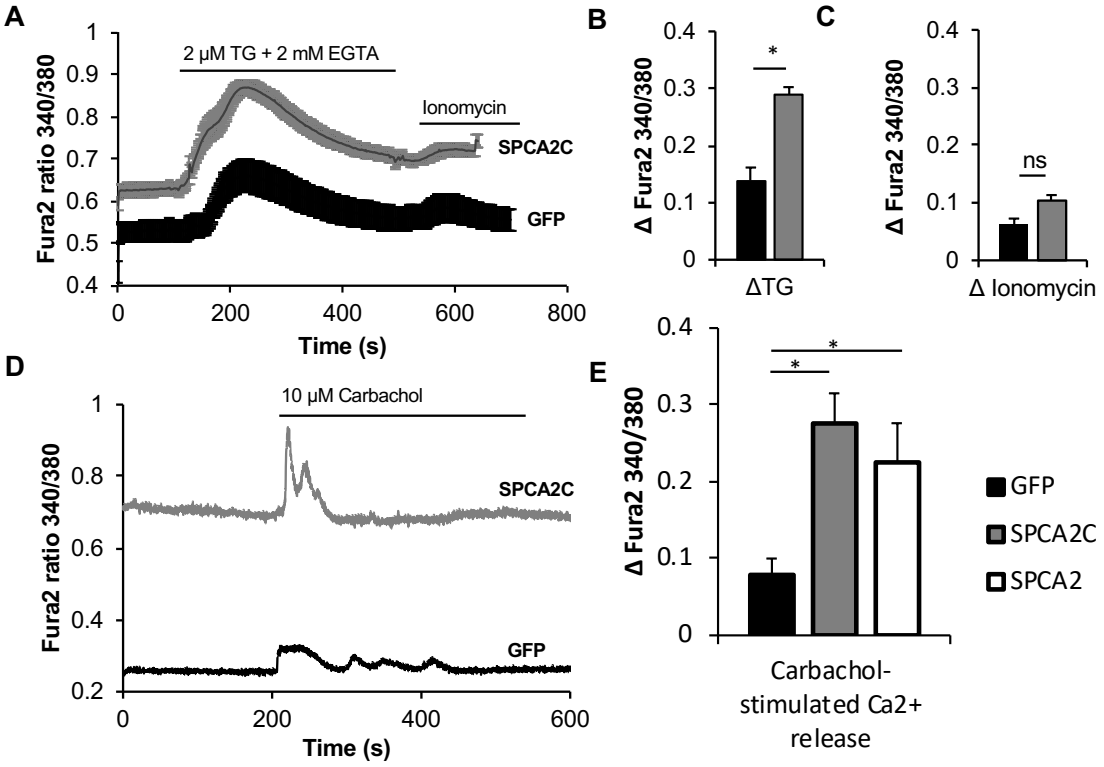
A
2 µM TG + 2 mM EGTA
Ionomycin
SPCA2C
GFP
Fura2 ratio 340/380
Time (s)
B
Δ Fura2 340/380
ΔTG
C
ns
Δ Ionomycin
D
10 µM Carbachol
SPCA2C
GFP
Fura2 ratio 340/380
Time (s)
E
Δ Fura2 340/380
Carbachol-stimulated Ca2+ release
GFP
SPCA2C
SPCA2

Figure 3.4 SPCA2C increases ER Ca^{2+} stores in HEK-Orai1^{YFP} cells.

(A) Ratiometric Fura2 analysis showing the response to TG or ionomycin treatment in HEK-Orai1^{YFP} cells expressing GFP (n=22) or GFP+SPCA2C^{FLAG} (n=23). Maximal change in cytosolic Ca^{2+} based on Fura2 340/380 ratio in response to **(B)** TG or **(C)** ionomycin (1 μm). Values expressed as mean +/- SEM; *P<0.05. **(D)** Ratiometric Fura2 traces showing response to carbachol stimulation in HEK293A cells expressing GFP (n=8) or GFP+SPCA2C^{FLAG} (n=8). **(E)** Maximal change in cytosolic Ca^{2+} based on Fura2 340/380 ratio in response to carbachol in HEK293A cells expressing GFP (n=8) or GFP+SPCA2C^{FLAG} (n=8), or GFP+SPCA2^{MYC} (n=6). Values expressed as mean +/- SEM; *p<0.05.

3.3.4. SPCA2C increases ER Ca^{2+} stores

The localization of SPCA2C to the ER suggests it affects Ca^{2+} stores and Ca^{2+} release from this organelle. To examine ER Ca^{2+}, HEK-Orai1^{YFP} cells expressing GFP +/- SPCA2C were incubated in 1.8 mM extracellular Ca^{2+} then treated with TG, which inhibits SERCA pumps, thereby promoting emptying of ER-associated Ca^{2+} stores (Sagara & Inesi, 1991). ER Ca^{2+} levels were assessed by monitoring the transient increase in cytosol Ca^{2+} after TG treatment using Fura2, as done previously (Feng et al., 2010; He et al., 1997). Cells expressing SPCA2C^{FLAG} showed a significant increase in cytosolic Ca^{2+} following TG treatment relative to GFP-expressing cells ($\Delta R_{340/380}$ = 0.289 ± 0.013 vs. 0.139 ± 0.016; $p<0.05$, Figure 3.4A, B) suggesting SPCA2C increased Ca^{2+} levels in the ER. Subsequent treatment with ionomycin to empty all other Ca^{2+} stores showed no significant differences in cytosolic Ca^{2+} between GFP or SPCA2C^{FLAG}-transfected cells ($\Delta R_{340/380}$ = 0.063 ± 0.001 and 0.103 ± 0.001, respectively; Figure 3.4A, C) indicating increased Ca^{2+} levels following SPCA2C expression were specific to the ER.

TG has been reported to also inhibit the full length SPCA2 (Yamamoto et al., 2016), so it is possible the increases in cytosolic Ca^{2+} upon TG treatment are the result of combined ER and Golgi emptying of Ca^{2+}. Therefore, ER Ca^{2+} stores were further tested by treating cells with carbachol, an acetylcholine receptor agonist that induces ER store-specific Ca^{2+} release through IP_3-mediated IP_3R activation. Cells were incubated in 1.8 mM extracellular Ca^{2+}, then treated with carbachol. In both SPCA2C^{FLAG} and GFP expressing HEK-Orai1^{YFP} cells, peak release of Ca^{2+} occurred rapidly upon carbachol stimulation (Figure 3.4D). However, significantly more Ca^{2+} was released in response to carbachol in SPCA2C^{FLAG}-expressing cells compared to GFP expressing HEK-Orai1^{YFP} cells ($\Delta R_{340/380}$= 0.276 ± 0.04 vs. 0.080 ± 0.02, Figure 3.4D, E). HEK-

Orai1^{YFP} cells expressing full length SPCA2^{MYC} also showed a significantly greater release of Ca^{2+} in response to carbachol relative to GFP-expressing cells ($\Delta R_{340/380}$= 0.226 ± 0.05 vs. 0.080 ± 0.02, Figure 3.4E).

3.3.5. SPCA2C increases Ca^{2+} influx across the plasma membrane after ER store emptying

While increased ER Ca^{2+} levels in cells expressing SPCA2C^{FLAG} could be due to enhanced Ca^{2+} uptake from the cytosol, SPCA2C does not contain the domains required for Ca^{2+}ATPase activity capable of moving Ca^{2+} against the steep concentration gradient. Since SPCA2C localized to the ER, interacted with Orai1 and promoted increased ER Ca^{2+} stores, SPCA2C's effect on SOCE was examined. If SPCA2 is involved in SOCE, increased Ca^{2+} uptake and re-localization to interact with Orai1 should be observed upon Ca^{2+} store depletion. Using Fura2 ratiometric imaging, cytosolic Ca^{2+} influx was measured in HEK-Orai1^{YFP} cells expressing GFP +/- SPCA2C^{FLAG} during incremental add back of Ca^{2+} following store depletion with TG and EGTA. HEK-Orai1^{YFP} cells expressing SPCA2C showed significantly greater Ca^{2+} influx following addition of Ca^{2+} back to the media, compared to GFP-only expressing ($\Delta_{R340/380}$ at 6 mM Ca^{2+}= 0.08 ± 0.005 vs. 0.03 ± 0.005; $p<0.05$, Figure 3.5A, B), indicating that SPCA2C influences Ca^{2+} influx rates after store depletion. Similar experiments with HEK-Orai1^{YFP} cells expressing SPCA2C^{FLAG} + STIM1^{mCherry} resulted in significantly greater resting levels of cytosolic Ca^{2+} at rest compared to STIM1^{mCherry}-only expressing cells ($R_{340/380}$= 0.803 ± 0.027 vs. 0.683 ± 0.017; $p<0.0001$, Figure 3.5C, D). However, no further increase in ER Ca^{2+} release or SOCE occurred when STIM1^{mCherry} and SPCA2C^{FLAG} were co-expressed ($\Delta R_{340/380}$ at 6 mM Ca^{2+}= 0.24 ± 0.03 and 0.24 ± 0.02; respectively, Figure 3.5D). Next, we examined the localization of SPCA2C in response ER Ca^{2+} store depletion. As observed previously, some co-

localization between SPCA2C^{FLAG} and Orai1^{YFP} was readily observed under resting Ca^{2+} levels (Figure 3.2A). Upon TG treatment and concomitant chelation of extracellular Ca^{2+} using EGTA, no increase in SPCA2C^{FLAG}-Orai1^{YFP} co-localization occurred (Figure 3.6B). Conversely, HEK-Orai1^{YFP} cells expressing STIM1^{mCherry} showed prominent Orai1-STIM1 puncta upon TG treatment, consistent with SOCE (Figure 3.6C, D). When STIM1^{mCherry} and SPCA2C^{FLAG} were co-expressed in HEK-Orai1^{YFP} cells and treated with TG, STIM1^{mCherry} and Orai1^{YFP} again formed distinct foci that were largely devoid of SPAC2C^{FLAG} accumulation (Figure 3.6E, F). These results suggest the ability of SPCA2C to increase ER Ca^{2+} and affect the response to ER store depletion may be independent of Orai1. Indeed, we previously showed SPCA2C increased cytosolic Ca^{2+} in HEK293A cells, which did not show detectable Orai1 expression (Chapter 2).

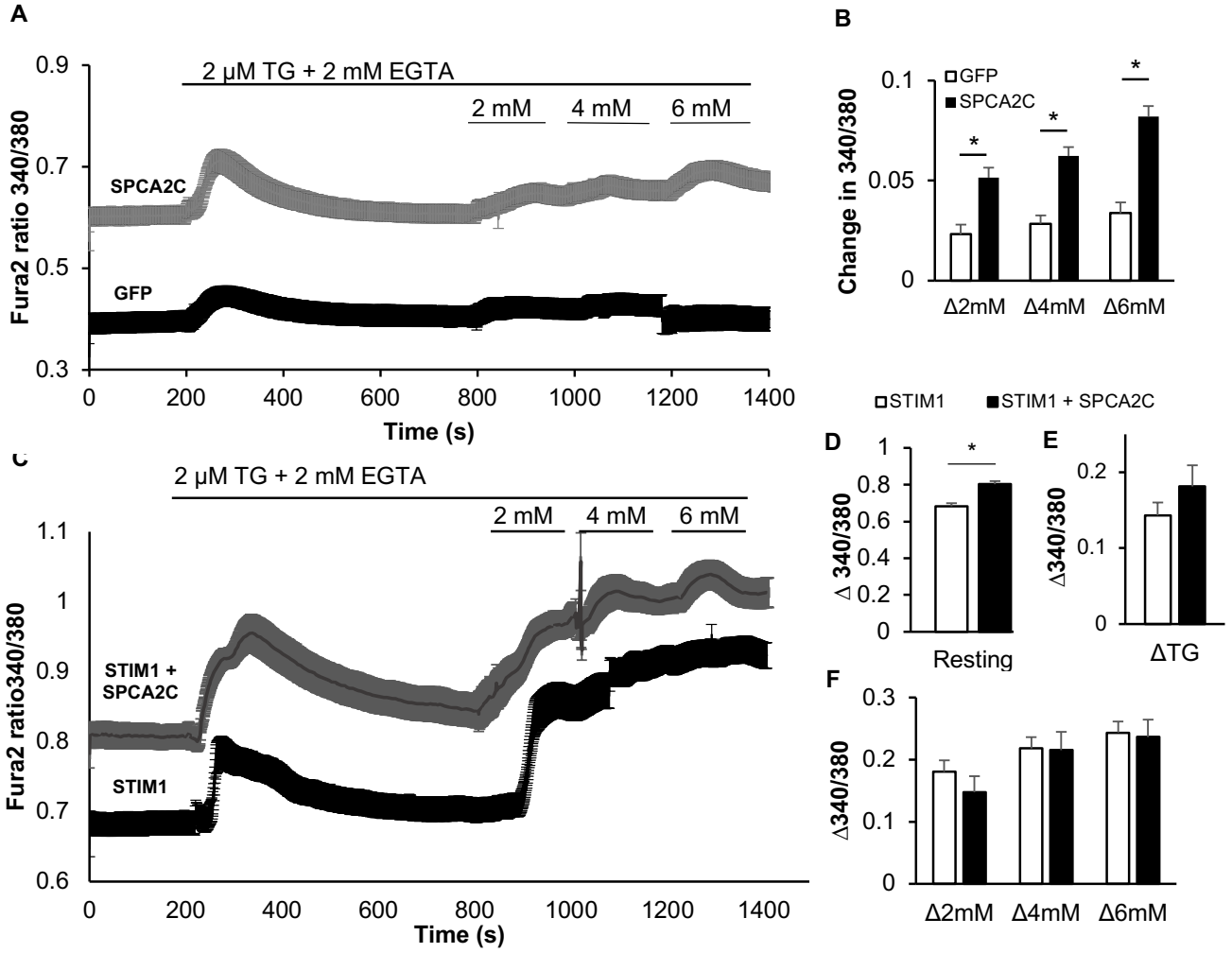
A
2 μM TG + 2 mM EGTA
2 mM
4 mM
6 mM
SPCA2C
GFP
Fura2 ratio 340/380
Time (s)
B
GFP
SPCA2C
Change in 340/380
Δ2mM
Δ4mM
Δ6mM
C
2 μM TG + 2 mM EGTA
2 mM
4 mM
6 mM
STIM1 +
SPCA2C
STIM1
Fura2 ratio340/380
Time (s)
STIM1
STIM1 + SPCA2C
D
Δ 340/380
Resting
E
Δ340/380
ΔTG
F
Δ340/380
Δ2mM
Δ4mM
Δ6mM

Figure 3.5 SPCA2C increases cytosolic Ca^{2+} after store depletion.

(A) Ratiometric Fura2 traces showing response to TG followed by increasing extracellular Ca^{2+} to the media in HEK-Orai1^{YFP} expressing GFP +/- SPCA2C^{FLAG}, or **(C)** STIM1^{mCherry}/GFP +/- SPCA2C^{FLAG}. **(B)** Maximal changes in cytosolic Ca^{2+} following Ca^{2+} addback quantified for SPCA2C^{FLAG}+GFP (n=33) or GFP alone (n=28). **(C)** Ratiometric Fura2 traces showing response to TG and Ca^{2+} addback in HEK-Orai1^{YFP} expressing STIM1^{mCherry}/GFP +/-SPCA2C^{FLAG}. **(D)** Quantification of resting Ca^{2+} levels, response to TG, and maximal change in cytosolic Ca^{2+} following Ca^{2+} addition quantified for SPCA2C^{FLAG}+STIM1^{mCherry}+GFP (n=25) or STIM1^{mCherry}+GFP (n=33)**.** Values expressed as mean +/- SEM; *p<0.0001.

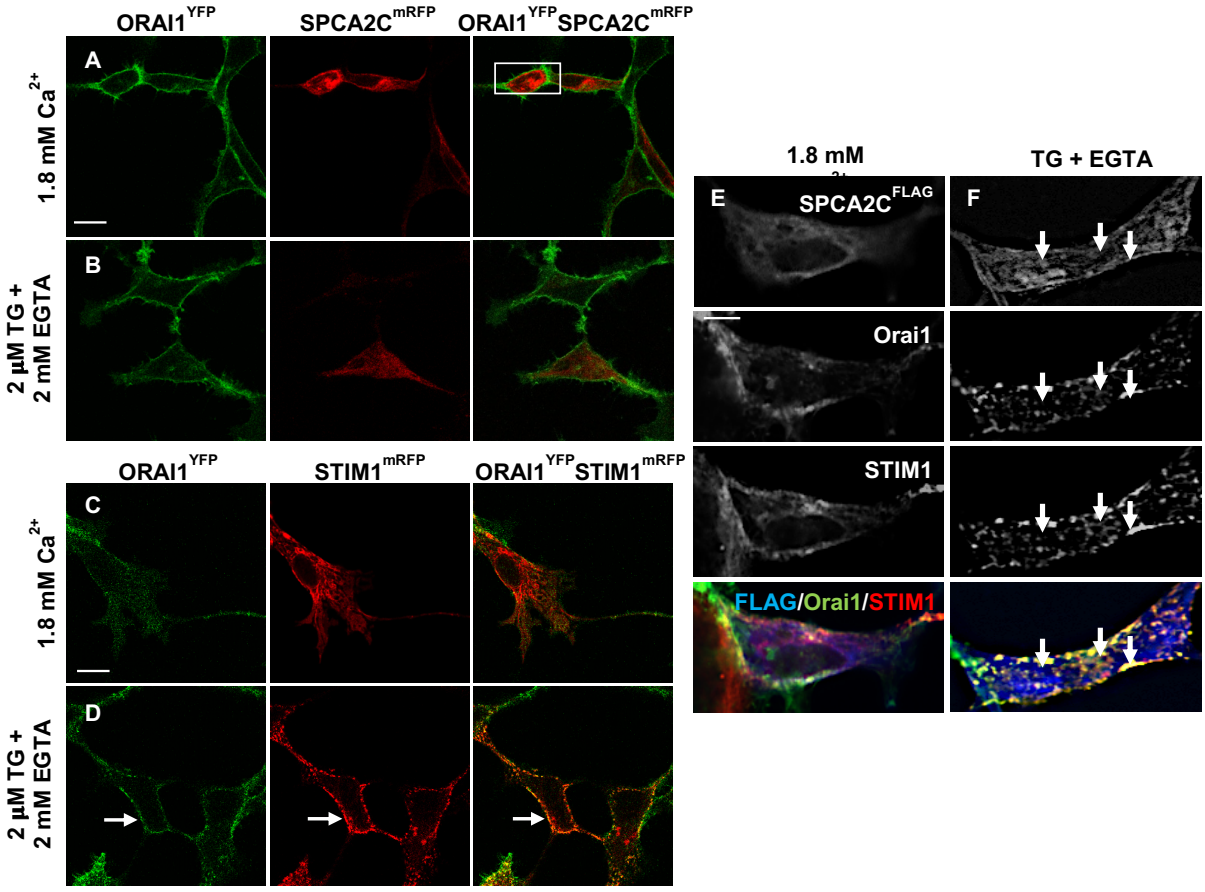
ORAI1YFP
SPCA2CmRFP
ORAI1YFPSPCA2CmRFP
A
1.8 mM Ca2+
B
2 µM TG +
2 mM EGTA
ORAI1YFP
STIM1mRFP
ORAI1YFPSTIM1mRFP
C
1.8 mM Ca2+
D
2 µM TG +
2 mM EGTA
1.8 mM
TG + EGTA
E
SPCA2CFLAG
Orai1
STIM1
FLAG/Orai1/STIM1
F

Figure 3.6 SPCA2C localization in HEK-Orai1YFP cells does not change when ER stores are depleted.

Fluorescent localization of **(A, B)** SPCA2C^{RFP} or **(C, D)** STIM1^{mCherry} in HEK-Orai1^{YFP} cells under **(A, C)** physiological Ca^{2+} conditions (1.8 mM Ca^{2+}) or **(B, D)** following thapsigargin (TG) treatment. STIM1^{mCherry} protein forms puncta co-localizing with Orai1^{YFP} (white arrow) following emptying of ER stores by treatment with 2 μM TG. Scale bar = 2.5 μm. Co-IF for STIM1^{mCherry} and SPCA2C^{FLAG} **(E)** under physiological Ca^{2+} conditions (1.8 mM Ca^{2+}) or **(F)** following TG treatment in HEK-Orai1^{YFP} (green) cells expressing SPCA2C^{FLAG} (blue) and STIM1^{mCherry} (red). Scale bar = 2.5 μm.

3.3.6. SPCA2C can increase Ca^{2+} influx after store depletion independent of Orai1

To determine if Orai1 is required for increased Ca^{2+} influx under resting condition or following ER Ca^{2+} store depletion, HEK293A cells were transfected with $SPCA2C^{FLAG}$ (Figure 3.7). Fura2 imaging was used to assess Ca^{2+} uptake with the addition of extracellular Ca^{2+} independent of ER Ca^{2+} store depletion (i.e. SICE). HEK293A cells expressing $SPCA2C^{FLAG}$ showed no significant increases in Ca^{2+} influx rate with the addition of extracellular Ca^{2+} (Figure 3.7A) suggesting the ability of SPCA2C to enhance SICE is dependent on the presence of Orai1. However, as observed in HEK-$Orai1^{YFP}$ cells, Ca^{2+} release from ER stores after treatment with TG and EGTA was significantly higher in HEK293A cells expressing $SPCA2C^{FLAG}$ compared to cells expressing GFP only ($\Delta R_{340/380}$= 0.133 ± 0.018 vs. 0.036 ± 0.009; $p<0.0001$, Figure 3.7B, C), and treatment with ionomycin showed no difference in Ca^{2+} release from other organelles (Figure 3.7D). Upon addition of Ca^{2+} back to the media after store depletion by TG and EGTA, Fura2 measurements showed HEK293A cells expressing $SPCA2C^{FLAG}$ had significantly increased Ca^{2+} influx ($\Delta R_{340/380}$ at 6 mM= 0.070 ± 0.005 vs. 0.029 ± 0.002; $p<0.001$, Figure 3.7C, E), indicating SPCA2C increased Ca^{2+} influx across the plasma membrane, after store depletion, even in the absence of Orai1.

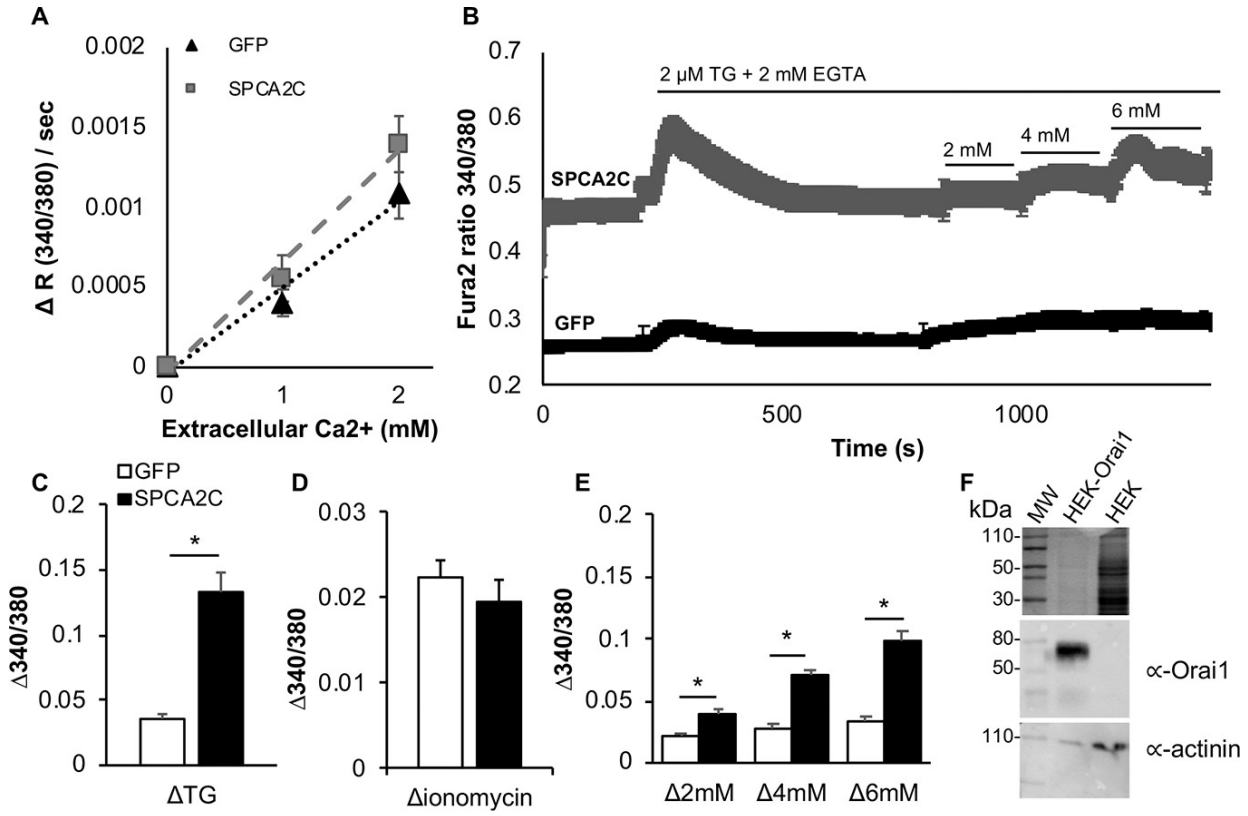
A
GFP
SPCA2C
Δ R (340/380) / sec
Extracellular Ca2+ (mM)
B
2 μM TG + 2 mM EGTA
2 mM
4 mM
6 mM
SPCA2C
GFP
Fura2 ratio 340/380
Time (s)
C
GFP
SPCA2C
Δ340/380
ΔTG
D
Δ340/380
Δionomycin
E
Δ340/380
Δ2mM
Δ4mM
Δ6mM
F
kDa
MW
HEK-Orai1
HEK
∝-Orai1
∝-actinin

Figure 3.7 SPCA2C increases Ca^{2+} entry during rest and after store depletion in the absence of Orai1.

(**A**) Rate of Ca^{2+} influx in cells exposed to increasing extracellular Ca^{2+} (GFP: n = 29 [0 mM], 25 [1.0 mM], 34 [2.0 mM]; GFP+SPCA2: n = 29 [0 mM], 33 [1.0 mM], 30 [2.0 mM]). **(B)** Ratiometric Fura2 traces showing representative trace in response to TG and Ca^{2+} addback in HEK 293 cells expressing GFP +/- SPCA2C. Maximal response to **(C)** TG, **(D)** ionomycin (1 μM), or **(E)** increasing Ca^{2+}**. (F)** Western blot showing no Orai1 expression in HEK293A cells. HEK293A cells expressing $Orai1^{YFP}$ have been included as a positive control, and western blotting for α-actinin provided as a loading control. Significantly more protein has been loaded for HEK293A cells to ensure no Orai1 expression is observed. Values expressed as mean +/- SEM; *P<0.0001.

3.3.7. SPCA2C does not increase nuclear translocation of NFAT

This data suggests that SPCA2C functions to increase cytosolic Ca^{2+}. Previous studies indicated the ability of full length SPCA2 to increase cytosolic Ca^{2+} leads to increased NFAT localization (Feng et al., 2010). To determine if the elevation of cytosolic Ca^{2+} signaling upon SPCA2C expression promotes a similar nuclear localization of NFAT, we co-transfected $SPCA2C^{mRFP}$ and EGFP-NFAT into HEK293A cells and examined NFAT localization (Figure 3.8). On its own, NFAT localizes to the cytoplasm (Figure 3.8A). As a control, we treated EGFP-NFAT expressing cells with TG, which resulted in almost complete NFAT translocation (Figure 3.8B). Interestingly, expression of $SPCA2C^{mRFP}$ did not enhance NFAT localization (Figure 3.8C), suggesting the increased in cytosolic Ca^{2+} levels were not high enough to stimulate translocation under the conditions tested. We performed similar experiments with a full length SPCA2 ($SPCA2C^{MYC}$; Figure 3.8D). While nuclear localization was increased (Figure 3.8E), translocation was often incomplete, maintaining partial EGFP-NFAT accumulation in the cytosol.

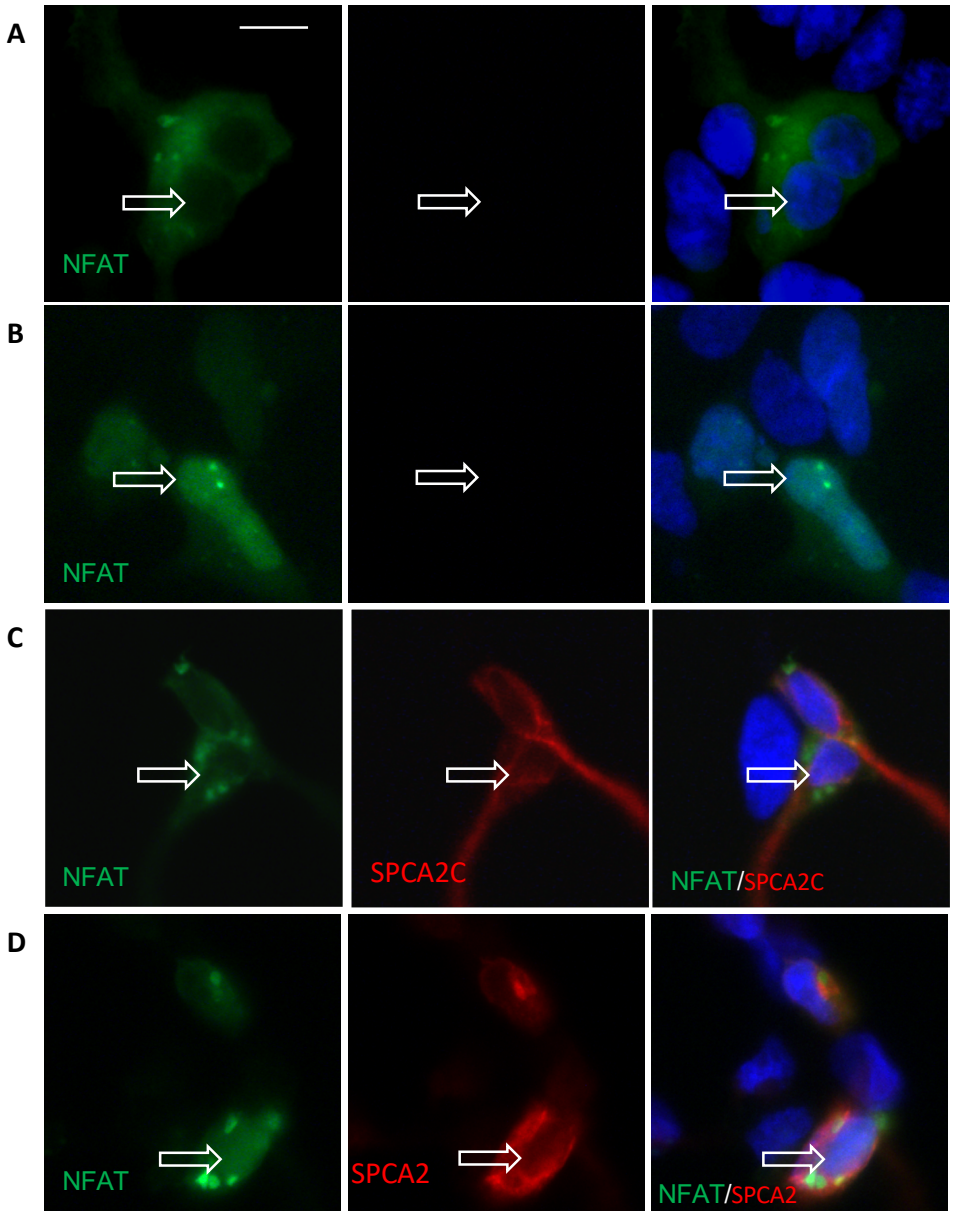
A
NFAT
B
NFAT
C
NFAT
SPCA2C
NFAT/SPCA2C
D
NFAT
SPCA2
NFAT/SPCA2

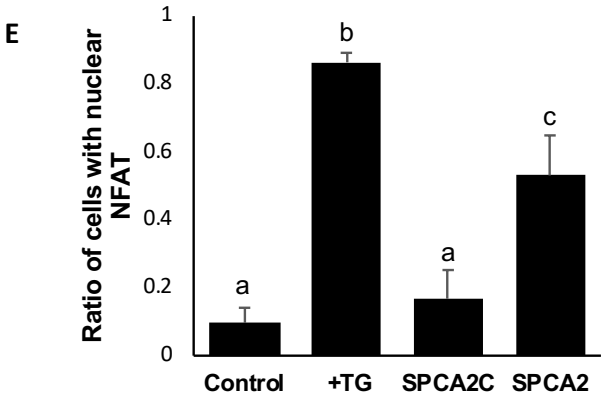
E
Ratio of cells with nuclear NFAT
1
0.8
0.6
0.4
0.2
0
a
b
a
c
Control
+TG
SPCA2C
SPCA2

Figure 3.8 SPCA2C expression does not enhance NFAT-EGFP nuclear localization in HEK293A cells.

SPCA2C^{mRFP} (n=89; **C**) or SPCA2^{MYC} (n=112; **D**) and localization assessed by fluorescent microscopy. As a positive control. NFAT-EGFP only-expressing cells were treated with TG (n=112; **B**). Arrows indicate individual nuclei of transfected cells. (**E**) Quantification of the percent of transfected cells that showed NFAT nuclear localization. Numbers in brackets indicate the total number of cells counted over three experiments. Letters indicate statistically different values. Magnification bars = 10 μm.

3.4 Discussion

Regulation of Ca^{2+} homeostasis is crucial for proper cell function, requiring several pathways to rapidly move Ca^{2+} into and out of the cytosol. One family of proteins involved in Ca^{2+} homeostasis is the secretory pathway Ca^{2+}ATPases, which consists of SPCA1 and SPCA2. Both SPCA proteins have been linked to Ca^{2+} homeostasis pathways not requiring ATPase function (Cross et al., 2013; Feng et al., 2010; Smaardijk et al., 2018). In this study, we characterized the function of SPCA2C, the only isoform of SPCA2 expressed in pancreatic acinar cells. SPCA2C contains the last four transmembrane domains of the full-length SPCA2 protein but lacks most of the domains required for Ca^{2+}ATPase activity. Our results indicated forced expression of $SPCA2C^{FLAG}$ increased Ca^{2+} influx in HEK293A cells through a store-independent mechanism dependent on Orai1, similar to full length SPCA2. However, $SPCA2C^{FLAG}$ also increased resting cytosolic Ca^{2+} concentrations, elevated Ca^{2+} levels in the ER, and promoted increased store-mediated Ca^{2+} influx, all independent of Orai1. These results suggest SPCA2C affects multiple pathways regulating cytosolic Ca^{2+} and does so through known and unknown mechanisms.

$SPCA2C^{FLAG}$ readily interacts with $Orai1^{YFP}$ when expressed in HEK-$Orai1^{YFP}$ cells. This is consistent with previous findings that showed only the C-terminal of SPCA2, which is maintained in SPCA2C, was required for Orai1 interaction (Feng et al., 2010). The previous study also indicated that only C- terminal portions of SPCA2 elicited increased Ca^{2+} influx, (Feng et al., 2010) confirming interactions between Orai1 and the C-terminal part of SPCA2 are functionally relevant on their own. Indeed, our results showed SPCA2C enhanced Orai1's ability to promote SICE. Unlike SPCA2, which localizes predominantly to the Golgi, we showed SPCA2C has a different localization pattern, accumulating also in the ER. This is consistent with

studies that examined localization of C terminal truncations of SPCA2 that showed a broad subcellular localization compared to full length SPCA2 (Smaardijk et al., 2017), and is also similar to the localization we previously documented in pancreatic acinar cells (Garside et al., 2010). This difference in localization patterns between SPCA2 and SPCA2C may account for the ability of SPCA2C to promote increased cytosolic Ca^{2+} levels relative to the full-length SPCA2 levels. We suggest full length SPCA2 would normally have limited interaction with Orai1 due to a lack of co-localization, and, therefore, different SPCA2 isoforms may be required for the different physiological roles related to Orai1and other Ca^{2+} influx channels. By localizing to the main Ca^{2+} storage department within the cell, SPCA2C has an increased opportunity to interact and effect Ca^{2+} levels throughout the cell.

The differential expression pattern may also account for differences in cell type-specific requirements for SICE. SPCA2C is the only SPCA2 isoform expressed to appreciable levels in acinar cells. The expression of SPCA2C and ability to interact with Orai1 may indicate a greater physiological role for SICE in maintaining Ca^{2+} at appropriate levels, where ER Ca^{2+} stores are essential for enzyme exocytosis. Linking SPCA2C specifically to acinar cell physiology may also explain differences observed in NFAT localization following expression of SPCA2 or SPCA2C. While our analysis of SPCA2 did not result in complete NFAT nuclear localization, some was observed in the majority of cells. Conversely, SPCA2C did not increase NFAT nuclear localization even though cytosolic Ca^{2+} levels were increased. Previous studies suggested that breast cancer cell line phenotypes are a pathological consequence of over-expressing SPCA2 and the resultant increase in NFAT translocation (Feng et al., 2010). We are currently examining whether alterations in SPCA2C expression can affect acinar cell biology.

Despite its ability to interact with Orai1, SPCA2C's contribution to Orai1 function appears to be limited to SICE. Expressing SPCA2C increased cytosolic and ER Ca^{2+}, and increased influx of Ca^{2+} following ER-store depletion regardless of Orai1 expression. Previous studies examining the ability of full length SPCA2 (Feng et al., 2010; Smaardijk et al., 2018) and SPCA1 (Smaardijk et al., 2018) to increase Ca^{2+} influx, indicated this occurred solely through SICE and specifically increased Golgi, but not ER Ca^{2+} stores (Smaardijk et al., 2018, 2017). SPCA2 expression did not affect ER stores, (Feng et al., 2010) while over-expression of SPCA1 promoted Golgi swelling and stress (Smaardijk et al., 2018, 2017). These results suggest that at least SPCA1 may have a pathophysiological role in SICE. Given SPCA2C's expression pattern in the pancreas, and its decreased expression following induction of injury (chapter 2), we suggest that SPCA2C, unlike SPCA1, has a unique physiological role in SICE.

It is tempting to suggest Orai1 interactions with SPCA2C and STIM1 reflect a switch from a normal physiological role to a stress-induced response. Co-expression of $STIM1^{mCherry}$ and $SPCA2C^{FLAG}$ in HEK-$Orai1^{YFP}$ cells eliminated Orai1-SPCA2C interaction and disrupted the cellular localization of $SPCA2C^{FLAG}$. Therefore, it appears STIM1 and SPCA2C bind to similar molecular regions on Orai1. The α-helical secondary structure predicted for the C-terminal domain of SPCA2C is similar to the predominant secondary structure adopted by STIM1. Thus, SPCA2C binding with Orai1 may be mediated by intermolecular helix interactions as characterized for STIM1 and Orai1. This apparent competition is consistent with previous findings that complexes containing Orai1 and SPAC2 do not contain STIM1. (Feng et al., 2010) Also, we did not observe a change in STIM1-Orai1-mediated SOCE or localization when

SPCA2C^{FLAG} was expressed. However, SPCA2C^{FLAG} localization was affected by the presence of STIM1^{mCherry}, suggesting an interaction with Orai1 helps localize SPCA2C to the membrane. In confirmation of a role for Orai1 in SPCA2C localization, knock down of *Orai1* in SCp2 cells restricted SPCA2 localization to perinuclear region, with, less puncta near the membrane (Cross et al., 2013). In addition, while SPCA2C promotes increases in Ca^{2+} uptake following store depletion, these increases are modest, and emptying of ER stores did not result in increased co-localization of Orai1^{YFP} and SPCA2C^{FLAG}. The re-localization of SPCA2C^{FLAG} upon STIM1^{mCherry} expression does not appear to be strictly to the Golgi. Indeed, SPCA2C^{FLAG} localization occurs throughout the cytoplasm and analysis of cytosolic fractions revealed a decrease in overall SPCA2C^{FLAG} accumulation (data not shown) suggesting it is being degraded.

Surprisingly, membrane localization of SPCA2C^{FLAG} was not disrupted by STIM1^{mCherry} in the absence of Orai1^{YFP}. Therefore, while Orai1 interactions may be required for membrane localization of SPCA2C, this requirement is only necessary when Orai1 is stably expressed. This seeming conundrum may be due to altered expression of proteins involved in Ca^{2+} influx when Orai1^{YFP} is stably expressed. We and others have shown that HEK-Orai1^{YFP} cells have reduced cytosolic Ca^{2+} compared to parental HEK293A cells, which may be due to reduced expression of other channels that promote Ca^{2+} uptake. Therefore, STIM1 does not compete with proteins required for SPCA2C membrane localization in the absence of Orai1.

While we could not detect Orai1 protein in HEK293A cells, we cannot rule out potential interactions with other Orai proteins. To my knowledge, no studies have examined endogenous Orai2 or Orai3 protein function in HEK293A cells. However, cell-specific differences in the

types of Ca^{2+} channels activated by ER Ca^{2+} store depletion have been documented (Hong et al., 2011; Kim et al., 2011; Vigont et al., 2015), and these different channels may interact with SPCA2C. For example, transient receptor potential cation 1/3/6 (TRPC1/3/6) channels heavily influence SOCE. (Hong et al., 2011; Kim et al., 2011; Vigont et al., 2015) Increased Ca^{2+} levels are associated with the initiation of pancreatitis and altering intracellular Ca^{2+} in the context of pancreatitis affects the progression and severity of acinar cell injury. Targeted deletion of the *Trpc3* gene (Kim et al. 2011) or blocking Orai1 with a specific inhibitor (Wen et al., 2015) significantly decreased SOCE in acinar cells and decreased the severity of experimental pancreatitis in mice. Currently, clinical trials are underway using an Orai1 inhibitor in the treatment of pancreatitis. We showed a significant decrease in SPCA2C expression within four hours of inducing experimental pancreatitis in mice suggesting SPCA2C function is perturbed in response to injury. In addition, we have observed a complete loss of SPCA2C in *Mist1*$^{-/-}$ mice, which have altered Ca^{2+} homeostasis, reduced exocytosis function, and an increased susceptibility to pancreatic disease.

In conclusion, this is the first evidence that SPCA2C affects multiple, non-ATPase related pathways that control Ca^{2+} homeostasis. Given SPCA2C is the predominant isoform expressed in pancreatic acinar cells, our work suggests that it plays an important physiological role in regulating Ca^{2+} within these cells. Whether decreased expression during injury is protective by reducing the potential for increased Ca^{2+} influx, or damaging, is unknown. Altering expression of SPCA2C in pancreatic acinar cells, as well as during experimentally induced pancreatitis, is currently being explored.

Chapter 4

The role of SPCA2C in calcium homeostasis in pancreatic biology and pathology

The work in this chapter has yet to be submitted for publication but some experiments were carried out by Mckenzie Carter, including western blot analysis on HA tagged SPCA1C-BioID, streptavidin, and Orai1 in BioID experiments (Figure 4.9), under the supervision of M.Fenech. RNA-seq analysis of patient-specific pancreatic tumor xenografts was performed by Dr. Nicholas Fraunhoffer (Figure 4.1B). The rest of the experimental work in this chapter was performed by M. Fenech.

4.1 Introduction

The previous two chapters identified the relevance of SPCA2C to basic biological processes using HEK293A cells and asked whether it regulates Ca^{2+} signalling pathways affected by the full length SPCA2. These findings suggest SPCA2C contributes to pathways both related and unrelated to those known to involve SPCA2. Therefore, the goal of this chapter was to gain a wider perspective of SPCA2C function. Two approaches were taken to assess SPCA2C in the context of Ca^{2+} homeostasis: i) assess SPCA2C function following over-expression in pancreatic cell lines and ii) define the SPCA2C interactome.

The role of SPCA2C in Ca^{2+} homeostasis of pancreatic physiology was examined in 266.6 cells. 266.6 cells resemble a partially differentiated pancreatic acinar cell phenotype, derived from

mice. They express several digestive enzymes and respond to carbachol stimulation (Mareninova et al., 2006; Ornitz et al., 1985). 266.6 cells were chosen over AR42J cells, another pancreatic cell line derived from rat tissue, since it is difficult to exogenously express transfected genes in AR42J cells through standard transfection protocols. Alternatively, SPCA2C was examined in cell lines derived from patient-specific pancreatic tumor xenografts (PDTX). Each cell line was derived from patient resected tumors. These cells provide a small sample of pancreatic cancers that can be used to study i) if SPCA2C expression differs among cancer-derived samples, and ii) if Ca^{2+} homeostasis differs according to the expression levels of SPCA2C. In both 266.6 and PDTX lines, SPCA2C's effect on Ca^{2+} homeostasis was determined through over-expressing SPCA2C.

Since the results of Chapters 2 and 3 suggested SPCA2C regulates Ca^{2+} through more than just interacting with Orai1, an unbiased screen was performed in HEK-Orai1^{YFP} cells to identify putative interacting partners of SPCA2C. A proximity-dependent biotin identification (BioID) with SPCA2C was used to identify candidate proteins that closely associate with SCPA2C in HEK-Orai1^{YFP} cells. BioID involves generating a BirA fusion protein that mediates biotinylation of primary amines on proximate (*i.e.* within ~10-50 nm) proteins when incubated with biotin (Appendix 1.1). Therefore, expression of SPCA2C-BioID in the presence of biotin for 15-24 hours will generate a "history" of candidate protein-protein interactions. Biotinylated proteins can then be isolated and identified by mass spectrometry (Roux et al., 2013). Compared to other approaches, such as affinity capture or coimmunoprecipitation, BioID allows the capture of transient protein interactions and identifies candidate proteins that interact indirectly (i.e. through a complex) with SPCA2C. The BioID approach uses extremely tight biotin-streptavidin

interactions, which avoids the difficulties associated with directly detecting weak and more transient interactions. BioID has been successfully used to identify novel interactors for a variety of proteins (Abbasi & Schild-Poulter, 2019; Kim & Roux, 2016; Roux et al., 2012; Varnaite & MacNeill, 2016). In this study, BioID was able to identify 263 candidate proteins as SPCA2C interactors.

4.2 Methods

4.2.1 Plasmid construction

The *MCS-SPCA2C-BioID-HA* expression vector was generated by inserting PCR-amplified *Atp2c2c* coding sequence into the *NheI* and *BamHI* sites, using forward primer sequence *5′ CTAGGCTAGCGACGATCCTGAACAGA 3′* and reverse primer sequence *5′ AGTCGAGGATCCCTCCACGGAGTC 3′* into the BioID vector back bone (MCS-BioID2-HA), which was acquired from Addgene (Addgene plasmid # 74224; http://n2t.net/addgene:74224; RRID:Addgene_74224; Figure 4.1). The plasmid sequence was verified using the London Regional Genomics Facility (Western University, London, ON).

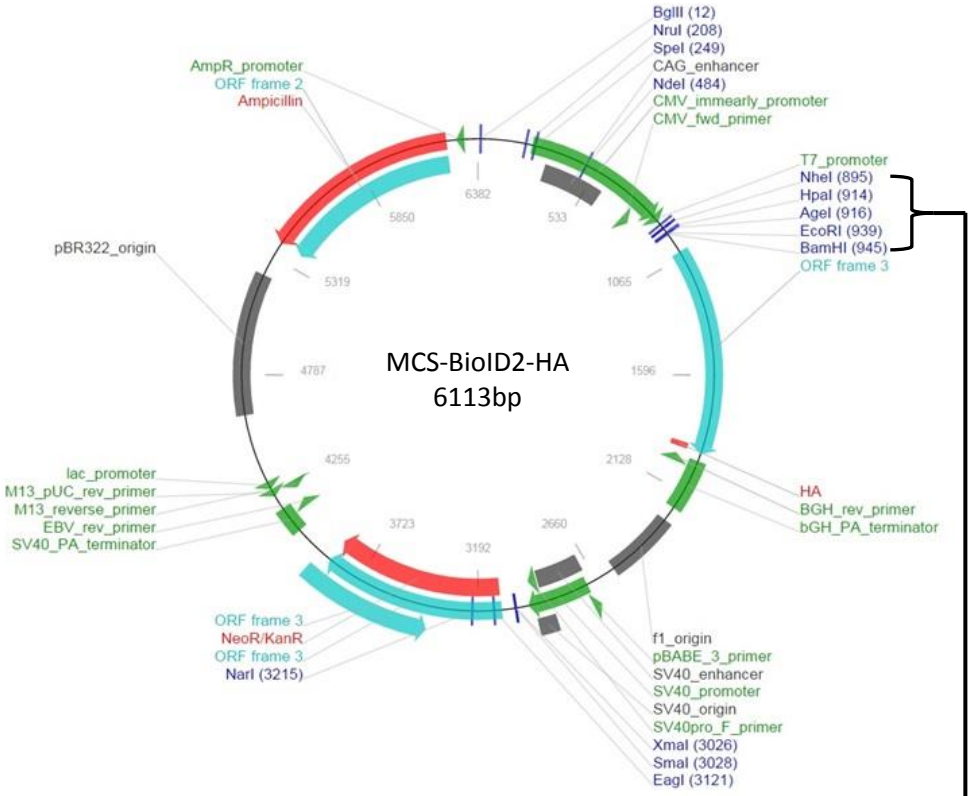


```
1       GCTAGCGCTCCACGGAGTGTCGGGGACACGATCCTGAACAGAGCCCTGATCCTGAGGGTCCTCATGTCGGCC
         NheI                                                          M  S  A
73      GCTGTCATCATAGGGGGGACCCTCTTTATCTTCTGGAGAGAGATCCCAGCGAACGGCACCAGCACCCCACGT
          A  V  I  I  G  G  T  L  F  I  F  W  R  E  I  P  A  N  G  T  S  T  P  R
145     ACAACCACCATGGCCTTCACCTGCTTCGTGTTTTTCGACCTCTTCAATGCCCTGAGCTGTCGCTCTCAGACC
         T  T  T  M  A  F  T  C  F  V  F  F  D  L  F  N  A  L  S  C  R  S  Q  T
217     AAGCTGATATTTGAGATTGGCTTTTTCCGGAACCGCATGTTCCTGTACTCAGTCCTTGGGTCCCTCCTGGGG
         T  T  I  F  E  I  G  F  F  R  N  R  M  F  L  Y  S  V  L  G  S  L  L  G
289     CAGCTGGCCGTGATCTATGCCCCGCCCCTACAAAAGGTCTTCCAGACTGAAAACCTGAGCGCGCTCGACCTG
         Q  L  A  V  I  Y  A  P  P  L  Q  K  V  F  Q  T  E  N  L  S  A  L  D  L
361     CTGCTGCTGACGGGCCTGGCCTCGTCTGTCTTCATTCTGTCGGAGCTGCTCAAGCTCTGGGAAAAGTTCTTG
         L  L  L  T  G  L  A  S  S  V  F  I  L  S  E  L  L  K  L  W  E  K  F  L
433     TCCAGAGCCAGGCCCACTCAGATGCTCCCGGAAGCTGTGGGATCC TTCAAG…
         S  R  A  R  P  T  Q  M  L  P  E  A  V  BamHI BioID
```

Figure 4.1 Plasmid map of SPCA2C-BioID-HA.

(**A**) *MCS-BioID2-HA* was purchased from Addgene. PCR amplification was used to generate the sequence shown in (**B**). Both the plasmid and PCR product were digested with *NheI* and *BamHI* and subsequently ligated together.

4.2.2 Cell culture, transfection and biotinylation

HEK293A cells were cultured at 37 °C in 5% CO_2 as previously stated (section 2.2.4). For biotinylation experiments, cells were transfected when they reached 70-80% confluence with *MCS-SPCA2C-BioID-HA* or *MCS-BioID-HA* using JetPrime Transfection Kit (Polyplus, NY). 24 hours after transfection cells were incubated for 24 hours with media supplemented with 50 μM biotin.

Cancer cells were cultured in DMEM/F12 media (ThermoFisher, Waltham, MA) supplemented with 10 mM nicotinamide (Sigma Aldrich, Oakville, ON), 5 mg/mL D-glucose (Sigma-Aldrich, Oakville, ON), 5 mL/L insulin-transferrin-selenium (Corning BV, Corning, NY), 5% Nu-serum IV (Corning BV,), 25 μg/mL bovine pituitary extract (BPE; ThermoFisher, Waltham, MA), 20 ng/mL Epidermal Growth Factor (EGF; Corning BV,), 5 nmol/L 3,3',5-Triiodo-L-Thyronine (T3; Sigma-Aldrich, Oakville, ON), 1 μmol/L dexamethasone (Sigma-Aldrich, Oakville, ON), 100 ng/mL cholera toxin (Sigma-Aldrich, Oakville, ON), and antibiotics (penicillin G 100U.mL, streptomycin 100 μg/mL, amphotericin B 0.25 μg/mL; Gibco-BRL, Grand Island, NY).

4.2.3 Calcium imaging

Ca^{2+} imaging was done as previously described (section 3.2.4). Following transfection, cells were loaded with 2 μM Fura2-AM in culture media for 30 minutes at 37 °C and 5% CO_2. Cells were washed once with HBSS supplemented with 1.8 mM Ca^{2+} (unless otherwise stated) and incubated at 37°C for 10 minutes in HBSS before beginning each experiment. Fura2 emissions were measured as previously described (Section 3.2.4) in individual cells. Resting cytosolic Ca^{2+}

levels were established over 100 seconds. To assess unstimulated Ca^{2+} influx, cells were treated with 2 mM EGTA (Ca^{2+} chelator). The difference between Fura2 ratios before and after addition of EGTA was taken as an indicator of the level of constitutive Ca^{2+} influx. To measure ER Ca^{2+} stores, cells were treated 2 μM thapsagargin (TG) after the EGTA treatment. To measure all other Ca^{2+} stores, cells were subsequently treated with 1 μM ionomycin. Relative Ca^{2+} stores levels were determined by the difference between max peak of Fura2 ratios after TG or ionomycin and Fura2 ratios before treatment for the ER and other stores, respectively.

4.2.4 Protein collection and western blotting

Cytosolic and membrane enriched protein fractions were collected as previously described (section 3.2.5). Proteins were resolved on 12% polyacrylamide gels and transferred to a PVDF membrane (ThermoFisher, Waltham, MA). After blocking in 5% non-fat dried milk (NFDM) in tris-buffered saline and 0.1% Tween 20 (TBST) for 30 min, membranes were incubated with primary antibodies diluted in 5% NFDM in TBS overnight at 4°C. Antibodies included rabbit α-Orai1 (1:500; Cell Signaling Technologies, Danvers, MA) or mouse α-hemagglutinin (HA; 1:500; Abcam, Cambridge, MA). Primary antibodies were detected using horseradish peroxidase (HRP)-conjugated α-rabbit (1:10,000; Cell Signaling Technologies, Danvers, MA) or α-mouse (1:10,000; Cell Signaling Technologies) secondary antibodies (diluted in in TBS) for 1 hour. For detection of biotinylated proteins, membranes were blocked with 1% (w/v) bovine serum albumin (BSA) and 0.2% (v/v) Triton X-100 in PBS for 30 minutes. Membranes were incubated with HRP-conjugated streptavidin (1:10,000; Abcam, Cambridge, MA) diluted in 1% (w/v) BSA, 0.2% (v/v) Triton X-100 in phosphate buffered saline (PBS) for 40 minutes. Antibody signals were detected using enhanced chemiluminescence.

4.2.5 Immunofluorescence analysis

HEK293A cells were transfected with *MCS-SPCA2C-BioID-HA* or *MCS-BioID-HA* and incubated with biotin as described above. Twenty-four hours after incubation in biotin, cells were fixed in 4% (v/v) formalin. To detect SPCA2C-BioID-HA and BioID-HA, cells were incubated for 30 minutes in blocking solution [PBS, 5% BSA, 1% (v/v) tritonX-100], and subsequently incubated for 1 hour at room temperature with primary mouse α-HA (1:500; Abcam, Cambridge, MA) diluted in blocking solution. Cells were washed with PBS, and subsequently incubated for 1 hour with FITC labeled secondary goat α-mouse antibody (1:250; ThermoFisher, Waltham, MA) diluted in PBS. Biotinylated proteins were detected by incubating samples in Alexa Flour 594-conjugated streptavidin (1:1000; ThermoFisher, Waltham, MA) diluted in blocking solution for 1 hour. Nuclei were visualized by incubating cells in DAPI (diluted 1:1000 in PBS; ThermoFisher) for 5 minutes. Images were acquired using a Leica DM5500B Microscope.

4.2.6 Preparation of extracts for BioID

Four 72 cm^2 flasks were prepared for each experimental and control condition. HEK-Orai1^{YFP} cells were transfected with *MCS-SPCA2C-BioID-HA* or *MCS-BioID-HA* as noted in 4.2.2. Twenty-four hours later, cells were washed in PBS. Whole cell extracts were prepared using lysis buffer (50 mM Tris·Cl pH 7.4, 500 mM NaCl, 0.2% SDS (w/v), 1 g/mL leupeptin, 10 g/mL aprotinin, 1 g/mL pepstatin, 1 mM DTT). Triton X-100 [final concentration 2% (w/v)] was added to dilute SDS and prevent it from precipitating at 4°C. Samples were sonicated on ice, twice for 30 seconds at output level 4 (Sonic Dismemborator Model 100). 50 mM Tris·Cl pH 7.4

was added to double the volume, and samples underwent another round of sonication. Samples were centrifuged for 10 minutes at 16,500 RCF at 4°C. Supernatants were transferred to new microcentrifuge tubes.

4.2.7 Streptavidin Pull-Down of biotinylated proteins

Streptavidin-conjugated proteins were isolated as previously described (Mehus et al., 2016). Briefly, whole cell extracts were incubated with equilibrated magnetic Dynabeads (MyOne Strepavadin C1; Invitrogen) overnight at 4°C. Beads were washed twice in wash buffer 1 (2% SDS w/v), once in wash buffer 2 [0.1% (w/v) deoxycholic acid, 1% (v/v) Triton X-100, 1 mM EDTA, 500 mM NaCl, 50 mM HEPES; pH7.5] and once in wash buffer 3 [0.5% (w/v) deoxycholic acid, 0.5% (w/v) NP-40, 1 mM EDTA, 250 mM LiCl, 10 mM Tris·Cl; pH 7.4]. A 50µL aliquot was removed for western blot analysis, and the remaining sample resuspended in 50 mM Tris·Cl, pH 7.4. Beads were re-centrifuged and resuspended in 50 mM ammonium bicarbonate.

4.2.8 On-bead trypsin digests

Proteins bound to magnetic beads were reduced using 100 mM DTT for 30 minutes and then alkylated at RT for 30 minutes in the dark with 1 M iodoacetamine (IAA; Sigma-Aldrich, Oakville, ON). Proteins were digested by agitating samples at 37°C for 4 hours with LysC (FUJIFILM Wako Pure Chemical Corporation, USA), overnight with Tryp-LysC (Promega, Madison, WI), and finally 4 hours in mass-spectrometry-grade trypsin (Promega, Madison, WI). The missed cleavage rate for samples was an average of 12.7%. Magnetic beads were centrifuged and pelleted with a magnet. Supernatants were dried by speed vacuum before

resuspension in 0.1% trifluoroacetic acid (Fisher, Ottawa, ON). Samples were desalted using C18 Zip Tips (Sigma-Aldrich, Oakville, ON) before drying by speed vacuum again and subsequently resuspended in 0.1% formic acid (Fisher, Ottawa, ON).

4.2.9 Liquid chromatography (C) electrospray ionizing (ESI) tandem mass spectrometry (MS)

Samples were submitted to the University of Western Ontario Biological Mass Spectrometry Laboratory (BMSL, London, CA) for analysis by high-resolution LC-ESI-MS/MS. Peptides were identified using an ACQUITY M-Class UHPLC system (Waters) connected to an Orbitrap Elite mass spectrometer (ThermoFisher, Waltham, MA). Approximately 1 μg of sample was injected onto an ACUITY UPCL M-Class Symmetry C18 Trap Column, 5 μm, 180 μm x 2 mm, trapped for 6 minutes at a flow rate of 5 μl/minute in 99% solution A 0.1% formic acid (FA) in water) and 1% solution B (0.1% FA in acetonitrile (SCN)). ACUITY UPLC M-Class peptide BEH C18 columns (130 Å, 1.7 μm, 75 μm x 250 mm) were used to separate peptides. Separation was performed at a flow rate of 300 nL/minute at 7-23% solution B for 179 minutes, 23-35% solution B for 60 minutes, then 95% solution B and washing. Samples were run in positive ion mode.

4.2.10 Mass spectrometry data analysis

Raw MS files were searched in PEAKS studio version X (Bioinformatics Solutions Inc., Waterloo, ON, Canada) using the Human Uniprot database to match peptides to proteins sequences. Maximum missed cleavages were set to 3 fragment mass deviation at 20 ppm, fragment mass error tolerance was set to 0.8 Da. Protein and peptide false discover rate (FDR) was set to 1%. Cysteine carbamidomethylation was set as a fixed modification while oxidation

(Met), amide deamidation (Asp/Gln), and acetylation (protein) were set as variable modifications with a maximum number of modifications per peptide set to 10. All other settings were left as default.

4.2.11 Statistics

N values are provided within the figure or figure legends for each experiment. Data is shown as mean +/- standard error of the mean (SEM), and statistical significance was determined using unpaired t-tests or two-way ANOVA followed by Tukey's posthoc test.

4.3 Results

4.3.1 Pancreatic cell types express TRPC3 and STIM1 proteins involved in SOCE.

To determine if the proteins required for SOCE and SICE are present in 266.6 and PDTX cell lines, western blot analysis was performed on whole cell extracts from these lines. PDTX lines include the AO-IPC, AR-IPC, H-NOR, L-NOR, 01-048 cells. HEK-Orai1^{YFP} cells transfected with STIM1^{mCherry} or parental HEK293A cells were included as controls (Figure 4.2A). Orai1 was only detected in HEK-Orai1^{YFP} cells, while TRPC3 and STIM1 were detected in HEK293A, 266.6 and all PDTX lines (Figure 4.2A). RNA-seq analysis (data provided by Dr. Nicholas Fraunhoffer) suggested AO-IPC cells have relatively high *STIM1* expression and low *TRPC3* and *ATP2C1* expression. While 01-048 cells exhibited the highest expression of *TRPC3* and *ATP2C1*, L-NOR cells express *TRPC3*, *STIM1* and *ATP2C1* all at relatively low levels (Figure 4.2). *ORAI1* expression was not detected in any cell line. RNA sequencing analysis indicates *ATP2C2* expression levels also differ between PDTX cell lines. AO-IPC cells have the highest *ATP2C2* expression among all PDTX lines, while 01-048 cells express relatively low amounts (Figure 4.2). To determine if there was a correlation between *ATP2C2* expression and cytosolic

Ca^{2+} levels, one high expressing (AO-IPC) and two low-expressing (L-NOR and 01-048) PDTX lines were chosen for analysis.

Fura2 ratiometric imaging was used to measure resting cytosolic Ca^{2+} levels in each cell line. Representative Fura2 ratiometric traces are provided for each type in Figure 4.3. At rest, AO-IPC cells (*ATP2C2*^{HI} cells) had significantly higher resting cytosolic Ca^{2+} levels compared to L-NOR cells (*ATP2C2*^{LO}; Fura2 340/380 ratio = 0.83 ± 0.006 vs. 0.81 ± 0.007; $p<0.001$; Figure 4.3 and 4.4A). The resting Ca^{2+} levels of 01-048 cells were significantly higher than L-NOR (Fura2 340/380 ratio = 0.85 ± 0.008 vs. 0.81 ± 0.007; $p<0.001$; Figure 4.4A) and not significantly different compared to AO-IPC cells. This suggests that the relative levels of *ATP2C2* do not alone dictate resting cytosolic Ca^{2+} levels.

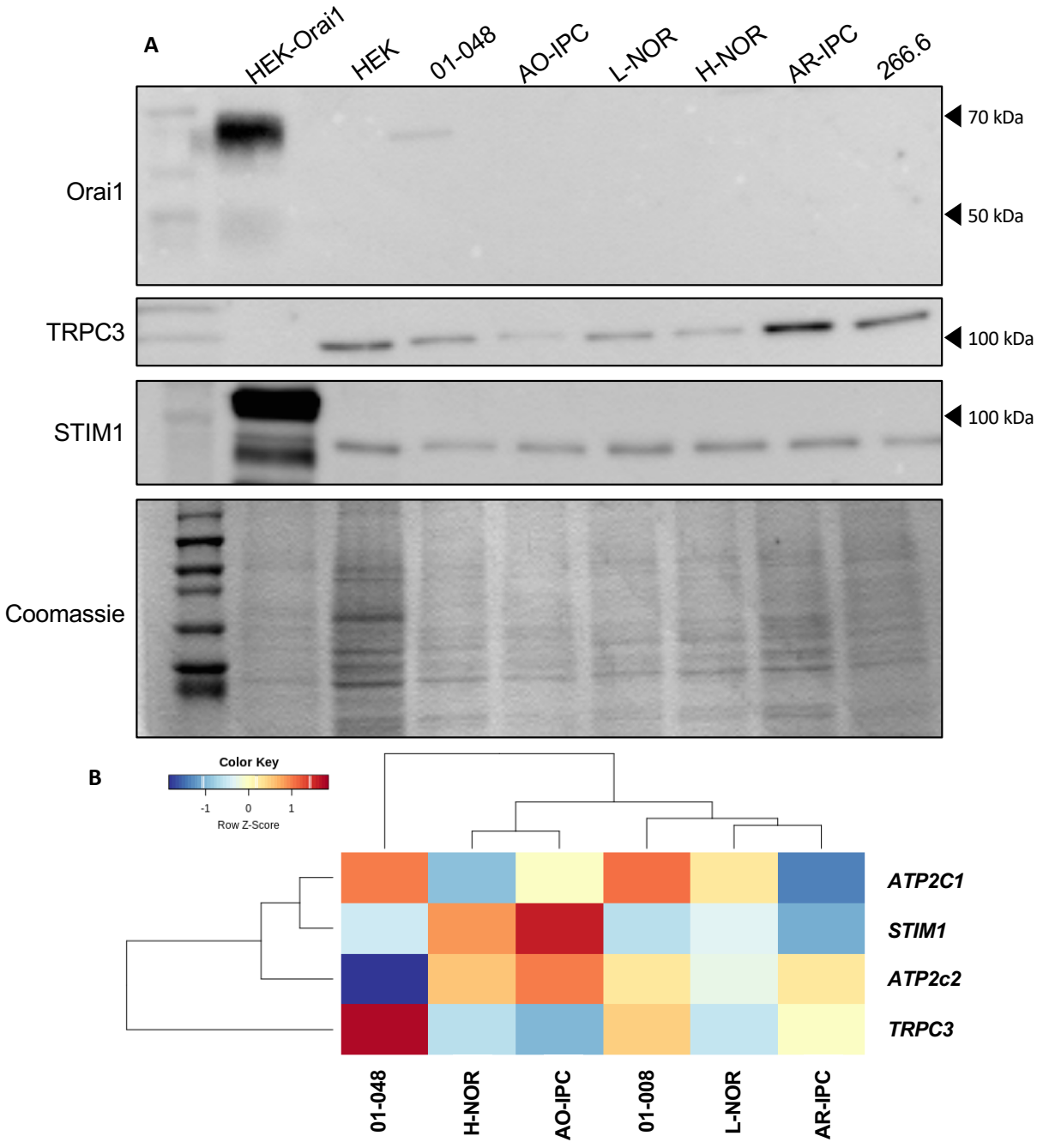
A
HEK-Orai1
HEK
01-048
AO-IPC
L-NOR
H-NOR
AR-IPC
266.6
Orai1
70 kDa
50 kDa
TRPC3
100 kDa
STIM1
100 kDa
Coomassie
B
Color Key
-1
0
1
Row Z-Score
ATP2C1
STIM1
ATP2c2
TRPC3
01-048
H-NOR
AO-IPC
01-008
L-NOR
AR-IPC

Figure 4.2 Expression of SOCE regulators in pancreatic cancer cell lines.

(A) Representative western blot analysis for Orai1, TRPC3 and STIM1 in 266.6 cells and PDTX lines. HEK-ORAI1^{YFP} transfected with STIM1 (positive control) and HEK293A cells (negative control) were included. Theoretical size of Orai1/Orai1^{YFP}, STIM1/STIM1^{mCherry} and TRPC3 is ~33/59 kDa, ~77/106 kDa, and ~100 kDa, respectivly. **(B)** Heat map from RNA-seq analysis of gene expression from the various PDTX lines showing *ATP2C2*, *STIM1, ATP2C1* and *TRPC3* expression in pancreatic cancer cell lines. Lower row Z-scores (blue) indicate relatively less mRNA expression.

A

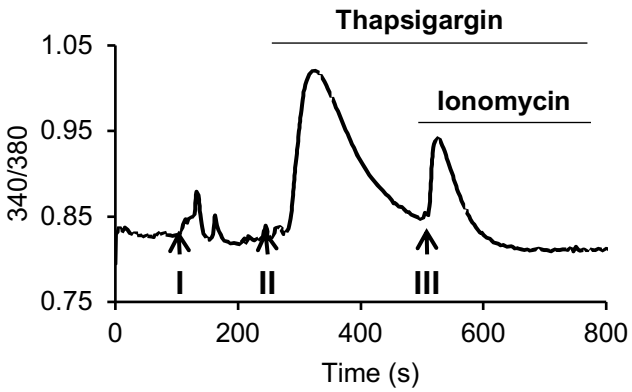
Thapsigargin
Ionomycin
1.05
0.95
0.85
0.75
340/380
I
II
III
0
200
400
600
800
Time (s)

B

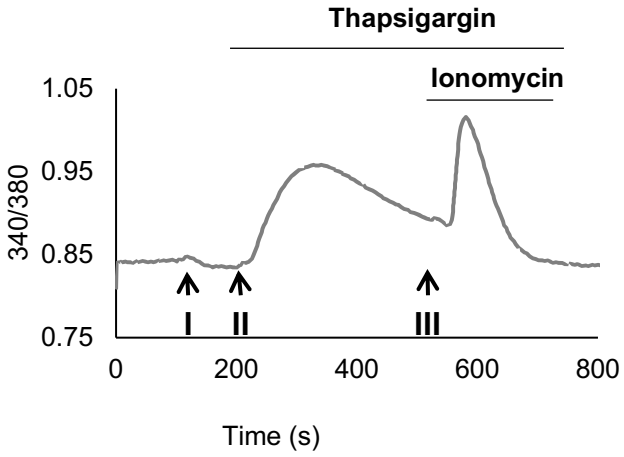
Thapsigargin
Ionomycin
1.05
0.95
0.85
0.75
340/380
I
II
III
0
200
400
600
800
Time (s)

C

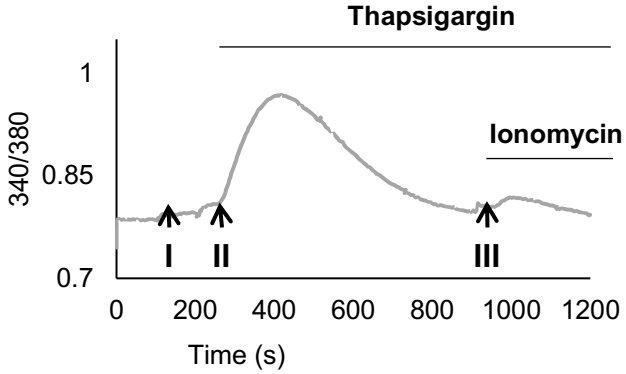
Thapsigargin
Ionomycin
1
0.85
0.7
340/380
I
II
III
0
200
400
600
800
1000
1200
Time (s)

Figure 4.3 Analysis of Ca^{2+} stores in PDTX lines.

(A) *ATP2C2^{HI}* (AO-IPC) and **(B)** *ATP2C2^{LO}* (L-NOR and 01-048F1) cell lines were loaded with 2 μM Fura2 and resting Ca^{2+} levels assessed. Cells were supplemented with 2 mM EGTA (I) followed by 2 μM TG 100 s later (II). Once cells reached steady Ca^{2+} states, 1 μM ionomycin (III) was added. Traces are representative of the average response observed in n=3 experiments. These results are used for quantitative analysis in Figure 4.4.

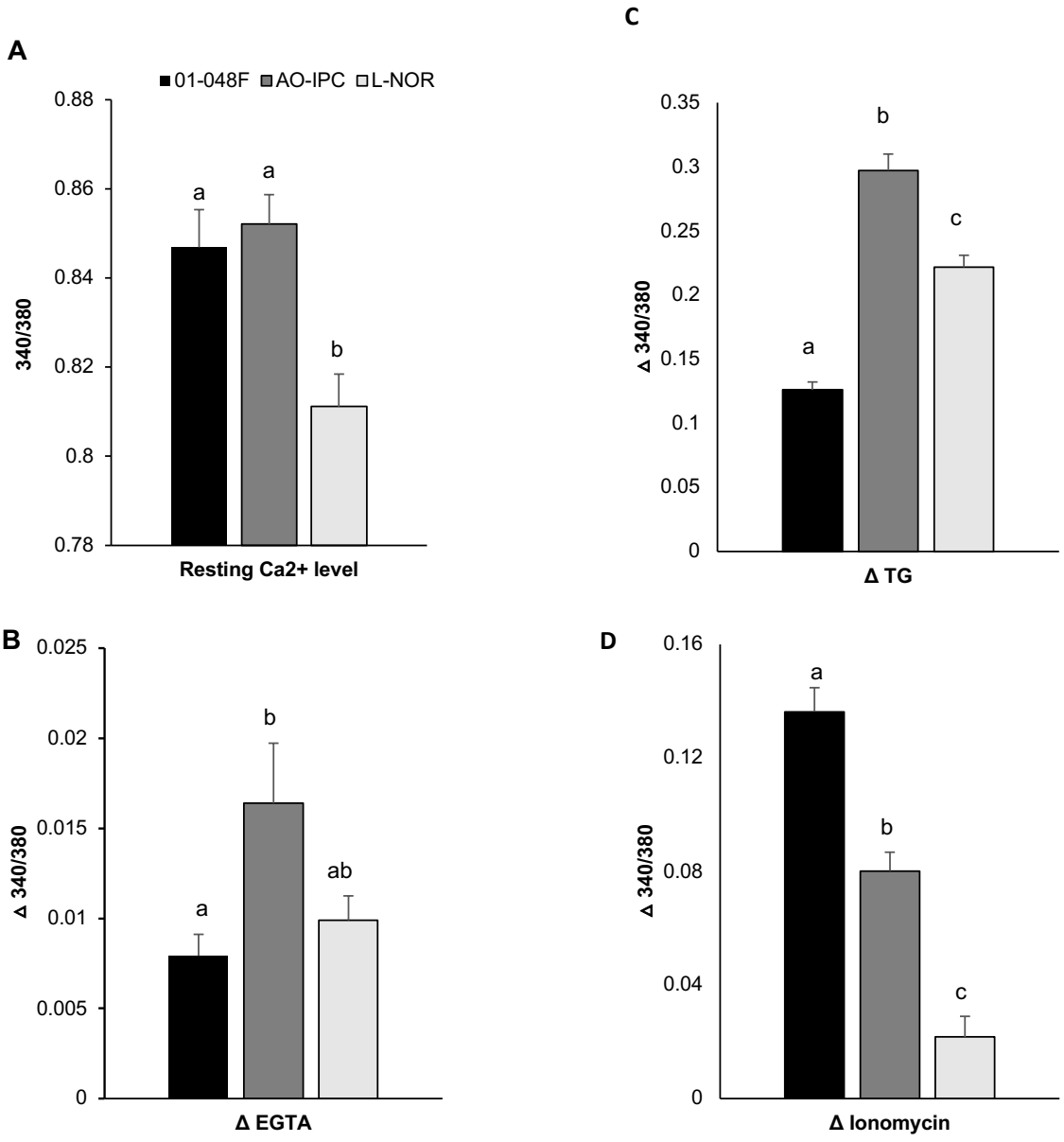
A
01-048F
AO-IPC
L-NOR
340/380
0.88
0.86
0.84
0.82
0.8
0.78
a
a
b
Resting Ca2+ level
C
Δ 340/380
0.35
0.3
0.25
0.2
0.15
0.1
0.05
0
a
b
c
Δ TG
B
Δ 340/380
0.025
0.02
0.015
0.01
0.005
0
a
b
ab
Δ EGTA
D
Δ 340/380
0.16
0.12
0.08
0.04
0
a
b
c
Δ Ionomycin

Figure 4.4 Analysis of Ca^{2+} signaling in PDTX lines L-NOR, 01-048, and AO-IPC.

Ratiometic Fura2 imaging was used to (**A**) quantify resting Ca^{2+} levels, (**B**) assess levels of constitutive Ca^{2+} influx by monitoring the loss of cytosolic Ca^{2+} after external Ca^{2+} chelation using 2 mM EGTA (**C**) measure ER Ca^{2+} store levels based on TG treatment, and (**D**) measure non-ER Ca^{2+} store levels based on 1 μM ionomycin treatment. Letters represent significant differences among groups. Error bars represent mean +/- SEM. Data are means from 3 separate experiments. Total number of cells for AO-IPC (n=52), 01-048 (n=45), and L-NOR (n=50).

Next, Fura2 ratiometric imaging was used to test Ca^{2+} influx into cells. Cells were treated with 2 mM EGTA to chelate all extracellular Ca^{2+}, therefore eliminating Ca^{2+} influx. The difference between cytosolic Ca^{2+} levels (approximated by the change in Fura2 ratios) before and after the addition of EGTA reflects the relative level of constitutive Ca^{2+} influx involved in maintaining basal cytosolic Ca^{2+} concentrations. Ca^{2+} influx in AO-IPC (*ATP2C2*^{HI} cells) was significantly greater than in 01-048 (*ATP2C2*^{LO}; Fura2 Δ340/380 ratio = 0.016 ± 0.003 vs. 0.008 ± 0.001; $p<0.05$; Figure 4.4B). There were no significant differences in Ca^{2+} influx rates between L-NOR (*ATP2C2*^{LO}) and AO-IPC (*ATP2C2*^{HI}), however, there was a trending decrease in L-NOR Ca^{2+} influx rates and no significant differences between 01-048 (*ATP2C2*^{LO}) cells (Figure 4.4B).

To determine the relative levels of Ca^{2+} in ER stores, cells were treated with TG. Ca^{2+} release from the ER after TG addition was significantly higher in AO-IPC (*ATP2C2*^{HI}) cells compared to 01-048 (*ATP2C2*^{LO}; Fura2 Δ340/380 ratio = 0.3 ± 0.01 vs. 0.13 ± 0.006; $p<0.0001$; Figure 4.4C) and L-NOR cells (Fura2 Δ340/380 ratio = 0.3 ± 0.01 vs. 0.22 ± 0.009; $p<0.0001$; Figure 4.4C). 01-048 cells released significantly more Ca^{2+} from ER stores then L-NOR cells (Fura2 Δ340/380 ratio = 0.13 ± 0.006 vs. 0.22 ± 0.009; $p<0.0001$; Figure 4.4C). These data suggests that at higher expression levels of *ATP2C2* may correlate with increased stores of ER Ca^{2+}. However, this correlation does not extend to the two *ATP2C2*^{LO} cell lines, suggesting that the relative levels of *ATP2C2* do not alone dictate the level of Ca^{2+} in ER stores.

The relative levels of Ca^{2+} stored in all other organelles were tested by treating cells with ionomycin after ER stores were emptied using TG. AO-IPC cells had significantly lower Ca^{2+} release after ionomycin treatment when compared to 01-048 cells (Fura2 Δ340/380 ratio = 0.08 ±

0.011 vs. 0.13 ± 0.01; p<0.0001; Figure 4.4C). 01-048 cells had significantly greater release of Ca^{2+} after ionomycin treatment compared to L-NOR cells (Fura2 Δ340/380 ratio = 0.13 ± 0.01 vs. 0.02 ± 0.002; p<0.05; Figure 4.4D). These results suggest higher cytosolic Ca^{2+} levels, constitutive Ca^{2+} influx across the plasma membrane and Ca^{2+} release from ER stores in AO-IPC cells may be correlated to higher levels of *ATP2C2* expression. However, *ATP2C2* levels need to be viewed in light of other Ca^{2+} handeling proteins, any correlation may be complicated by differential expression of other mediators of Ca^{2+} handling in the cells. In addition, analysis of *Atp2c2* expression does not distinguish full length *ATP2C2* from *ATP2C2C*. Therefore, to test if SPCA2C can increase Ca^{2+} levels and responses, the effects of SPCA2C over-expression was examined on cytosolic Ca^{2+} levels, Ca^{2+}influx and ER Ca^{2+} stores using transient transfection in 01-048 cells. The 01-048 cell line was chosen because these cells have relatively low *ATP2C2* expression.

4.3.2 Increased SPCA2C expression increases resting cytosolic Ca^{2+} in 01-048 cells

To determine if SPCA2C over-expression in 01-048 cells affects cytosolic Ca^{2+} levels, *pcDNA3-SPCA2C^{mRFP}* was transfected with *pcDNA-GFP* into 01-048 cells and cytosolic Ca^{2+} levels measured by Fura2 analysis. 01-048 cells over-expressing SPCA2C had significantly increased cytosolic Ca^{2+} levels compared to control GFP-only transfected cells (Fura2 340/380 ratio = 0.87 ± 0.004 vs. 0.84 ± 0.010; P < 0.05; Figure 4.5A, B) consistent with the findings that SPCA2C affects resting cytosolic Ca^{2+} levels.

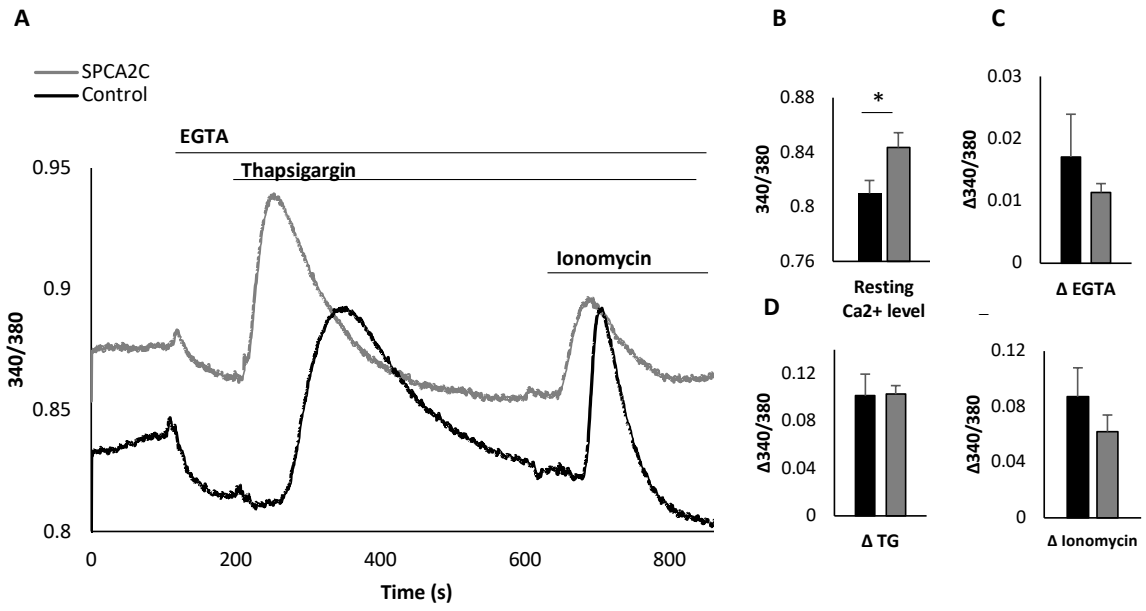
A
SPCA2C
Control
EGTA
Thapsigargin
Ionomycin
340/380
Time (s)
B
340/380
Resting
Ca2+ level
C
Δ340/380
Δ EGTA
D
Δ340/380
Δ TG
Δ340/380
Δ Ionomycin

Figure 4.5 Increasing SPCA2C expression elevates resting cytosolic Ca^{2+} levels in 01-048 cells.

(**A**) Ratiometric Fura2 analysis in 01-048 cells transfected with $SPCA2C^{mRFP}$ and GFP (n=20) or GFP alone (control; n=16). Resting levels were measured for the first 100 s before supplemented with 2 mM EGTA to measure relative level of constitutive Ca^{2+} influx, followed by 2μM TG to measure ER Ca^{2+} stores. Once cytosolic Ca^{2+} reached a steady state, 1 μM ionomycin (I) was added, to measure non-ER Ca^{2+} stores. Traces are representative of the average response observed in n=3 experiments. Resting levels (**B**) maximal change in cytosolic Ca^{2+} based on Fura2 340/380 ratio in response to addition of EGTA (**C**) TG (**D**) and ionomycin (**E**)were measured. Values are expressed as means +/- SEM; *P<0.05.

To determine if increased cytosolic Ca^{2+} levels in SPCA2C-over expressing cells were due to increased constitutive Ca^{2+} influx, 2 mM EGTA was added to the extracellular media to chelate Ca^{2+}, halting Ca^{2+} influx. The relative loss in cytosolic C^{2+} upon chelation of extracellular Ca^{2+} with EGTA was not different for 01-048 cells over-expressing $SPCA2C^{mRFP}$ compared to control GFP only transfected cells (Figure 4.5C), consistent with findings in HEK293A, cells which showed increased SPCA2C expression does not increase constitutive Ca^{2+} influx rates at rest without Orai1 expression. Finally, 01-048 cells were treated with TG and ionomycin to examine Ca^{2+} levels in ER stores and non-ER stores, respectively. No significant differences were observed when comparing the relative Ca^{2+} release after TG or ionomycin treatment in SPCA2C-expressing vs. non-expressing 01-048 cells (Figure 4.5C, D). These experiments indicate over-expression of SPCA2C in 01-048 cells increased cytosolic Ca^{2+} levels but did not increase ER Ca^{2+} stores. This may suggest an alternative function for SPCA2C in this line or reflect altered expression of other Ca^{2+} handling proteins.

4.3.4 SPCA2C over-expression increases cytosolic Ca^{2+} and Ca^{2+} influx across the plasma membrane in 266.6 cells.

To determine if SPCA2C affects pancreatic acinar cell cytosolic Ca^{2+} levels and Ca^{2+} handling, $SPCA2C^{mRFP}$ was transiently over-expressed in 266.6 cells. Examination of resting cytosolic Ca^{2+} levels using Fura2 ratiometric imaging showed significantly increased cytosolic Ca^{2+} levels in 266.6 cells over-expressing SPCA2C compared to control GFP transfected cells (Fura2 340/380 ratio = 0.82 ± 0.008 vs. 0.75 ± 0.014; $p<0.0001$; Figure 4.6A, B). To determine if increased cytosolic Ca^{2+} levels were due to increased constitutive Ca^{2+} influx, EGTA was added to the extracellular media. 266.6 cells over-expressing SPCA2C showed a greater drop in

cytosolic Ca^{2+} upon chelation of extracellular Ca^{2+} compared to control GFP transfected cells (Fura2 340/380 ratio = 0.04 ± 0.002 vs. 0.02 ± 0.003; $p<0.01$; Figure 4.6C) suggesting that over-expression of SPCA2C may be increasing the number of interactions with Ca^{2+} channels on the plasma membrane, thereby enhancing constitutive Ca^{2+} influx. However, ER Ca^{2+} levels appeared to be significantly lower in SPCA2C over-expressing 266.6 cells based on Ca^{2+} release following TG treatment compared to GFP control cells (Fura2 340/380 ratio = 0.08 ± 0.008 vs. 0.12 ± 0.015; $p<0.001$; Figure 4.6D). No significant difference in non-ER stores Ca^{2+} levels was observed based on ionomycin treatment.

Since TG can also promote Ca^{2+} release from the Golgi, ER store-specific Ca^{2+} release was assessed by treating cells with carbachol. There was no difference in Ca^{2+} release from ER stores in response to carbachol between 266.6 cells expressing SPCA2C or control GFP only cells (Figure 4.7), suggesting increased SPCA2C expression in 266.6 cells does not increase Ca^{2+} levels in the ER stores.

Combined, these results suggest increased expression of SPCA2C in 266.6 cells increased resting cytosolic Ca^{2+} levels and Ca^{2+} influx across the plasma membrane. However, unlike HEK293A cells, over-expression of SPCA2C did not increase ER Ca^{2+} stores in 266.6 cells.

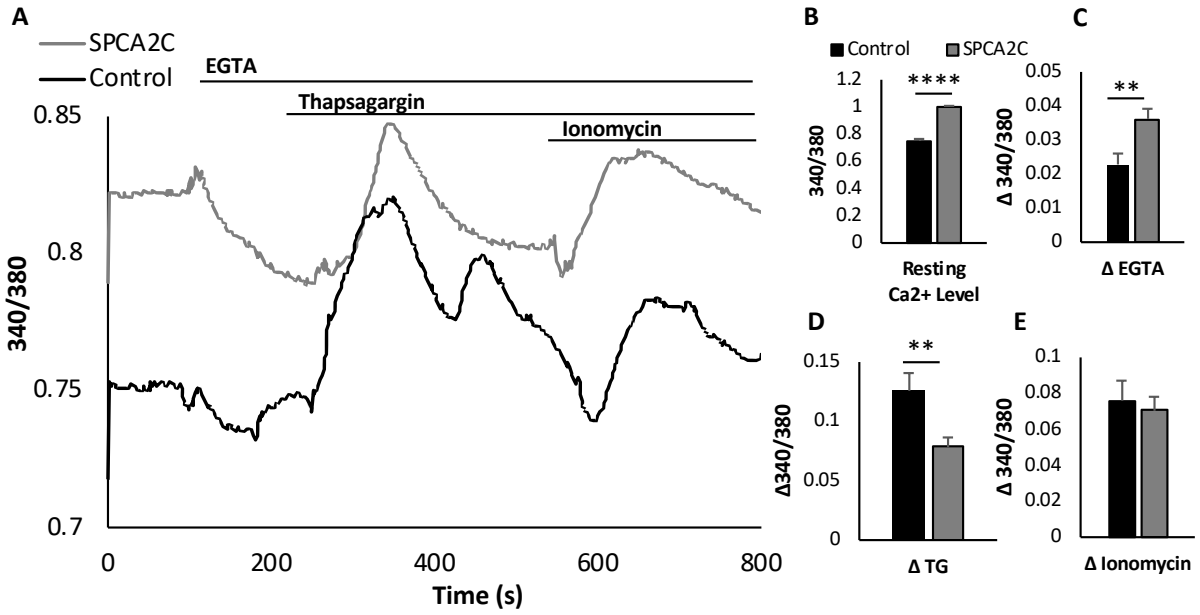
A
SPCA2C
Control
EGTA
Thapsagargin
Ionomycin
0.85
0.8
0.75
0.7
340/380
0
200
400
600
800
Time (s)
B
Control
SPCA2C
****
1.2
1
0.8
0.6
0.4
0.2
0
340/380
Resting
Ca2+ Level
C
**
0.05
0.04
0.03
0.02
0.01
0
Δ 340/380
Δ EGTA
D
**
0.15
0.1
0.05
0
Δ340/380
Δ TG
E
0.1
0.08
0.06
0.04
0.02
0
Δ 340/380
Δ Ionomycin

Figure 4.6 Increasing SPCA2C expression elevates resting cytosolic Ca^{2+} levels and Ca^{2+} influx in 266.6 cells.

(**A**) Ratiometric Fura2 analysis in 266.6 cells transfected with $SPCA2C^{mRFP}$ and GFP (n=42) or GFP alone (control; n=43). The number of cells examined was extended over three experiments. Resting levels were measured for the first 100 s before addition of 2 mM EGTA to assess the level of constitutive Ca^{2+} influx, followed by 2 μM TG to measure the levels of the ER Ca^{2+} stores. Once cytosolic Ca^{2+} reached a steady state, 1 μM ionomycin was added, to measure Ca^{2+} release from non-ER Ca^{2+} stores. Traces are representative of the average response from n=3 separate experiments. Resting levels (**B**) maximal change in cytosolic Ca^{2+} based on Fura2 340/380 ratio in response to addition of EGTA (**C**) TG (**D**) and ionomycin (**E**)were measured. Values are expressed as mean +/- SEM; *P<0.001. **P<0.0001.

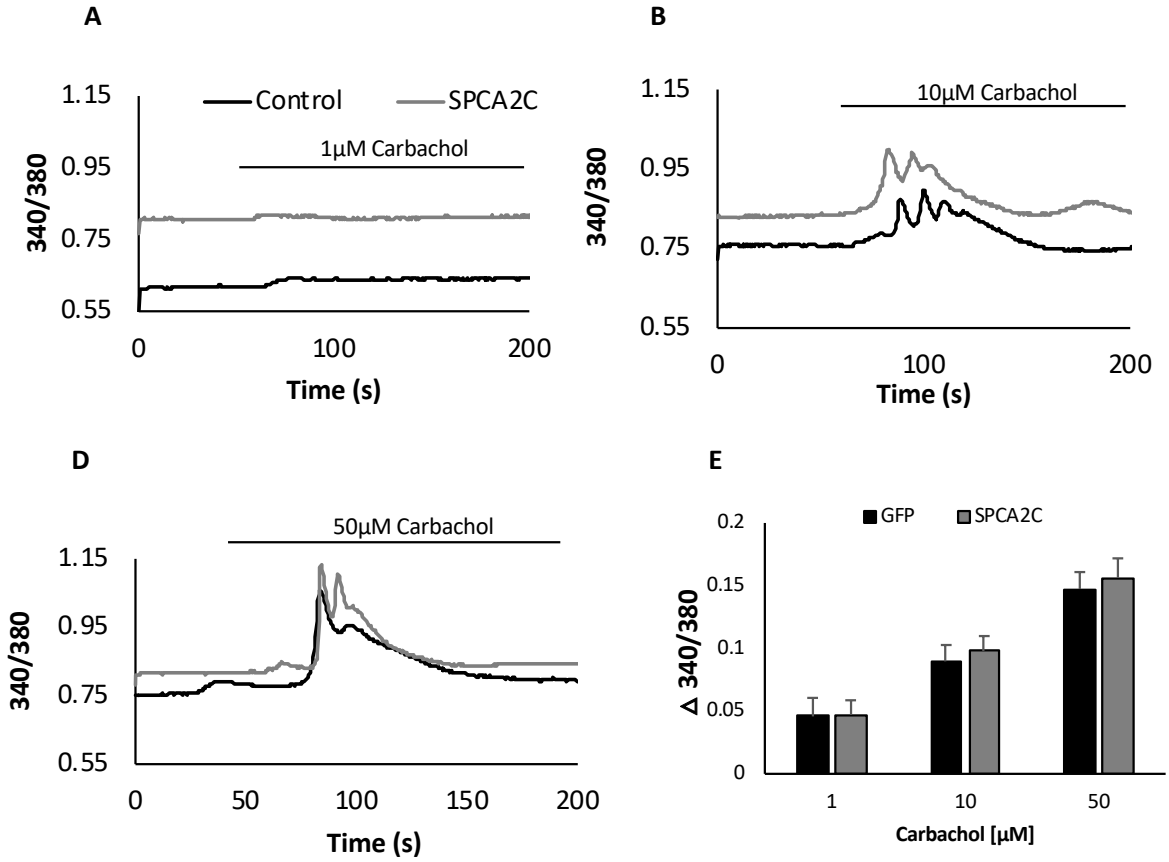
A
Control
SPCA2C
1µM Carbachol
340/380
1.15
0.95
0.75
0.55
0
100
200
Time (s)
B
10µM Carbachol
340/380
1.15
0.95
0.75
0.55
0
100
200
Time (s)
D
50µM Carbachol
340/380
1.15
0.95
0.75
0.55
0
50
100
150
200
Time (s)
E
GFP
SPCA2C
Δ 340/380
0.2
0.15
0.1
0.05
0
1
10
50
Carbachol [µM]

Figure 4.7 Increased SPCA2C expression does not affect carbachol stimulated Ca^{2+} response in 266.6 cells.

Fura2 ratiometric analysis of 266.6 cells transfected with $SPCA2C^{mRFP}$ and GFP or GFP alone (control). Resting levels were measured for the first 60s before buffer was supplemented with 1, 10, or 50 μM carbachol (**A, B, C**; respectively)**.** Traces are representative single cell responses. Ca^{2+} release from the ER was approximated by the difference in Fura2 340/380 ratio from resting to max peak after carbachol addition. Experiments were conducted 3 times, number of cells total for GFP control (1 μM, n=13; 10 μM, n=34; 50 μM, n=35) and $SPCA2C^{mRFP}$ (1 μM, n=34; 10 μM, n=30; 50 μM, n=39; **E**). Values are expressed as means +/- SEM.

4.3.5 Characterization of the expression, localization and functionality of SPCA2C-BioID-HA in HEK23A cells.

My data suggests, SPCA2C affects Ca^{2+} homeostasis through mechanisms both involving and independent of Orai1. Therefore, to identify other SPCA2C interactors that might be involved in Ca^{2+} homeostasis, a BioID protein-proximity detection assay was performed. The BioID assay was carried out in HEK-Orai1^{YFP} cells, as they provide an internal established control for interactions between SPCA2C and Orai1.

To validate SPCA2C-BioID-HA expression and its ability to biotinylate interacting protein partners, *MCS-SPCA2C-BioID-HA* and empty *MCS-BioID-HA* vectors were transiently transfected into HEK293A cells. 24 hours after transfection media was supplemented with biotin for 24 hours. IF analysis for HA showed SPCA2C-BioID-HA localized within cytosolic regions and near the cell periphery, consistent with SPCA2C^{FLAG} and SPCA2C^{mRFP} localization observed in section 3.3.3. Streptavidin-Alex Fluor 568 revealed that the biotinylation in SPCA2C-BioID expressing cells was localized within the cytosol, near the cell periphery (Figure 4.8A), which is different than the nuclear localization observed for the biotinylation pattern using empty BioID-HA vector expressing cells (Figure 4.8B).

To confirm localization of SPCA2C-BioID-HA to the correct cellular compartment, samples of cytosol and membrane enriched fractions were used in western blot analysis. The western blot confirmed expression of SPCA2C-BioID-HA and biotinylation in the membrane fraction of *MCS-SPCA2C-BioID-HA* transfected cells. The western blot showed that the membrane fraction of BioID-HA transfected cells contained relatively few bands (Figure 4.9A). Furthermore, the

streptavidin-banding pattern in SPCA2C-BioID-HA whole cell protein lysates was retained after isolation of biotinylated protein with streptavidin coated Dynabeads (Figure 4.9B).

4.3.6 Identification of SPCA2C candidate protein interactors using BioID.

Using transient transfection of SPCA2C-BioID-HA and BioID-HA (control) in HEK-Orai1^{YFP} cells, a large-scale BioID experiment was performed, testing for biotinylation prior to MS submission (Figure 4.10B). Biotin modifications are rare in mammalian cells, with the exception of pyruvate carboxylase, acetyl-CoA carboxylase 1 and 2, propionyl-CoA carboxylase alpha chain, and methylcrotonoyl-CoA carboxylase subunit alpha (Roux et al., 2012). The presence of the carboxylases in the MS results confirms the successful capture of biotinylated proteins. Indeed, one or more of these carboxylases were detected in my system.

A list of 480 proteins was detected by mass spectrometry (MS) in the SPCA2C-BioID-HA pull-down. These proteins were referenced against the list of 336 proteins detected in the empty control BioID pull-down (Figure 4.10A). Proteins listed in both SPCA2C-BioID-HA and BioID-HA MS lists were omitted from further analysis. In total, 263 proteins were uniquely identified in the SPCA2C-BioID-HA group. Orai1 was among the list of SPCA2C-BioID-HA proteins, confirming the screen identified known interacting partners for SPCA2C.

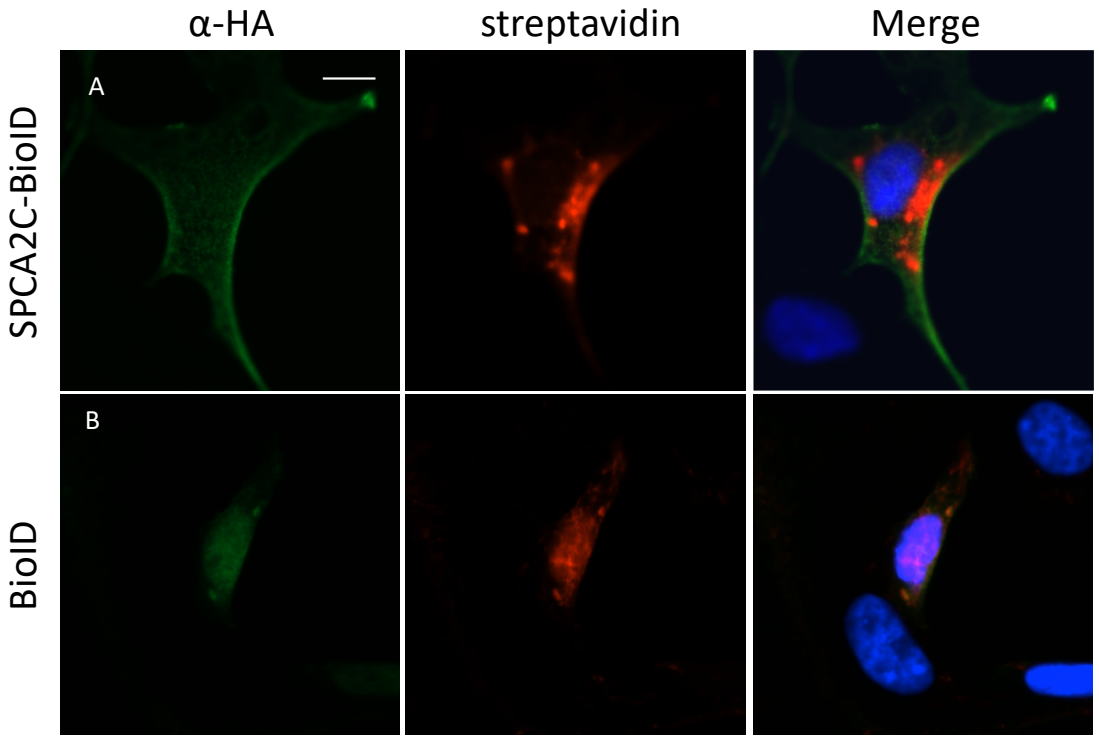
α-HA
streptavidin
Merge
SPCA2C-BioID
BioID
A
B

Figure 4.8 Expression of BioID and SPCA2C-BioID in HEK293A cells.

SPCA2C-BioID-HA (**A**) or BioID-HA (**B**) fusion protein was transiently expressed in HEK293A cells. Cells were incubated in 50uM biotin for 24 hours then fixed. Immunofluorescence was performed with anti-HA (green), and streptavidin-Alexa Flour 568 (red). Scale bar=10 μm.

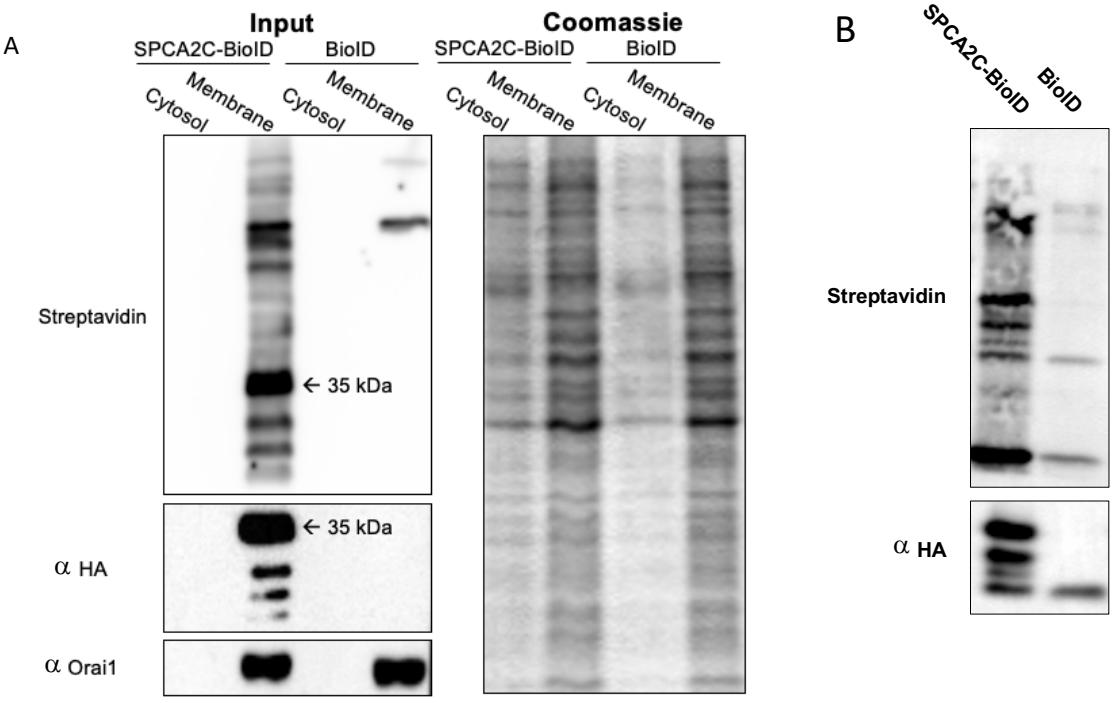
A
Input
Coomassie
SPCA2C-BioID
BioID
SPCA2C-BioID
BioID
Cytosol
Membrane
Cytosol
Membrane
Cytosol
Membrane
Cytosol
Membrane
Streptavidin
← 35 kDa
← 35 kDa
α HA
α Orai1
B
SPCA2C-BioID
BioID
Streptavidin
α HA

Figure 4.9 Characterization of SPCA2C-BioID-HA functionality for biotin-labelling proteins in HEK-Orai1^{YFP} cells.

MCS-SPCA2C-BioID-HA and *MCS-BioID-HA* fusion plasmids were separately expressed in HEK-Orai1^{YFP} cells incubated in 50 μM biotin for 24 hours. Western blot was performed on cytosolic and membrane enriched protein lysates for α-HA, α-Orai1 (blot showing Orai1^{YFP}) and streptavidin-HRP **(A)**. Whole cell lysates were incubated in streptavidin-coupled dynabeads and western blot performed for anti-HA and streptavidin-HRP **(B)** to show presence of SPCA2C-BioID-HA and biotinylated proteins, using a streptavidin pull-down before mass spectrometry**.**

To determine if the BioID screen validated previous findings on cellular localization and function, bioinformatics pathway analysis was performed using this list of 263 proteins using the online web tool gProfiler (https://biit.cs.ut.ee/gprofiler/gost). GO analysis of cellular compartments (GO:CC) identified the ER membrane as a highly enriched pathways based on the list of putative interactors ($P_{adj} = 5.04x10^{-35}$; Figure 4.10D). This supports previous IF analysis localizing SPCA2C to the ER. KEGG pathway analysis also identified ER-related processes such as protein processing in the ER and protein export ($P_{adj} = 1.9x10^{-6}$ Figure 4.10C), again supportive of our previous findings that SPCA2C localizes and functions in the ER. Finally, Human Protein Atlas (HPA) analysis terms included pancreas; exocrine glandular cells and salivary gland; glandular cells ($P_{adj} = 1.22x10^{-5}$ and $P_{adj} = 0.0015$, respectively; Figure 5.10B). These terms support expectations that SPCA2C is important in acinar cell physiology.

4.3.7 Using the Contaminant Repository for Affinity Purification to create a stringent list of interaction candidates.

Since BioID and affinity purification coupled to MS are now widely used approaches for the identification of protein-protein interactors, a Contaminant Repository for Affinity Purification has been created online (Mellacheruvu et al., 2013; https://www.crapome.org). Using this resource improves characterization of background associated with a given experimental protocol. This list contains more than 3300 proteins, which makes it a very stringent control. However, because the list is extensive, it may falsely eliminate true interactors of SPCA2C. Nevertheless, using a more stringent approach that omitted proteins found in the contaminant list and the BioID negative control, a refined list of 71 candidate interacting proteins was identified (Figure 4.11A). This list also included positive control Orai1. Bioinformatic analysis was performed and

a refined list of GO, KEGG and Reactome pathways identified. Even after this stringent refinement, GO cell compartment analysis still suggested localization of interacting partners to the ER ($P_{adj} = 1.34x10^{-20}$; Figure 4.11D), which strongly supports our previous localization and functional analysis of SPCA2C in cells. Some terms identified by KEGG analysis, such as ribosomes and glycolysis, could be artifacts of the BioID screen. KEGG pathway analysis suggested candidate protein interactors play a role in SNARE interaction in vesicular transport ($P_{adj} = 0.028$; Figure 4.12C). Vesicular transport in the exocytosis of enzymes is the main function of pancreatic acinar cells and relies heavily on proper Ca^{2+} regulation, which Reactome analysis suggests as a likely function of the identified candidate interactors ($P_{adj} = 0.02$; Figure 4.11B).

As mentioned, the contaminant repository may eliminate *bona fide* SPCA2C interaction partners. Therefore, all putative interactors in the less stringent list of 263 proteins should not be discredited completely. In future work, verifying the protein interactions identified by the BioID assay should be done to confirm the identify of novel binding partners for SPCA2C.

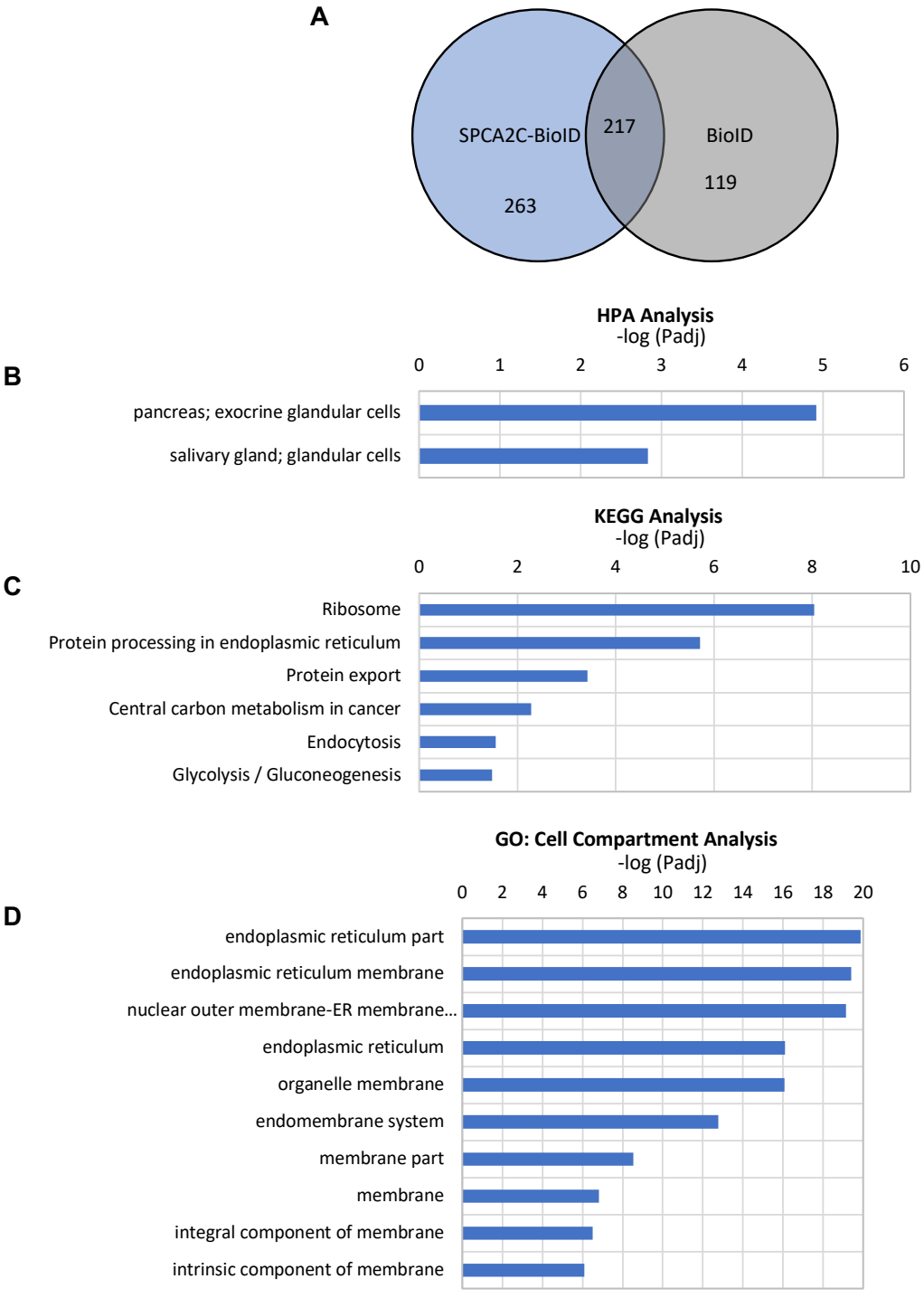
A
SPCA2C-BioID
263
217
BioID
119
B
HPA Analysis
-log (Padj)
0
1
2
3
4
5
6
pancreas; exocrine glandular cells
salivary gland; glandular cells
C
KEGG Analysis
-log (Padj)
0
2
4
6
8
10
Ribosome
Protein processing in endoplasmic reticulum
Protein export
Central carbon metabolism in cancer
Endocytosis
Glycolysis / Gluconeogenesis
D
GO: Cell Compartment Analysis
-log (Padj)
0
2
4
6
8
10
12
14
16
18
20
endoplasmic reticulum part
endoplasmic reticulum membrane
nuclear outer membrane-ER membrane...
endoplasmic reticulum
organelle membrane
endomembrane system
membrane part
membrane
integral component of membrane
intrinsic component of membrane

Figure 4.10 KEGG, GO and HPA pathways based on protein interaction candidates from BioID screen.

(**A**) Venn diagram comparing the overlap of peptides obtained in BioID-HA and SPCA2C-BioID-HA MS analysis. Bioinformatic analysis of the 263 unique proteins biotinylated by SPCA2C-BioID-HA, after excluding negative control protein. The pathways identified in Gene Ontology (**B**) KEGG (**C**), and HPA (**D**) analysis suggest specific roles and localization patterns for SPCA2C.

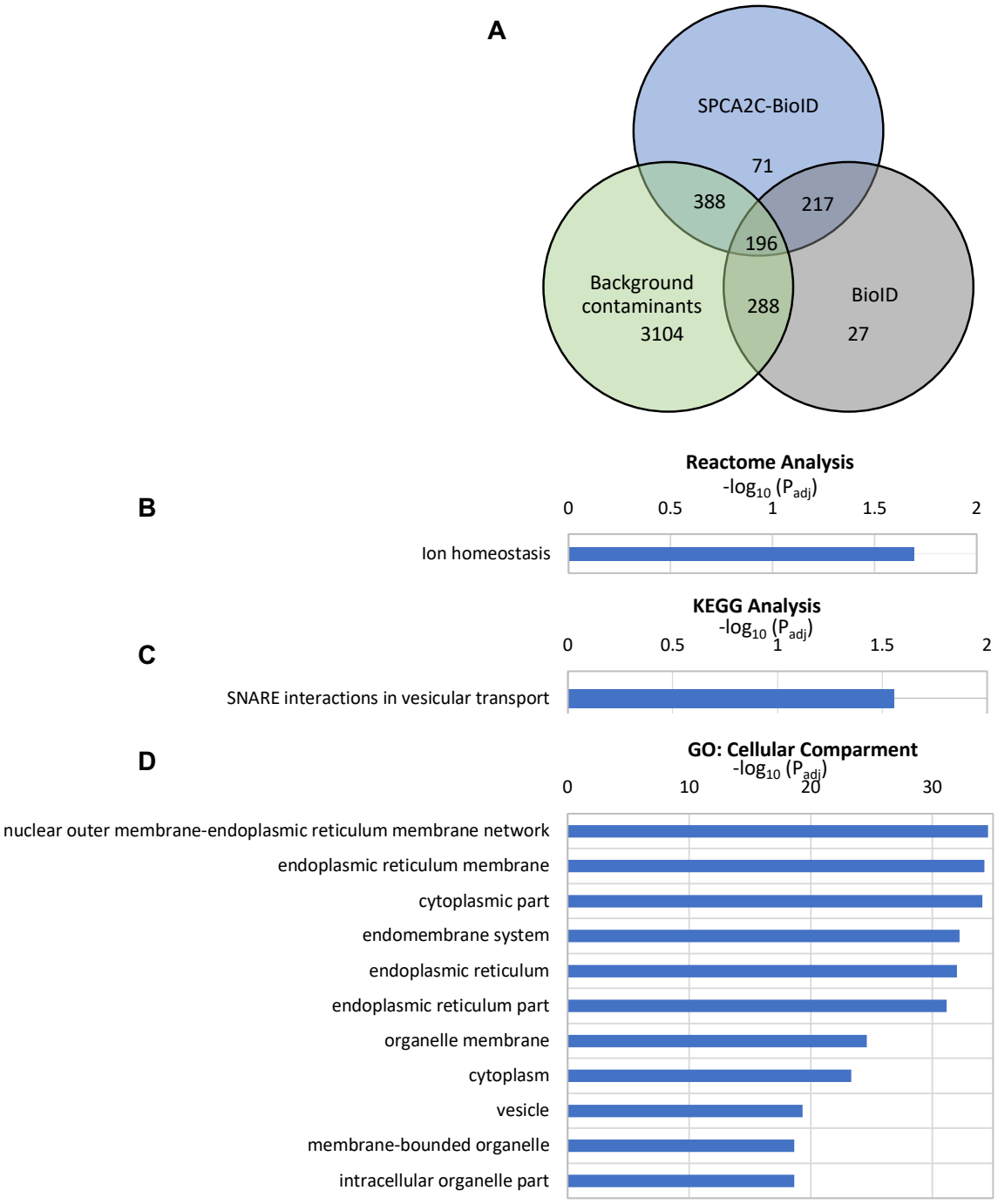
A
SPCA2C-BioID
71
388
217
196
Background contaminants
3104
288
BioID
27
B
Reactome Analysis
-log10 (Padj)
0
0.5
1
1.5
2
Ion homeostasis
C
KEGG Analysis
-log10 (Padj)
0
0.5
1
1.5
2
SNARE interactions in vesicular transport
D
GO: Cellular Comparment
-log10 (Padj)
0
10
20
30
nuclear outer membrane-endoplasmic reticulum membrane network
endoplasmic reticulum membrane
cytoplasmic part
endomembrane system
endoplasmic reticulum
endoplasmic reticulum part
organelle membrane
cytoplasm
vesicle
membrane-bounded organelle
intracellular organelle part

Figure 4.11 KEGG, GO and Reactome pathways based on protein interaction candidates identified using the BioID screen.

(**A**) Venn diagram comparing the number of proteins identified in the BioID-HA control and SPCA2C-BioID-HA compared to the contaminant repository list. Analysis of the 71 identified proteins unique to SPCA2C-BioID-HA, after excluding negative control and common contaminate proteins, by determining enriched terms and pathways from Gene Ontology (**B**) KEGG (**C**), and Reactome (**D**).

4.4 Discussion

Both SPCA2 and SPCA2C have been linked to Ca^{2+} homeostasis pathways requiring Orai1. However, our functional data in Chapters 2 and 3 suggest SPCA2C is also involved in regulating Ca^{2+} through non-Orai1 mediated pathways as well. Therefore, in this Chapter, two approaches were taken to gain a broader understanding of SPCA2C function. First, the effects of over-expressing *ATP2C2* on cytosolic Ca^{2+} levels before and after stimulation were examined in pancreatic cell lines. Similar to findings in breast cancer (Dang et al., 2017; Feng et al., 2010), pancreatic PDTX cell lines differed in expression levels of *ATP2C2* RNA, and a PDTX cell line expressing high *ATP2C2* RNA levels had increased cytosolic Ca^{2+} levels, constitutive Ca^{2+} influx and ER Ca^{2+} release in response to TG compared to PDTX cell lines with a lower expression of *ATP2C2* RNA expression level. SPCA2C over-expression in both PDTX cells or 266.6 cells, increased resting cytosolic Ca^{2+} levels. However, there was also no change in ER Ca^{2+} levels with SPCA2C over-expression, which is different than findings in HEK293A cells. Second, a BioID screen was performed in HEK-Orai1^{YFP} cells to identify other interactors of SPCA2C that might be related to Ca^{2+} homeostasis. The BioID screen also supports localization of SPCA2C to the ER as a primary function and confirmed the interaction with Orai1. In addition, the screen identified 71 (most stringent) to 263 (least stringent) putative SPCA2C interacting proteins for future analysis. These results strongly support a complex, yet significant role for SPCA2C in multiple Ca^{2+} regulating pathways.

ATP2C2^{HI} expression levels in PDTX lines had increased constitutive Ca^{2+} influx and ER Ca^{2+} stores, compared to *ATP2C2^{LO}* PDTX lines. However, although resting cytosolic Ca^{2+} levels were greater in *ATP2C2^{HI}* 01-048 cells compared to *ATP2C2^{LO}* L-NOR cells, there was no

difference between *ATP2C2*^{HI} 01-048 cells and *ATP2C2*^{LO} AO-IPC cells; which suggests that Ca^{2+} regulation in these cells may be influenced by differential expression of other Ca^{2+} regulators. Furthermore, since there is no reliable SPCA2C antibody available, it is difficult to assess if increased *Atp2c2* RNA transcript directly increases SPCA2 or SPCA2C protein abundance. Also, the assay did not distinguish whether full-length *ATP2C2* or *ATP2C2C* is expressed in the PDTX lines. The full-length or a longer isoform of SPCA2 may be expressed in the PDTX lines, which could produce an alternative function in these cells. Alternate isoforms of SPCA2 could be less effective at increasing cytosolic Ca^{2+} levels, as full-length SPCA2 was shown to increase cytosolic Ca^{2+} to a lesser degree compared to SPCA2C (chapter 2).

Over-expression of SPCA2C in 01-048 cells, which endogenously express relatively low, but not absent amounts of *Atp2c2*, increased cytosolic Ca^{2+} levels but not constitutive Ca^{2+} influx or ER Ca^{2+} stores. This is different than previous findings in HEK293A cells where SPCA2C over expression increased both cytosolic and ER stored Ca^{2+}. While this discrepancy could be due to SPCA2C localizing differently between 01-048 and HEK293A cells, intracellular SPCA2C localization analysis by co-IF did not differ from HEK293A cells. Alternatively, while these pancreatic cancer cells are derived from pancreatic acinar cells (Xu et al., 2019), they are pathologically enhanced cells with changes to their original expression levels of Ca^{2+} related proteins likely, which is evidenced by differential expression of *STIM1*, *TRPC3*, and *ATP2C1* between cells. Furthermore, the overall organization and function of Ca^{2+} signaling proteins may be changed. An example of this change is the fact that 01-048 cells did not respond to carbachol, an acetylcholine agonist, which should induce intracellular oscillatory Ca^{2+} signals. In an attempt

to resolve this issue, I examined SPCA2C over-expression in 266.6 cells as a physiological model of pancreatic acinar cells.

SPCA2C over-expression in the physiological pancreatic cell line, 266.6 cell line increased resting cytosolic Ca^{2+} levels. However, unlike in HEK293A cells, Ca^{2+} responses to treatment with TG were lower when SPCA2C was over-expressed. This suggests that over-expression of SPCA2C may decrease ER stored Ca^{2+} in 266.6 cells. However, when ER store-specific Ca^{2+} release was stimulated by carbachol, an acetylcholine receptor agonist that results in IP_3-mediated IP_3R activation, no difference in Ca^{2+} release from ER stores between 266.6 cells over-expressing SPCA2C or control GFP cells was observed. Note that there is already endogenous expression of SPCA2C in 266.6 cells, which could be masking any differences between the control and over-expression cells. Over-expression of SPCA2C may elicit a protective mechanism by the cell to ensure ER Ca^{2+} stores do not cause cellular distress.
For example, a novel ER Ca^{2+} channel encoded by the transmembrane and coiled-coil domains 1 (TMCO1) gene forms active tetrameric channels that extrude Ca^{2+} from the ER above a certain Ca^{2+} concentration, thereby preventing ER Ca^{2+} overload (Wang et al., 2016).

The unbiased screen for putative SPCA2C interacting protein partners identified pathways that reflect localization and function of SPCA2C to the ER. Bioinformatics analysis supported previous findings from Chapters 2 and 3 that SPCA2C localizes to the ER and GO cellular compartment analysis suggests that SPCA2C also localizes to vesicles. KEGG pathway analysis suggests a link to the SNARE complex pathway. These two findings suggest a role for SPCA2C in regulated exocytosis of enzymes in pancreatic acinar cells, as well as, Ca^{2+} regulation.

Indeed, Reactome pathway analysis of candidate interacting partners identified Ca^{2+} ion homeostasis as an enriched pathway, supporting our findings from previous cell experiments that SPCA2C is involved in cytosolic and ER Ca^{2+} levels. Furthermore, after excluding the BioID negative control proteins and common contaminants repository list, all 71 proteins identified by BioID were sorted based on protein class with 8.8% of proteins belonging to Ca^{2+} binding proteins. Among the list of 71 candidate proteins 9 were functionally characterized as binding Ca^{2+} directly or to be involved in Ca^{2+} homeostasis (Appendix table 1.2). To confirm an interaction between SPCA2C and candidates identified by the BioID screen other methods such as co-IP or frequency resonance energy transfer (FRET) could be used, followed by evaluation of the functional relevance of such an interaction via mutation. Following up on putative interactions identified by BioID analysis will be key in further elucidating the functional mechanisms of SPCA2C.

For example, among the 9 proteins identified, Aspartyl/asparaginyl beta-hydroxylase isoform 8 (ASPH) is of particular interest because it has been characterized as a membrane-bound Ca^{2+} sensing protein and structural component of the ER-plasma membrane junctions. ASPH regulates the activity of CRAC channels in T-cells (Srikanth et al., 2012). An interaction between SPCA2C and ASPH could be readily confirmed using co-IP in HEK293A cells.

RyR was also identified by the BioID assay. As discussed in section 1.4.1, RyR play an important role in shaping Ca^{2+} signals in pancreatic acinar cells. There have also been reports of RyR playing a role in activating Orai1-composed CRAC channels to influence Ca^{2+} signaling

and homeostasis (Lin et al., 2016). Therefore, the RyR is another interesting candidate, which should be confirmed by co-IP.

In conclusion, increased expression of SPCA2C in 266.6 cells, a model of pancreatic acinar cell physiology, suggests that it plays an important physiological role in regulating cytosolic Ca^{2+} levels and basal Ca^{2+} influx within these cells. In pancreatic pathology, *ATP2C2*^{HI} was associated with increases in constitutive Ca^{2+} influx and increased ER Ca^{2+} store levels in PDTX cell lines, suggesting that relative increases in endogenous expression of SPCA2 increases ER Ca^{2+} store levels and constitutive Ca^{2+} influx. Furthermore, this is the first evidence that SPCA2C may affect pathways of vesicle trafficking and enzyme exocytosis, which rely on Ca^{2+} signalling to function. Further studies are needed to confirm SPCA2C protein-protein interactions and the mechanism of SPCA2C's actions in these pathways.

Chapter 5

Conclusions and Discussion

5.1 Conclusions:

The following discoveries were made through my research presented in this thesis:

1. SPCA2C is transcribed from an alternative transcriptional start site.
2. The region upstream of *Atp2c2c* acts as a promoter, driving expression of SPCA2C.
3. *Atp2c2c* expression is significantly decreased after inducing pancreatitis in mice.
4. SPCA2C shows a more expansive area of localization in the cell compared to SPCA2, also localizing to the ER.
5. SPCA2C interacts with Orai1 and increases store-independent Ca^{2+} entry.
6. SPCA2C increases ER stored Ca^{2+} stores and Ca^{2+} influx across the plasma membrane after ER store depletion in HEK293A cells. These roles are independent of Orai1.
7. Patient-derived tumour xenograft (PDTX) lines from pancreatic tumours express variable levels of *ATP2C2*. These lines also express *TRPC3*, *STIM1*, and *ATP2C1*, but mRNA and protein levels are not correlated.
8. Relative levels of *ATP2C2* expression partially correlate to cytosolic Ca^{2+}, constitutive Ca^{2+} influx and ER Ca^{2+} levels. Exogenous SPCA2C over-expression increases cytosolic Ca^{2+} levels in an $ATP2C2^{LO}$ PDTX cell lines.
9. SPCA2C over-expression increases cytosolic Ca^{2+} and constitutive Ca^{2+} influx in 266.6 cells, a mouse pancreatic acinar cell line.
10. Candidate SPCA2C binding partners belong to pathways that regulate Ca^{2+} ion homeostasis and localize to the ER and secretory vesicles.

5.2 General Discussion

The purpose of this thesis was to determine the function of SPCA2C in Ca^{2+} homeostasis. Previous work on SPCA2C suggested roles in Ca^{2+} homeostasis that lie outside ATPase function. Since Ca^{2+} is a critical regulator of multiple cellular processes, and the pancreas relies on precise Ca^{2+} regulation, I functionally characterized SPCA2C in both pancreatic and non-pancreatic cells. My research shows that SPCA2C regulates cytosolic Ca^{2+} levels and contributes to pathways influencing ER Ca^{2+} levels. Through an unbiased screen, I identified a number of proteins that putatively interact with SPCA2C that will form the basis of future hypothesises and research projects. Combined, this work confirmed a functional importance and identified novel roles for SPCA2C in calcium biology.

5.2.1 The regulation of cytosolic Ca^{2+} levels by SPCA2C

The experiments in this thesis strongly support a role for SPCA2C in increasing cytosolic Ca^{2+} levels. In HEK293A cells, SPCA2C over-expression increased cytosolic levels independent of Orai1 expression. A Ca^{2+} regulatory role was also demonstrated in mouse acinar 266.6 cells, and the 01-048 PDTX cell line. The passage of Ca^{2+} across the plasma membrane cannot be due to Ca^{2+}ATPase activity as the C-terminal truncation of SPCA2C completely lacks the E1-E2 hydrolase domain, and several transmembrane domains containing a Ca^{2+} binding site. Although it is possible that the four remaining transmembrane domains of SPCA2C form a Ca^{2+} channel alone or after homo-multimerization, this scenario seems unlikely give the Ca^{2+} permeation pathways in full length Ca^{2+}ATPases is primarily formed by transmembrane helices outside the transmembrane domains retained in SPCA2C (Palmgren & Nissen, 2011). Therefore, SPCA2C must contribute to Ca^{2+} influx through alternative pathways.

Surprisingly, SPCA2C is able to increase cytosolic Ca^{2+} with limited localization to the plasma membrane. Most SPCA2C is localized to the ER or Golgi. This localization suggests SPCA2C activates Ca^{2+} channels on the plasma membrane to influence Ca^{2+} influx through communication between the ER and plasma membrane, possibly through closely apposed regions and/or junctional complexes. Such a model is supported by the putative protein interactors identified in the BioID screen, including Aspartyl/asparaginyl beta-hydroxylase (ASPH), which has shown to be a structural component of ER-plasma membrane junctions (Srikanth et al., 2012). Although the ability of SPCA2C to influence SICE initially appears to be dependent on Orai1, resting cytosolic Ca^{2+} levels were still elevated in HEK293A cells not expressing Orai1. Furthermore, cytosolic levels were also increased when SPCA2C was over-expressed 266.6 and 01-048 cells, which do not express Orai1. Therefore, this work suggests that SPCA2C constitutively increases cytosolic Ca^{2+} levels by either directly or indirectly regulating more than one Ca^{2+} channel on the plasma membrane, while primarily localizing to the ER.

5.2.2 SPCA2C's contribution to other Ca^{2+} regulating pathways including ER Ca^{2+} stores

In all cell types studied in this thesis, SPCA2C localizes more often to the ER, rather than the Golgi apparatus. ER-localized SPCA2C expression patterns are similar to localization previously documented in pancreatic acinar cells (Garside et al., 2010) and consistent with studies that examined localization of C-terminal truncations of SPCA2 (Jones, 1999). Furthermore, GO compartment analysis of proteins identified in the BioID experiment suggest localization of SPCA2C to the ER. Thus, there is strong evidence that the main function of SPCA2C is driven through localization to this subcellular compartment. Ca^{2+} release from the ER propagates all

global cellular signals (Berridge, 2007). For example, Ca^{2+} release from the ER is particularly important for exocytosis in pancreatic acinar cells, which relies on proper spatiotemporal global Ca^{2+} signals. Importantly, disruptions in ER Ca^{2+} release are strongly tied to pancreatic pathology (Zhou et al., 1996). Since my studies support a role for SPCA2C in regulating ER Ca^{2+} concentrations, this suggests that SPCA2C may be dysfunctional in pancreatic pathologies such as pancreatitis. In HEK293A cells, which do not express SPCA2 or SPCA2C, SPCA2C over-expression increases ER Ca^{2+} stores. However, in the pancreatic acinar 266.6 cells and the PTDX line 01-048 cell line, SPCA2C over-expression did not increase ER Ca^{2+} levels. This difference may be due to endogenous expression of SPCA2C or the full length SPCA2 in 266.6 and 01-048 cells. Over-expression of SPCA2C in cells that already express SPCA2C may not further increase functionality within the cell (*i.e.* increasing cytosolic and ER stores within the cell). In fact, artificially high CCK signalling can actually inhibit exocytosis (Roettger et al., 1997). Alternatively, the discrepancy could be due to mechanisms that protect against ER Ca^{2+} overload in these pancreatic cell types. Such mechanisms have been described previously to be mediated by transmembrane and coiled-coil domains 1 (TMCO1) protein, which forms an active channel to extrude Ca^{2+} when ER levels become too high (Wang et al., 2016).

My work provides strong support for a role for SPCA2C in pathways that exclude Orai1 and ATPase function. Several putative SPCA2C-interacting partners were identified using BioID. KEGG and GO analysis supported our Fura2 ratiometric imaging experiments, as it also suggests SPCA2C is involved in Ca^{2+} ion homeostasis in the ER. Furthermore, GO cellular compartment analysis identified vesicles and KEGG pathway analysis identified SNARE interactions involved in vesicular transport as enriched pathways based on a stringently refined protein candidate list.

These terms listed by the bioinformatics analysis of interaction candidates support a theory that SPCA2C might be involved in vesicle transport. Vesicle transport in pancreatic acinar cells is regulated by Ca^{2+} signalling and is very important to pancreatic physiology. Future studies should involve exploring the role of SPCA2C in pathways specific to Ca^{2+} mediated vesicle transport. For example, carbachol-induced exocytosis assays in SPCA2C knock-down or over-expression experiments could be done in 266.6 cells. These experiments could be followed up with exocytosis experiments in primary acinar cells from a pancreas-specific *Atp2c2c* knockout model.

5.2.3 Interacting partners of SPCA2C

This study confirmed interaction between SPCA2C and Orai1 in HEK293A cells and that the effect of SPCA2C on SICE in HEK293A cells can be Orai1-dependent. Despite the ability of SPCA2C to interact with Orai1, SPCA2C was able to increase cytosolic and ER stores independent of Orai1. Specifically, SPCA2C was able to increase cytosolic Ca^{2+} in 266.6 and 01-048, which also do not express Orai1. HEK293A cells, 266.6 and 01-048 cells all express TRPC3, a SOCE associated Ca^{2+} channel. TRPC3 plays a role in pancreatic pathology. Blocking TRPC3 in mouse models of induced pancreatitis decreases the severity of cellular injury (Hong et al., 2011; Kim et al., 2011; Vigont et al., 2015). Therefore, it is attractive to suggest SPCA2C enhances cytosolic Ca^{2+} levels using TRPC3 as an interacting protein partner. Unfortunately, HEK-Orai1^{YFP} cells do not expresses TRPC3 to detectable levels and so it was not identified as a candidate protein by the BioID experiment. Further experiments should verify an interaction between these two proteins. A candidate cell line to test this in would be the 266.6 cells as they represent acinar cells, express SPCA2C endogenously, and express high levels of TRPC3.

Although the BioID screen did not detect TRPC3, several other interesting potential interacting proteins were identified. Among a refined list of 71 candidates, 9 were functionally characterized as binding Ca^{2+} directly or to be involved in Ca^{2+} homeostasis. Of course, these interactions will have to be confirmed by other methods such as FRET or co-immunoprecipitation. HEK-Orai1^{YFP} cells were a good model for the first BioID experiment because they included an internal positive control that is Orai1. Furthermore, SPCA2C over-expression analysis first conducted in HEK293A cells lead us to believe SPCA2C was interacting with other endogenously expressed Ca^{2+} channels in these cells. Performing the BioID screen in these cells assisted in uncovering dozens of candidate interactors.

5.3 Study limitations and future directions

Through over-expression data, my work illustrates SPCA2C regulates Ca^{2+} homeostasis in multiple cell lines. However, overexpression of SPCA2C in acinar cells may limit the ability to determine SPCA2C's effect on the exocrine pancreas *in vivo*. My data suggests SPCA2C is important in regulating cytosolic and potentially ER Ca^{2+} levels, which would make it important for pancreatic acinar cell function. However, SPCA2C over-expression in pancreatic acinar cells *in vivo* may disrupt proper Ca^{2+} regulation by abnormally increasing calcium in cytosol and/or ER and acinar cells may undergo apoptosis or necrosis in response. This could lead to the onset of acute pancreatitis. SPCA2C expression is significantly decreased early in induced pancreatitis in mice, possibly due to a protective mechanism by cells to combat dysregulated Ca^{2+} levels and decrease injury. This also supports a scenario that over-expressing SPCA2C would increase the severity of pancreatitis. I attempted to address such a question by generating transgenic mice that would over-express SPCA2C specifically in pancreatic acinar cells. Although a number of potential founder mice were identified with a *Atp2c2c* transgene in their DNA, no *Atp2c2c*/SPCA2C^{FLAG} expression could be detected in isolated pancreatic tissue from these mice. In a second attempt to over-express SPCA2C *in vivo,* I used intrapancreatic ductal infusion of an adeno-associated virus carrying a

transgene to over express SPCA2C. However, again, I was unable to detect $SPCA2C^{FLAG}$ expression in protein isolated from these mice. In both cases, I suspect that the transgene was silenced *in vivo* and therefore not able to express $SPCA2C^{FLAG}$ to detectable levels. Since over-expression of SPCA2C *in vivo* proves to be a challenging route for further analysis, I think pancreas-specific *Atp2c2c* knockout models will be a critical next step to confirm the importance of SPCA2C in acinar cell function.

A conditional *Atp2c2c* knock-out mouse model will also be useful to follow up on the pathways identified by bioinformatic analysis of proximity protein candidates, which supports a role for SPCA2C in vesicular biology. To date, neither SPCA2 or SPCA2C has been studied within the context of vesicle maturation/transport or zymogen granule exocytosis in pancreatic acinar cells. Exocytosis assays from primary acinar cells isolated from an *Atp2c2c* knockout model in mice, as mentioned above, could be used to further explore a role for SPCA2C in vesicle transport or zymogen granule exocytosis in pancreatic acinar cells. RAB8A and VAS1, two proteins involved in vesicle transport and membrane fusion, were identified by the BioID analysis. Confirming an interaction between SPCA2C and these proteins by co-IP could help uncover the role of SPCA2C in this pathway. Other attractive protein interaction candidates were identified by BioID analysis; for example, coiled-coil domain-containing protein 47 (CCD47), which is involved in the regulation of Ca^{2+} homeostasis in the ER (Yamamoto et al., 2014). The information on CCD47 is limited, however, it remains in interesting candidate to investigate further. Initial screening using qRT-PCR can be done to determine if CCD47 is expressed to appreciable levels in pancreatic acinar cells. Additional experiments should include confirming an interaction between CCD47 and SPCA2C, as well as, examining the effect of an SPCA2C-CCD47 interaction on Ca^{2+} conductance, or ER Ca^{2+} store levels in cells.

We have identified a novel isoform of SPCA2 in the pancreas of mice, however, there is still limited data on SPCA2 isoforms found in humans. The DNA sequence similarity between SPCA2 human and mice is 84.7% conserved (determined by Clustal Omega; Sievers et al. 2011).

Nevertheless, to ensure that the functions I uncover using the mouse homolog of the SPCA2C isoform is translatable to humans, when and where SPCA2C is expressed in human tissues should be analyzed.

5.4 Conclusion

This study defined a pancreas-specific isoform of SPCA2, termed SPCA2C, which is transcribed from an alternative transcriptional start site and functions in the ER and possibly plasma membrane region to affect multiple Ca^{2+} signalling pathways.

References

Abbasi, S., & Schild-Poulter, C. (2019). Mapping the Ku Interactome Using Proximity-Dependent Biotin Identification in Human Cells. *Journal of Proteome Research*, *18*(3), 1064–1077. https://doi.org/10.1021/acs.jproteome.8b00771

Ahuja, M., Schwartz, D. M., Tandon, M., Son, A., Zeng, M., Swaim, W., … Muallem, S. (2017). Orai1-Mediated Antimicrobial Secretion from Pancreatic Acini Shapes the Gut Microbiome and Regulates Gut Innate Immunity. *Cell Metabolism*, *25*(3), 635–646. https://doi.org/10.1016/j.cmet.2017.02.007

Altshuler, I., Vaillant, J. J., Xu, S., & Cristescu, M. E. (2012). The evolutionary history of sarco(endo)plasmic calcium ATPase (SERCA). *PloS One*, *7*(12), e52617–e52617. https://doi.org/10.1371/journal.pone.0052617

Anantamongkol, U., Takemura, H., Suthiphongchai, T., Krishnamra, N., & Horio, Y. (2007). Regulation of Ca2+ mobilization by prolactin in mammary gland cells: possible role of secretory pathway Ca2+-ATPase type 2. *Biochemical and Biophysical Research Communications*, *352*(2), 537–542. https://doi.org/10.1016/j.bbrc.2006.11.055

Anderson, L. N., Cotterchio, M., & Gallinger, S. (2009). Lifestyle, dietary, and medical history factors associated with pancreatic cancer risk in Ontario, Canada. *Cancer Causes & Control : CCC*, *20*(6), 825–834. https://doi.org/10.1007/s10552-009-9303-5

Antebi, A., & Fink, G. R. (1992). The yeast Ca(2+)-ATPase homologue, PMR1, is required for normal Golgi function and localizes in a novel Golgi-like distribution. *Molecular Biology of the Cell*, *3*(6), 633–654. https://doi.org/10.1091/mbc.3.6.633

Arredouani, A., Guiot, Y., Jonas, J.-C., Liu, L. H., Nenquin, M., Pertusa, J. A., … Gilon, P. (2002). SERCA3 ablation does not impair insulin secretion but suggests distinct roles of

different sarcoendoplasmic reticulum Ca(2+) pumps for Ca(2+) homeostasis in pancreatic beta-cells. *Diabetes*, *51*(11), 3245–3253. https://doi.org/10.2337/diabetes.51.11.3245

Badaoui, M., Mimsy-Julienne, C., Saby, C., Van Gulick, L., Peretti, M., Jeannesson, P., … Ouadid-Ahidouch, H. (2018). Collagen type 1 promotes survival of human breast cancer cells by overexpressing Kv10.1 potassium and Orai1 calcium channels through DDR1-dependent pathway. *Oncotarget*, *9*(37), 24653–24671. https://doi.org/10.18632/oncotarget.19065

Baughman, J. M., Perocchi, F., Girgis, H. S., Plovanich, M., Belcher-Timme, C. A., Sancak, Y., … Mootha, V. K. (2011). Integrative genomics identifies MCU as an essential component of the mitochondrial calcium uniporter. *Nature*, *476*(7360), 341–345. https://doi.org/10.1038/nature10234

Beauvois, M. C., Arredouani, A., Jonas, J.-C., Rolland, J.-F., Schuit, F., Henquin, J.-C., & Gilon, P. (2004). Atypical Ca2+-induced Ca2+ release from a sarco-endoplasmic reticulum Ca2+-ATPase 3-dependent Ca2+ pool in mouse pancreatic beta-cells. *The Journal of Physiology*, *559*(Pt 1), 141–156. https://doi.org/10.1113/jphysiol.2004.067454

Berridge, M J, Lipp, P., & Bootman, M. D. (2000). The versatility and universality of calcium signalling. *Nature Reviews. Molecular Cell Biology*, *1*(1), 11–21. https://doi.org/10.1038/35036035

Berridge, Michael John. (2007). Calcium signalling, a spatiotemporal phenomenon. In J. Krebs & M. B. T.-N. C. B. Michalak (Eds.), *Calcium* (Vol. 41, pp. 485–502). Elsevier. https://doi.org/https://doi.org/10.1016/S0167-7306(06)41019-X

Bezprozvanny, I., Watras, J., & Ehrlich, B. E. (1991). Bell-shaped calcium-response curves of Ins(1,4,5)P3- and calcium-gated channels from endoplasmic reticulum of cerebellum.

Nature, *351*(6329), 751–754. https://doi.org/10.1038/351751a0

Brini, M., Cali, T., Ottolini, D., & Carafoli, E. (2013). The plasma membrane calcium pump in health and disease. *The FEBS Journal*, *280*(21), 5385–5397. https://doi.org/10.1111/febs.12193

Bruce, J. I. E. (2013). PMCA. https://doi.org/10.3998/panc.2013.7

Burnham, D. B., McChesney, D. J., Thurston, K. C., & Williams, J. A. (1984). Interaction of cholecystokinin and vasoactive intestinal polypeptide on function of mouse pancreatic acini in vitro. *The Journal of Physiology*, *349*, 475–482. Retrieved from http://www.ncbi.nlm.nih.gov/pmc/articles/PMC1199349/

Camello, P., Gardner, J., Petersen, O. H., & Tepikin, A. V. (1996). Calcium dependence of calcium extrusion and calcium uptake in mouse pancreatic acinar cells. *The Journal of Physiology*, *490 (Pt 3*, 585–593. https://doi.org/10.1113/jphysiol.1996.sp021169

Chantome, A., Potier-Cartereau, M., Clarysse, L., Fromont, G., Marionneau-Lambot, S., Gueguinou, M., … Vandier, C. (2013). Pivotal role of the lipid Raft SK3-Orai1 complex in human cancer cell migration and bone metastases. *Cancer Research*, *73*(15), 4852–4861. https://doi.org/10.1158/0008-5472.CAN-12-4572

Churchill, G. C., Okada, Y., Thomas, J. M., Genazzani, A. A., Patel, S., & Galione, A. (2002). NAADP Mobilizes Ca2+ from Reserve Granules, Lysosome-Related Organelles, in Sea Urchin Eggs. *Cell*, *111*(5), 703–708. https://doi.org/https://doi.org/10.1016/S0092-8674(02)01082-6

Criddle, D. N., Murphy, J., Fistetto, G., Barrow, S., Tepikin, A. V, Neoptolemos, J. P., … Petersen, O. H. (2006). Fatty acid ethyl esters cause pancreatic calcium toxicity via inositol trisphosphate receptors and loss of ATP synthesis. *Gastroenterology*, *130*(3), 781–793.

https://doi.org/10.1053/j.gastro.2005.12.031

Cross, B. M., Hack, A., Reinhardt, T. A., & Rao, R. (2013). SPCA2 regulates Orai1 trafficking and store independent Ca2+ entry in a model of lactation. *PloS One*, *8*(6), e67348. https://doi.org/10.1371/journal.pone.0067348; 10.1371/journal.pone.0067348

Csordas, G., Golenar, T., Seifert, E. L., Kamer, K. J., Sancak, Y., Perocchi, F., … Hajnoczky, G. (2013). MICU1 controls both the threshold and cooperative activation of the mitochondrial Ca(2)(+) uniporter. *Cell Metabolism*, *17*(6), 976–987. https://doi.org/10.1016/j.cmet.2013.04.020

Dang, D., Prasad, H., & Rao, R. (2017). Secretory pathway Ca(2+) -ATPases promote in vitro microcalcifications in breast cancer cells. *Molecular Carcinogenesis*, *56*(11), 2474–2485. https://doi.org/10.1002/mc.22695

Deng, H., & Xiao, H. (2017). The role of the ATP2C1 gene in Hailey-Hailey disease. *Cellular and Molecular Life Sciences : CMLS*, *74*(20), 3687–3696. https://doi.org/10.1007/s00018-017-2544-7

Dode, L., Andersen, J. P., Vanoevelen, J., Raeymaekers, L., Missiaen, L., Vilsen, B., & Wuytack, F. (2006). Dissection of the functional differences between human secretory pathway Ca2+/Mn2+-ATPase (SPCA) 1 and 2 isoenzymes by steady-state and transient kinetic analyses. *The Journal of Biological Chemistry*, *281*(6), 3182–3189. https://doi.org/10.1074/jbc.M511547200

Dolai S., Liang T., Cosen-Binker L. I., Lam P. P. L., G. H. Y. (2012). Regulation of Physiologic and Pathologic Exocytosis in Pancreatic Acinar Cells. https://doi.org/10.3998/panc.2012.12

Dong, X.-P., Wang, X., & Xu, H. (2010). TRP channels of intracellular membranes. *Journal of Neurochemistry*, *113*(2), 313–328. https://doi.org/10.1111/j.1471-4159.2010.06626.x

Dormer, R. L., & Williams, J. A. (1981). Secretagogue-induced changes in subcellular Ca2+ distribution in isolated pancreatic acini. *The American Journal of Physiology*, *240*(2), G130-40.

Faddy, H. M., Smart, C. E., Xu, R., Lee, G. Y., Kenny, P. A., Feng, M., … Monteith, G. R. (2008). Localization of plasma membrane and secretory calcium pumps in the mammary gland. *Biochemical and Biophysical Research Communications*, *369*(3), 977–981. https://doi.org/10.1016/j.bbrc.2008.03.003; 10.1016/j.bbrc.2008.03.003

Feng, M., Grice, D. M., Faddy, H. M., Nguyen, N., Leitch, S., Wang, Y., … Rao, R. (2010). Store-independent activation of Orai1 by SPCA2 in mammary tumors. *Cell*, *143*(1), 84–98. https://doi.org/10.1016/j.cell.2010.08.040

Feske, S., Gwack, Y., Prakriya, M., Srikanth, S., Puppel, S.-H., Tanasa, B., … Rao, A. (2006). A mutation in Orai1 causes immune deficiency by abrogating CRAC channel function. *Nature*, *441*(7090), 179–185. https://doi.org/10.1038/nature04702

Finch, E. A., Turner, T. J., & Goldin, S. M. (1991). Calcium as a coagonist of inositol 1,4,5-trisphosphate-induced calcium release. *Science (New York, N.Y.)*, *252*(5004), 443–446.

Futatsugi, A., Nakamura, T., Yamada, M. K., Ebisui, E., Nakamura, K., Uchida, K., … Mikoshiba, K. (2005). IP3 receptor types 2 and 3 mediate exocrine secretion underlying energy metabolism. *Science (New York, N.Y.)*, *309*(5744), 2232–2234. https://doi.org/10.1126/science.1114110

Gaisano, H. Y., Ghai, M., Malkus, P. N., Sheu, L., Bouquillon, A., Bennett, M. K., & Trimble, W. S. (1996). Distinct cellular locations of the syntaxin family of proteins in rat pancreatic acinar cells. *Molecular Biology of the Cell*, *7*(12), 2019–2027.

Gaisano, H. Y., Lutz, M. P., Leser, J., Sheu, L., Lynch, G., Tang, L., … Salapatek, A. M. (2001).

Supramaximal cholecystokinin displaces Munc18c from the pancreatic acinar basal surface, redirecting apical exocytosis to the basal membrane. *The Journal of Clinical Investigation*, *108*(11), 1597–1611. https://doi.org/10.1172/JCI9110

Galione, A. (2011). NAADP Receptors. *Cold Spring Harbor Perspectives in Biology* , *3*(1). https://doi.org/10.1101/cshperspect.a004036

Galione, A. (2015). A primer of NAADP-mediated Ca2+ signalling: From sea urchin eggs to mammalian cells. *Cell Calcium*, *58*(1), 27–47. https://doi.org/https://doi.org/10.1016/j.ceca.2014.09.010

Garside, V. C., Kowalik, A. S., Johnson, C. L., DiRenzo, D., Konieczny, S. F., & Pin, C. L. (2010). MIST1 regulates the pancreatic acinar cell expression of Atp2c2, the gene encoding secretory pathway calcium ATPase 2. *Experimental Cell Research*, *316*(17), 2859–2870. https://doi.org/10.1016/j.yexcr.2010.06.014; 10.1016/j.yexcr.2010.06.014

GENAZZANI, A. A., & GALIONE, A. (1996). Nicotinic acid-adenine dinucleotide phosphate mobilizes Ca2+ from a thapsigargin-insensitive pool. *Biochemical Journal*, *315*(3), 721–725. https://doi.org/10.1042/bj3150721

Gerasimenko, J. V, Maruyama, Y., Yano, K., Dolman, N. J., Tepikin, A. V, Petersen, O. H., & Gerasimenko, O. V. (2003). NAADP mobilizes Ca2+ from a thapsigargin-sensitive store in the nuclear envelope by activating ryanodine receptors. *The Journal of Cell Biology*, *163*(2), 271–282. https://doi.org/10.1083/jcb.200306134

Gerasimenko, J. V, Sherwood, M., Tepikin, A. V, Petersen, O. H., & Gerasimenko, O. V. (2006). NAADP, cADPR and IP₃ all release Ca²⁺ from the endoplasmic reticulum and an acidic store in the secretory granule area. *Journal of Cell Science*, *119*(2), 226 LP – 238. https://doi.org/10.1242/jcs.02721

Giovannucci, D. R., Groblewski, G. E., Sneyd, J., & Yule, D. I. (2000). Targeted phosphorylation of inositol 1,4,5-trisphosphate receptors selectively inhibits localized Ca2+ release and shapes oscillatory Ca2+ signals. *The Journal of Biological Chemistry*, *275*(43), 33704–33711. https://doi.org/10.1074/jbc.M004278200

Gonzalez, A., Schulz, I., & Schmid, A. (2000). Agonist-evoked mitochondrial Ca2+ signals in mouse pancreatic acinar cells. *The Journal of Biological Chemistry*, *275*(49), 38680–38686. https://doi.org/10.1074/jbc.M005667200

Gunderson, F. Q., Merkhofer, E. C., & Johnson, T. L. (2011). Dynamic histone acetylation is critical for cotranscriptional spliceosome assembly and spliceosomal rearrangements. *Proceedings of the National Academy of Sciences of the United States of America*, *108*(5), 2004–2009. https://doi.org/10.1073/pnas.1011982108

Halangk, W., Lerch, M. M., Brandt-Nedelev, B., Roth, W., Ruthenbuerger, M., Reinheckel, T., … Deussing, J. (2000). Role of cathepsin B in intracellular trypsinogen activation and the onset of acute pancreatitis. *The Journal of Clinical Investigation*, *106*(6), 773–781. https://doi.org/10.1172/JCI9411

He, H., Lam, M., McCormick, T. S., & Distelhorst, C. W. (1997). Maintenance of Calcium Homeostasis in the Endoplasmic Reticulum by Bcl-2. *The Journal of Cell Biology*, *138*(6), 1219 LP – 1228. https://doi.org/10.1083/jcb.138.6.1219

He, W., & Hu, Z. (2012). The role of the Golgi-resident SPCA Ca(2)(+)/Mn(2)(+) pump in ionic homeostasis and neural function. *Neurochemical Research*, *37*(3), 455–468. https://doi.org/10.1007/s11064-011-0644-6

Hong, J. H., Li, Q., Kim, M. S., Shin, D. M., Feske, S., Birnbaumer, L., … Muallem, S. (2011). Polarized but differential localization and recruitment of STIM1, Orai1 and TRPC channels

in secretory cells. *Traffic (Copenhagen, Denmark)*, *12*(2), 232–245. https://doi.org/10.1111/j.1600-0854.2010.01138.x

Hooper, R., & Patel, S. (2012). NAADP on target. *Advances in Experimental Medicine and Biology*, *740*, 325–347. https://doi.org/10.1007/978-94-007-2888-2_14

Hou, X., Pedi, L., Diver, M. M., & Long, S. B. (2012). Crystal structure of the calcium release-activated calcium channel Orai. *Science (New York, N.Y.)*, *338*(6112), 1308–1313. https://doi.org/10.1126/science.1228757

Hurwitz, S. (1996). Homeostatic control of plasma calcium concentration. *Critical Reviews in Biochemistry and Molecular Biology*, *31*(1), 41–100. https://doi.org/10.3109/10409239609110575

Husain, S. Z., Prasad, P., Grant, W. M., Kolodecik, T. R., Nathanson, M. H., & Gorelick, F. S. (2005). The ryanodine receptor mediates early zymogen activation in pancreatitis. *Proceedings of the National Academy of Sciences of the United States of America*, *102*(40), 14386–14391. https://doi.org/10.1073/pnas.0503215102

Jenkins, J., Papkovsky, D. B., & Dmitriev, R. I. (2016). The Ca2+/Mn2+-transporting SPCA2 pump is regulated by oxygen and cell density in colon cancer cells. *The Biochemical Journal*, *473*(16), 2507–2518. https://doi.org/10.1042/BCJ20160477

Johnson, C. L., Weston, J. Y., Chadi, S. A., Fazio, E. N., Huff, M. W., Kharitonenkov, A., … Pin, C. L. (2009). Fibroblast growth factor 21 reduces the severity of cerulein-induced pancreatitis in mice. *Gastroenterology*, *137*(5), 1795–1804. https://doi.org/10.1053/j.gastro.2009.07.064

Jones, D. T. (1999). Protein secondary structure prediction based on position-specific scoring matrices. *Journal of Molecular Biology*, *292*(2), 195–202.

https://doi.org/10.1006/jmbi.1999.3091

Kang, R., Lotze, M. T., Zeh, H. J., Billiar, T. R., & Tang, D. (2014). Cell death and DAMPs in acute pancreatitis. *Molecular Medicine (Cambridge, Mass.)*, *20*, 466–477. https://doi.org/10.2119/molmed.2014.00117

Kasai, H., Li, Y. X., & Miyashita, Y. (1993). Subcellular distribution of Ca2+ release channels underlying Ca2+ waves and oscillations in exocrine pancreas. *Cell*, *74*(4), 669–677. https://doi.org/10.1016/0092-8674(93)90514-q

Kim, D. I., & Roux, K. J. (2016). Filling the Void: Proximity-Based Labeling of Proteins in Living Cells. *Trends in Cell Biology*, *26*(11), 804–817. https://doi.org/http://dx.doi.org/10.1016/j.tcb.2016.09.004

Kim, M. S., Lee, K. P., Yang, D., Shin, D. M., Abramowitz, J., Kiyonaka, S., … Muallem, S. (2011). Genetic and pharmacologic inhibition of the Ca2+ influx channel TRPC3 protects secretory epithelia from Ca2+-dependent toxicity. *Gastroenterology*, *140*(7), 2107–2115, 2115.e1-4. https://doi.org/10.1053/j.gastro.2011.02.052

Kowalik, A. S., Johnson, C. L., Chadi, S. A., Weston, J. Y., Fazio, E. N., & Pin, C. L. (2007). Mice lacking the transcription factor Mist1 exhibit an altered stress response and increased sensitivity to caerulein-induced pancreatitis. *American Journal of Physiology.Gastrointestinal and Liver Physiology*, *292*(4), G1123-32. https://doi.org/10.1152/ajpgi.00512.2006

Kruger, B., Albrecht, E., & Lerch, M. M. (2000). The role of intracellular calcium signaling in premature protease activation and the onset of pancreatitis. *The American Journal of Pathology*, *157*(1), 43–50. https://doi.org/10.1016/S0002-9440(10)64515-4

Kuhlbrandt, W. (2004). Biology, structure and mechanism of P-type ATPases. *Nature Reviews.*

Molecular Cell Biology, *5*(4), 282–295. https://doi.org/10.1038/nrm1354

Lee, M. G., Xu, X., Zeng, W., Diaz, J., Wojcikiewicz, R. J., Kuo, T. H., … Muallem, S. (1997). Polarized expression of Ca2+ channels in pancreatic and salivary gland cells. Correlation with initiation and propagation of [Ca2+]i waves. *The Journal of Biological Chemistry*, *272*(25), 15765–15770.

Leite, M. F., Dranoff, J. A., Gao, L., & Nathanson, M. H. (1999). Expression and subcellular localization of the ryanodine receptor in rat pancreatic acinar cells. *The Biochemical Journal*, *337 (Pt 2*, 305–309.

Li, J., Zhou, R., Zhang, J., & Li, Z.-F. (2014). Calcium signaling of pancreatic acinar cells in the pathogenesis of pancreatitis. *World Journal of Gastroenterology : WJG*, *20*(43), 16146–16152. https://doi.org/10.3748/wjg.v20.i43.16146

Li Wen, Rajarshi Mukherjee, Wei Huang, R. S. (2016). Calcium signaling, mitochondria and acute pancreatitis: avenues for therapy. https://doi.org/10.3998/panc.2016.15

Lin, A. H. Y., Sun, H., Paudel, O., Lin, M.-J., & Sham, J. S. K. (2016). Conformation of ryanodine receptor-2 gates store-operated calcium entry in rat pulmonary arterial myocytes. *Cardiovascular Research*, *111*(1), 94–104. https://doi.org/10.1093/cvr/cvw067

Liou, J., Kim, M. L., Heo, W. Do, Jones, J. T., Myers, J. W., Ferrell, J. E. J., & Meyer, T. (2005). STIM is a Ca2+ sensor essential for Ca2+-store-depletion-triggered Ca2+ influx. *Current Biology : CB*, *15*(13), 1235–1241. https://doi.org/10.1016/j.cub.2005.05.055

Lloyd-Evans, E., Morgan, A. J., He, X., Smith, D. A., Elliot-Smith, E., Sillence, D. J., … Platt, F. M. (2008). Niemann-Pick disease type C1 is a sphingosine storage disease that causes deregulation of lysosomal calcium. *Nature Medicine*, *14*(11), 1247–1255. https://doi.org/10.1038/nm.1876

Longnecker, D. S. (2014). Anatomy and Histology of the Pancreas. https://doi.org/10.3998/panc.2014.3

Luik, R. M., Wu, M. M., Buchanan, J., & Lewis, R. S. (2006). The elementary unit of store-operated Ca2+ entry: local activation of CRAC channels by STIM1 at ER-plasma membrane junctions. *The Journal of Cell Biology*, *174*(6), 815–825. https://doi.org/10.1083/jcb.200604015

Luo, X., Shin, D. M., Wang, X., Konieczny, S. F., & Muallem, S. (2005). Aberrant localization of intracellular organelles, Ca2+ signaling, and exocytosis in Mist1 null mice. *The Journal of Biological Chemistry*, *280*(13), 12668–12675. https://doi.org/10.1074/jbc.M411973200

Luzio, J. P., Pryor, P. R., & Bright, N. A. (2007). Lysosomes: fusion and function. *Nature Reviews Molecular Cell Biology*, *8*(8), 622–632. https://doi.org/10.1038/nrm2217

Mallilankaraman, K., Doonan, P., Cardenas, C., Chandramoorthy, H. C., Muller, M., Miller, R., … Madesh, M. (2012). MICU1 is an essential gatekeeper for MCU-mediated mitochondrial Ca(2+) uptake that regulates cell survival. *Cell*, *151*(3), 630–644. https://doi.org/10.1016/j.cell.2012.10.011

Mareninova, O. A., Sung, K.-F., Hong, P., Lugea, A., Pandol, S. J., Gukovsky, I., & Gukovskaya, A. S. (2006). Cell death in pancreatitis: caspases protect from necrotizing pancreatitis. *The Journal of Biological Chemistry*, *281*(6), 3370–3381. https://doi.org/10.1074/jbc.M511276200

Matozaki, T., Sakamoto, C., Nishisaki, H., Suzuki, T., Wada, K., Matsuda, K., … Kasuga, M. (1991). Cholecystokinin inhibits phosphatidylcholine synthesis via a Ca(2+)-calmodulin-dependent pathway in isolated rat pancreatic acini. A possible mechanism for diacylglycerol accumulation. *The Journal of Biological Chemistry*, *266*(33), 22246–22253.

McGuffin, L. J., Bryson, K., & Jones, D. T. (2000). The PSIPRED protein structure prediction server. *Bioinformatics (Oxford, England)*, *16*(4), 404–405.

Meda, P., Findlay, I., Kolod, E., Orci, L., & Petersen, O. H. (1983). Short and reversible uncoupling evokes little change in the gap junctions of pancreatic acinar cells. *Journal of Ultrastructure Research*, *83*(1), 69–84. https://doi.org/10.1016/s0022-5320(83)90066-7

Mehus, A. A., Anderson, R. H., & Roux, K. J. (2016). Chapter One - BioID Identification of Lamin-Associated Proteins. In K. L. Wilson & A. B. T.-M. in E. Sonnenberg (Eds.), *Intermediate Filament Associated Proteins* (Vol. 569, pp. 3–22). Academic Press. https://doi.org/https://doi.org/10.1016/bs.mie.2015.08.008

Mignen, O., Thompson, J. L., & Shuttleworth, T. J. (2008). Both Orai1 and Orai3 are essential components of the arachidonate-regulated Ca2+-selective (ARC) channels. *The Journal of Physiology*, *586*(1), 185–195. https://doi.org/10.1113/jphysiol.2007.146258

Mogami, H., Nakano, K., Tepikin, A. V, & Petersen, O. H. (1997). Ca2+ flow via tunnels in polarized cells: recharging of apical Ca2+ stores by focal Ca2+ entry through basal membrane patch. *Cell*, *88*(1), 49–55.

Mukherjee, R., Mareninova, O. A., Odinokova, I. V, Huang, W., Murphy, J., Chvanov, M., … Sutton, R. (2016). Mechanism of mitochondrial permeability transition pore induction and damage in the pancreas: inhibition prevents acute pancreatitis by protecting production of ATP. *Gut*, *65*(8), 1333–1346. https://doi.org/10.1136/gutjnl-2014-308553

Murphy, J. A., Criddle, D. N., Sherwood, M., Chvanov, M., Mukherjee, R., McLaughlin, E., … Sutton, R. (2008). Direct activation of cytosolic Ca2+ signaling and enzyme secretion by cholecystokinin in human pancreatic acinar cells. *Gastroenterology*, *135*(2), 632–641. https://doi.org/10.1053/j.gastro.2008.05.026

Nathanson, M. H., Padfield, P. J., O'Sullivan, A. J., Burgstahler, A. D., & Jamieson, J. D. (1992). Mechanism of Ca2+ wave propagation in pancreatic acinar cells. *The Journal of Biological Chemistry*, *267*(25), 18118–18121.

Niederau, C., & Grendell, J. H. (1988). Intracellular vacuoles in experimental acute pancreatitis in rats and mice are an acidified compartment. *The Journal of Clinical Investigation*, *81*(1), 229–236. https://doi.org/10.1172/JCI113300

Okunade, G. W., Miller, M. L., Azhar, M., Andringa, A., Sanford, L. P., Doetschman, T., … Shull, G. E. (2007). Loss of the Atp2c1 secretory pathway Ca(2+)-ATPase (SPCA1) in mice causes Golgi stress, apoptosis, and midgestational death in homozygous embryos and squamous cell tumors in adult heterozygotes. *The Journal of Biological Chemistry*, *282*(36), 26517–26527. https://doi.org/10.1074/jbc.M703029200

Ong, H. L., Cheng, K. T., Liu, X., Bandyopadhyay, B. C., Paria, B. C., Soboloff, J., … Ambudkar, I. S. (2007). Dynamic assembly of TRPC1-STIM1-Orai1 ternary complex is involved in store-operated calcium influx. Evidence for similarities in store-operated and calcium release-activated calcium channel components. *The Journal of Biological Chemistry*, *282*(12), 9105–9116. https://doi.org/10.1074/jbc.M608942200

Ornitz, D. M., Palmiter, R. D., Hammer, R. E., Brinster, R. L., Swift, G. H., & MacDonald, R. J. (1985). Specific expression of an elastase-human growth hormone fusion gene in pancreatic acinar cells of transgenic mice. *Nature*, *313*(6003), 600–602. https://doi.org/10.1038/313600a0

Osipchuk, Y. V, Wakui, M., Yule, D. I., Gallacher, D. V, & Petersen, O. H. (1990). Cytoplasmic Ca2+ oscillations evoked by receptor stimulation, G-protein activation, internal application of inositol trisphosphate or Ca2+: simultaneous microfluorimetry and Ca2+ dependent Cl-

current recording in single pancreatic acinar cells. *The EMBO Journal*, *9*(3), 697–704.

Palmgren, M. G., & Nissen, P. (2011). P-type ATPases. *Annual Review of Biophysics*, *40*, 243–266. https://doi.org/10.1146/annurev.biophys.093008.131331

Pandol, S. J., Schoeffield, M. S., Fimmel, C. J., & Muallem, S. (1987). The agonist-sensitive calcium pool in the pancreatic acinar cell. Activation of plasma membrane Ca2+ influx mechanism. *The Journal of Biological Chemistry*, *262*(35), 16963–16968.

Park, M. K., Ashby, M. C., Erdemli, G., Petersen, O. H., & Tepikin, A. V. (2001). Perinuclear, perigranular and sub-plasmalemmal mitochondria have distinct functions in the regulation of cellular calcium transport. *The EMBO Journal*, *20*(8), 1863–1874. https://doi.org/10.1093/emboj/20.8.1863

Patel, S., Joseph, S. K., & Thomas, A. P. (1999). Molecular properties of inositol 1,4,5-trisphosphate receptors. *Cell Calcium*, *25*(3), 247–264. https://doi.org/10.1054/ceca.1999.0021

Patterson, R. L., Boehning, D., & Snyder, S. H. (2004). Inositol 1,4,5-trisphosphate receptors as signal integrators. *Annual Review of Biochemistry*, *73*, 437–465. https://doi.org/10.1146/annurev.biochem.73.071403.161303

Penny, C. J., Kilpatrick, B. S., Eden, E. R., & Patel, S. (2015). Coupling acidic organelles with the ER through Ca2+ microdomains at membrane contact sites. *Cell Calcium*, *58*(4), 387–396. https://doi.org/https://doi.org/10.1016/j.ceca.2015.03.006

Pestov, N. B., Dmitriev, R. I., Kostina, M. B., Korneenko, T. V, Shakhparonov, M. I., & Modyanov, N. N. (2012). Structural evolution and tissue-specific expression of tetrapod-specific second isoform of secretory pathway Ca2+-ATPase. *Biochemical and Biophysical Research Communications*, *417*(4), 1298–1303. https://doi.org/10.1016/j.bbrc.2011.12.135;

10.1016/j.bbrc.2011.12.135

Pin, C. L., Rukstalis, J. M., Johnson, C., & Konieczny, S. F. (2001). The bHLH transcription factor Mist1 is required to maintain exocrine pancreas cell organization and acinar cell identity. *The Journal of Cell Biology*, *155*(4), 519–530. https://doi.org/10.1083/jcb.200105060

Plovanich, M., Bogorad, R. L., Sancak, Y., Kamer, K. J., Strittmatter, L., Li, A. A., … Mootha, V. K. (2013). MICU2, a paralog of MICU1, resides within the mitochondrial uniporter complex to regulate calcium handling. *PloS One*, *8*(2), e55785. https://doi.org/10.1371/journal.pone.0055785

Ponnappa, B. C., Dormer, R. L., & Williams, J. A. (1981). Characterization of an ATP-dependent Ca2+ uptake system in mouse pancreatic microsomes. *The American Journal of Physiology*, *240*(2), G122-9. https://doi.org/10.1152/ajpgi.1981.240.2.G122

Prakriya, M., Feske, S., Gwack, Y., Srikanth, S., Rao, A., & Hogan, P. G. (2006). Orai1 is an essential pore subunit of the CRAC channel. *Nature*, *443*(7108), 230–233. https://doi.org/10.1038/nature05122

Pralong, W. F., Wollheim, C. B., & Bruzzone, R. (1988). Measurement of cytosolic free Ca2+ in individual pancreatic acini. *FEBS Letters*, *242*(1), 79–84.

Prasad, V., Okunade, G. W., Miller, M. L., & Shull, G. E. (2004). Phenotypes of SERCA and PMCA knockout mice. *Biochemical and Biophysical Research Communications*, *322*(4), 1192–1203. https://doi.org/10.1016/j.bbrc.2004.07.156

Rizzuto, R, Pinton, P., Carrington, W., Fay, F. S., Fogarty, K. E., Lifshitz, L. M., … Pozzan, T. (1998). Close contacts with the endoplasmic reticulum as determinants of mitochondrial Ca2+ responses. *Science (New York, N.Y.)*, *280*(5370), 1763–1766.

Rizzuto, Rosario, De Stefani, D., Raffaello, A., & Mammucari, C. (2012). Mitochondria as sensors and regulators of calcium signalling. *Nature Reviews Molecular Cell Biology*, *13*(9), 566–578. https://doi.org/10.1038/nrm3412

Rogers, T. B., Inesi, G., Wade, R., & Lederer, W. J. (1995). Use of thapsigargin to study Ca2+ homeostasis in cardiac cells. *Bioscience Reports*, *15*(5), 341–349. https://doi.org/10.1007/bf01788366

Ronco, V., Potenza, D. M., Denti, F., Vullo, S., Gagliano, G., Tognolina, M., … Moccia, F. (2015). A novel Ca2+-mediated cross-talk between endoplasmic reticulum and acidic organelles: Implications for NAADP-dependent Ca2+ signalling. *Cell Calcium*, *57*(2), 89–100. https://doi.org/https://doi.org/10.1016/j.ceca.2015.01.001

Roos, J., DiGregorio, P. J., Yeromin, A. V, Ohlsen, K., Lioudyno, M., Zhang, S., … Stauderman, K. A. (2005). STIM1, an essential and conserved component of store-operated Ca2+ channel function. *The Journal of Cell Biology*, *169*(3), 435–445. https://doi.org/10.1083/jcb.200502019

Roux, K. J., Kim, D. I., & Burke, B. (2013). BioID: a screen for protein-protein interactions. *Current Protocols in Protein Science*, *74*, Unit 19.23. https://doi.org/10.1002/0471140864.ps1923s74

Roux, K. J., Kim, D. I., Raida, M., & Burke, B. (2012). A promiscuous biotin ligase fusion protein identifies proximal and interacting proteins in mammalian cells. *The Journal of Cell Biology*, *196*(6), 801–810. https://doi.org/10.1083/jcb.201112098

Rudolph, H. K., Antebi, A., Fink, G. R., Buckley, C. M., Dorman, T. E., LeVitre, J., … Moir, D. T. (1989). The yeast secretory pathway is perturbed by mutations in PMR1, a member of a Ca2+ ATPase family. *Cell*, *58*(1), 133–145. https://doi.org/10.1016/0092-8674(89)90410-8

Sagara, Y., & Inesi, G. (1991). Inhibition of the sarcoplasmic reticulum Ca2+ transport ATPase by thapsigargin at subnanomolar concentrations. *The Journal of Biological Chemistry*, *266*(21), 13503–13506.

Sancak, Y., Markhard, A. L., Kitami, T., Kovacs-Bogdan, E., Kamer, K. J., Udeshi, N. D., … Mootha, V. K. (2013). EMRE is an essential component of the mitochondrial calcium uniporter complex. *Science (New York, N.Y.)*, *342*(6164), 1379–1382. https://doi.org/10.1126/science.1242993

Schwartz, S., Meshorer, E., & Ast, G. (2009). Chromatin organization marks exon-intron structure. *Nature Structural & Molecular Biology*, *16*(9), 990–995. https://doi.org/10.1038/nsmb.1659

Shalbueva, N., Mareninova, O. A., Gerloff, A., Yuan, J., Waldron, R. T., Pandol, S. J., & Gukovskaya, A. S. (2013). Effects of oxidative alcohol metabolism on the mitochondrial permeability transition pore and necrosis in a mouse model of alcoholic pancreatitis. *Gastroenterology*, *144*(2), 437-446.e6. https://doi.org/10.1053/j.gastro.2012.10.037

Sievers, F., Wilm, A., Dineen, D., Gibson, T. J., Karplus, K., Li, W., … Higgins, D. G. (2011). Fast, scalable generation of high-quality protein multiple sequence alignments using Clustal Omega. *Molecular Systems Biology*, *7*, 539. https://doi.org/10.1038/msb.2011.75

Smaardijk, S., Chen, J., Kerselaers, S., Voets, T., Eggermont, J., & Vangheluwe, P. (2018). Store-independent coupling between the Secretory Pathway Ca(2+) transport ATPase SPCA1 and Orai1 in Golgi stress and Hailey-Hailey disease. *Biochimica et Biophysica Acta. Molecular Cell Research*, *1865*(6), 855–862. https://doi.org/10.1016/j.bbamcr.2018.03.007

Smaardijk, S., Chen, J., Wuytack, F., & Vangheluwe, P. (2017). SPCA2 couples Ca2+ influx via

Orai1 to Ca2+ uptake into the Golgi/secretory pathway. *Tissue and Cell*, *49*(2), 141–149. https://doi.org/10.1016/j.tice.2016.09.004

Srikanth, S., Jew, M., Kim, K.-D., Yee, M.-K., Abramson, J., & Gwack, Y. (2012). Junctate is a Ca2+-sensing structural component of Orai1 and stromal interaction molecule 1 (STIM1). *Proceedings of the National Academy of Sciences of the United States of America*, *109*(22), 8682–8687. https://doi.org/10.1073/pnas.1200667109

Stathopulos, P. B., Schindl, R., Fahrner, M., Zheng, L., Gasmi-Seabrook, G. M., Muik, M., … Ikura, M. (2013). STIM1/Orai1 coiled-coil interplay in the regulation of store-operated calcium entry. *Nature Communications*, *4*, 2963. https://doi.org/10.1038/ncomms3963

Straub, S V, Giovannucci, D. R., & Yule, D. I. (2000). Calcium wave propagation in pancreatic acinar cells: functional interaction of inositol 1,4,5-trisphosphate receptors, ryanodine receptors, and mitochondria. *The Journal of General Physiology*, *116*(4), 547–560.

Straub, Stephen V, Giovannucci, D. R., Bruce, J. I. E., & Yule, D. I. (2002). A role for phosphorylation of inositol 1,4,5-trisphosphate receptors in defining calcium signals induced by Peptide agonists in pancreatic acinar cells. *The Journal of Biological Chemistry*, *277*(35), 31949–31956. https://doi.org/10.1074/jbc.M204318200

Streb, H., Heslop, J. P., Irvine, R. F., Schulz, I., & Berridge, M. J. (1985). Relationship between secretagogue-induced Ca2+ release and inositol polyphosphate production in permeabilized pancreatic acinar cells. *The Journal of Biological Chemistry*, *260*(12), 7309–7315.

Stuenkel, E. L., Tsunoda, Y., & Williams, J. A. (1989). Secretagogue induced calcium mobilization in single pancreatic acinar cells. *Biochemical and Biophysical Research Communications*, *158*(3), 863–869. https://doi.org/10.1016/0006-291x(89)92802-7

Sudbrak, R., Brown, J., Dobson-Stone, C., Carter, S., Ramser, J., White, J., … Monaco, A. P.

(2000). Hailey-Hailey disease is caused by mutations in ATP2C1 encoding a novel Ca(2+) pump. *Human Molecular Genetics*, *9*(7), 1131–1140.

Sudhof, T. C., & Rothman, J. E. (2009). Membrane fusion: grappling with SNARE and SM proteins. *Science (New York, N.Y.)*, *323*(5913), 474–477. https://doi.org/10.1126/science.1161748

Tait, S. W. G., & Green, D. R. (2013). Mitochondrial regulation of cell death. *Cold Spring Harbor Perspectives in Biology*, *5*(9), a008706. https://doi.org/10.1101/cshperspect.a008706

Tepikin, A. V, Voronina, S. G., Gallacher, D. V, & Petersen, O. H. (1992). Pulsatile Ca2+ extrusion from single pancreatic acinar cells during receptor-activated cytosolic Ca2+ spiking. *The Journal of Biological Chemistry*, *267*(20), 14073–14076.

Thorn, P., Lawrie, A. M., Smith, P. M., Gallacher, D. V, & Petersen, O. H. (1993). Local and global cytosolic Ca2+ oscillations in exocrine cells evoked by agonists and inositol trisphosphate. *Cell*, *74*(4), 661–668. https://doi.org/10.1016/0092-8674(93)90513-p

Tran, T., Jia, D., Sun, Y., & Konieczny, S. F. (2007). The bHLH domain of Mistl is sufficient to activate gene transcription. *Gene Expression*, *13*(4–5), 241–253.

Tsunoda, Y., Stuenkel, E. L., & Williams, J. A. (1990). Oscillatory mode of calcium signaling in rat pancreatic acinar cells. *The American Journal of Physiology*, *258*(1 Pt 1), C147-55. https://doi.org/10.1152/ajpcell.1990.258.1.C147

Vanoevelen, J., Dode, L., Van Baelen, K., Fairclough, R. J., Missiaen, L., Raeymaekers, L., & Wuytack, F. (2005). The secretory pathway Ca2+/Mn2+-ATPase 2 is a Golgi-localized pump with high affinity for Ca2+ ions. *The Journal of Biological Chemistry*, *280*(24), 22800–22808. https://doi.org/10.1074/jbc.M501026200

Varnaite, R., & MacNeill, S. A. (2016). Meet the neighbors: Mapping local protein interactomes by proximity-dependent labeling with BioID. *Proteomics*, *16*(19), 2503–2518. https://doi.org/10.1002/pmic.201600123

Vig, M., Peinelt, C., Beck, A., Koomoa, D. L., Rabah, D., Koblan-Huberson, M., … Kinet, J.-P. (2006). CRACM1 is a plasma membrane protein essential for store-operated Ca2+ entry. *Science (New York, N.Y.)*, *312*(5777), 1220–1223. https://doi.org/10.1126/science.1127883

Vigont, V., Kolobkova, Y., Skopin, A., Zimina, O., Zenin, V., Glushankova, L., & Kaznacheyeva, E. (2015). Both Orai1 and TRPC1 are Involved in Excessive Store-Operated Calcium Entry in Striatal Neurons Expressing Mutant Huntingtin Exon 1. *Frontiers in Physiology*, *6*, 337. https://doi.org/10.3389/fphys.2015.00337

Voronina, S. G., Gryshchenko, O. V, Gerasimenko, O. V, Green, A. K., Petersen, O. H., & Tepikin, A. V. (2005). Bile acids induce a cationic current, depolarizing pancreatic acinar cells and increasing the intracellular Na+ concentration. *The Journal of Biological Chemistry*, *280*(3), 1764–1770. https://doi.org/10.1074/jbc.M410230200

Wang, Q.-C., Zheng, Q., Tan, H., Zhang, B., Li, X., Yang, Y., … Tang, T.-S. (2016). TMCO1 Is an ER Ca2+ Load-Activated Ca2+ Channel. *Cell*, *165*(6), 1454–1466. https://doi.org/https://doi.org/10.1016/j.cell.2016.04.051

Wen, L., Voronina, S., Javed, M. A., Awais, M., Szatmary, P., Latawiec, D., … Sutton, R. (2015). Inhibitors of ORAI1 Prevent Cytosolic Calcium-associated Injury of Human Pancreatic Acinar Cells and Acute Pancreatitis in 3 Mouse Models. *Gastroenterology*. https://doi.org/10.1053/j.gastro.2015.04.015; 10.1053/j.gastro.2015.04.015

Williams, J. A. (2008). Receptor-mediated signal transduction pathways and the regulation of pancreatic acinar cell function. *Current Opinion in Gastroenterology*, *24*(5), 573–579.

https://doi.org/10.1097/MOG.0b013e32830b110c

Wu, M. M., Buchanan, J., Luik, R. M., & Lewis, R. S. (2006). Ca2+ store depletion causes STIM1 to accumulate in ER regions closely associated with the plasma membrane. *The Journal of Cell Biology*, *174*(6), 803–813. https://doi.org/10.1083/jcb.200604014

Wuytack, F., Raeymaekers, L., & Missiaen, L. (2002). Molecular physiology of the SERCA and SPCA pumps. *Cell Calcium*, *32*(5–6), 279–305. https://doi.org/10.1016/s0143416002001847

Xiang, M., Mohamalawari, D., & Rao, R. (2005). A novel isoform of the secretory pathway Ca2+,Mn(2+)-ATPase, hSPCA2, has unusual properties and is expressed in the brain. *The Journal of Biological Chemistry*, *280*(12), 11608–11614. https://doi.org/10.1074/jbc.M413116200

Xu, X., Zeng, W., Popov, S., Berman, D. M., Davignon, I., Yu, K., … Wilkie, T. M. (1999). RGS proteins determine signaling specificity of Gq-coupled receptors. *The Journal of Biological Chemistry*, *274*(6), 3549–3556. https://doi.org/10.1074/jbc.274.6.3549

Xu, Y., Liu, J., Nipper, M., & Wang, P. (2019). Ductal vs. acinar? Recent insights into identifying cell lineage of pancreatic ductal adenocarcinoma. *Annals of Pancreatic Cancer*, *2*. https://doi.org/10.21037/apc.2019.06.03

Yamamoto, Sachiko, Takehara, M., Kabashima, Y., Fukutomi, T., & Ushimaru, M. (2016). Identification of novel inhibitors of human SPCA2. *Biochemical and Biophysical Research Communications*, *477*(2), 266–270. https://doi.org/10.1016/j.bbrc.2016.06.055

Yamamoto, Shinichiro, Yamazaki, T., Komazaki, S., Yamashita, T., Osaki, M., Matsubayashi, M., … Kakizawa, S. (2014). Contribution of calumin to embryogenesis through participation in the endoplasmic reticulum-associated degradation activity. *Developmental*

Biology, *393*(1), 33–43. https://doi.org/10.1016/j.ydbio.2014.06.024

Yang, X., Jin, H., Cai, X., Li, S., & Shen, Y. (2012). Structural and mechanistic insights into the activation of Stromal interaction molecule 1 (STIM1). *Proceedings of the National Academy of Sciences of the United States of America*, *109*(15), 5657–5662. https://doi.org/10.1073/pnas.1118947109

Yule, D I, Ernst, S. A., Ohnishi, H., & Wojcikiewicz, R. J. (1997). Evidence that zymogen granules are not a physiologically relevant calcium pool. Defining the distribution of inositol 1,4,5-trisphosphate receptors in pancreatic acinar cells. *The Journal of Biological Chemistry*, *272*(14), 9093–9098. https://doi.org/10.1074/jbc.272.14.9093

Yule, D I, Lawrie, A. M., & Gallacher, D. V. (1991). Acetylcholine and cholecystokinin induce different patterns of oscillating calcium signals in pancreatic acinar cells. *Cell Calcium*, *12*(2–3), 145–151. https://doi.org/10.1016/0143-4160(91)90016-8

Yule, David I. (2015). Calcium Signaling in Pancreatic Acinar cells. https://doi.org/10.3998/panc.2015.24

Zeng, W., Xu, X., & Muallem, S. (1996). Gbetagamma transduces [Ca2+]i oscillations and Galphaq a sustained response during stimulation of pancreatic acinar cells with [Ca2+]i-mobilizing agonists. *The Journal of Biological Chemistry*, *271*(31), 18520–18526. https://doi.org/10.1074/jbc.271.31.18520

Zhang, S. L., Yeromin, A. V, Zhang, X. H.-F., Yu, Y., Safrina, O., Penna, A., … Cahalan, M. D. (2006). Genome-wide RNAi screen of Ca(2+) influx identifies genes that regulate Ca(2+) release-activated Ca(2+) channel activity. *Proceedings of the National Academy of Sciences of the United States of America*, *103*(24), 9357–9362. https://doi.org/10.1073/pnas.0603161103

Zhao, X. S., Shin, D. M., Liu, L. H., Shull, G. E., & Muallem, S. (2001). Plasticity and adaptation of Ca2+ signaling and Ca2+-dependent exocytosis in SERCA2(+/-) mice. *The EMBO Journal*, *20*(11), 2680–2689. https://doi.org/10.1093/emboj/20.11.2680

Zhou, W., Shen, F., Miller, J. E., Han, Q., & Olson, M. S. (1996). Evidence for altered cellular calcium in the pathogenetic mechanism of acute pancreatitis in rats. *The Journal of Surgical Research*, *60*(1), 147–155. https://doi.org/10.1006/jsre.1996.0024

Zhu, J., Lu, X., Feng, Q., & Stathopulos, P. B. (2018). A charge-sensing region in the stromal interaction molecule 1 luminal domain confers stabilization-mediated inhibition of SOCE in response to S-nitrosylation. *The Journal of Biological Chemistry*, *293*(23), 8900–8911. https://doi.org/10.1074/jbc.RA117.000503

Zhu, L., Tran, T., Rukstalis, J. M., Sun, P., Damsz, B., & Konieczny, S. F. (2004). Inhibition of Mist1 homodimer formation induces pancreatic acinar-to-ductal metaplasia. *Molecular and Cellular Biology*, *24*(7), 2673–2681. https://doi.org/10.1128/mcb.24.7.2673-2681.2004

Appendices

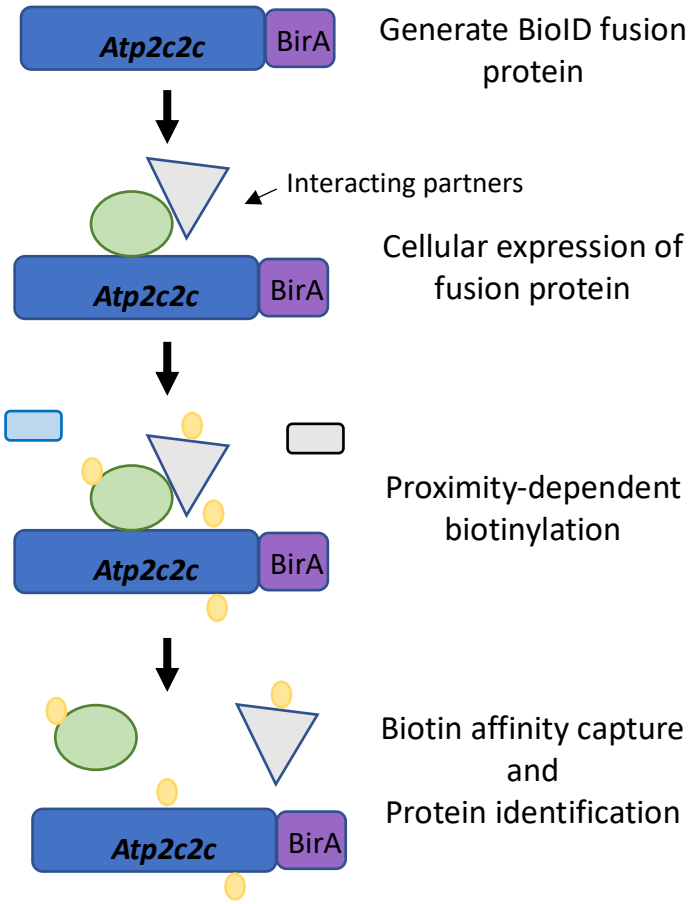
Atp2c2c
BirA
Generate BioID fusion protein
Interacting partners
Atp2c2c
BirA
Cellular expression of fusion protein
Atp2c2c
BirA
Proximity-dependent biotinylation
Atp2c2c
BirA
Biotin affinity capture and Protein identification

Appendix 1 . Experimental design and work flow of BioID.

SPCA2C-BioID-HA fusion protein was transiently expressed in HEK293A cells. Cells were incubated in 50uM biotin for 24 hours and total cell lysates were collected. Cell lysates were incubated in streptavidin-coupled dynabeads. Isolated proteins were sent for mass spectrometry.

Appendix 2. Summary table showing candidate SPCA2C interacting proteins identified using BioID MS analysis in PEAKS (after exclusion of negative control hits)

Gene name	-10logP[a]	Coverage (%)[b]	Area[c]	#Unique[d]	#Spec[e]	PTM[f]	Avg. Mass (Da)[g]
CKAP4	221.6	29	1.32E+07	14	31		66023
TLN1	209	7	2.42E+06	10	14	Carbamidomethylation	269765
TPD54	201.26	56	2.00E+07	11	26	Deamidation (NQ)	22238
RRBP1	199.85	12	8.89E+06	14	26	Carbamidomethylation	152472
ZCCHV	197.63	11	3.35E+06	8	10	Carbamidomethylation	101431
KTN1	195.88	12	4.01E+06	14	18	Deamidation (NQ)	156275
HS71L	193.39	13	1.77E+06	1	36		70375
DDX17	188.61	14	6.34E+06	7	17	Carbamidomethylation	80273
4F2	183.62	22	8.79E+06	9	17		67994
ITB1	180.73	13	8.85E+06	9	25	Carbamidomethylation; Deamidation (NQ)	88415
SPB1	179.94	10	5.64E+06	7	8	Carbamidomethylation	96558
TERA	179.26	16	4.66E+06	8	20	Carbamidomethylation	89322
STX5	175.23	20	1.46E+07	7	17	Carbamidomethylation	39673
TOIP1	172.02	16	6.06E+06	8	14		66248
HXK1	170.3	13	1.45E+07	10	14	Carbamidomethylation	102486
LYRIC	161.31	29	5.13E+06	10	15		63837
VAPB	158.77	30	3.55E+07	5	32	Carbamidomethylation; Deamidation (NQ)	27228
TMX1	154.62	22	8.32E+07	7	33	Carbamidomethylation	31791
RL18	153.09	20	7.87E+06	4	9		21634
PTN1	152.9	13	1.44E+07	5	17		49967
RL19	148.83	17	1.53E+07	4	11	Deamidation (NQ)	23466
DNM1L	147.06	10	7.21E+06	6	13		81877
UBXN4	147	20	2.88E+07	6	38	Carbamidomethylation	56778
F1142	146.06	15	1.70E+06	4	10	Carbamidomethylation	55468
RL40	145.95	46	1.79E+06	2	21	di-Glycine	14728
CCD47	144.48	14	1.48E+07	5	17		55874
LBR	144.2	7	3.23E+06	4	9		70703
MAVS	143.7	13	3.26E+06	4	10		56528
PSMD4	143.35	18	4.55E+06	4	10	Carbamidomethylation; Deamidation (NQ)	40737
IF5A1	142.67	36	8.80E+06	5	23	Deamidation (NQ)	16832
RL7A	139.84	20	4.13E+06	5	9	Carbamidomethylation	29996

RAB8A	137.12	29	8.52E+05	3	13	Deamidation (NQ)	23668
MAN1	137.1	7	4.02E+06	5	7	Carbamidomethylation	99997
NUPL2	136.22	14	4.27E+06	5	9	Carbamidomethylation	44872
RL32	134.81	27	1.72E+07	4	14	Carbamidomethylation; di-Glycine	15860
VAS1	129.88	7	8.16E+05	2	4		52026
SRPR	129.77	15	4.01E+06	6	7	Carbamidomethylation	69811
RAB1A	127.93	23	2.66E+06	2	14	Deamidation (NQ)	22678
CALX	127.02	9	5.67E+06	4	7		67568
STIP1	124.98	8	2.41E+06	3	4	Carbamidomethylation	62639
CHM4B	123.72	25	1.84E+06	4	6		24950
CLCC1	121.55	9	1.41E+06	4	4	Carbamidomethylation	62023
CLGN	121.24	7	2.64E+06	3	5		70039
PDIA3	120.89	8	2.75E+06	3	4		56782
DNJC7	119.75	8	1.96E+06	3	5	Carbamidomethylation	56441
MXRA7	119.39	18	2.37E+06	3	4		21466
RAB7A	116.6	17	2.39E+06	3	5		23490
NP1L1	114.24	7	3.83E+06	2	3		45374
SRP54	114.16	7	9.53E+05	3	4		55705
PP1G	113.94	8	9.39E+05	2	4	Carbamidomethylation	36984
HM13	113.23	8	4.40E+07	4	23		41488
TBB5	111.41	9	1.97E+06	2	7		49671
ARFG1	110.47	7	6.64E+05	2	3		44668
YKT6	110.38	14	1.34E+06	3	4		22418
PUR6	107.48	7	3.60E+05	2	2	Carbamidomethylation	47079
STT3B	107.11	6	1.97E+06	5	11		93674
RFC4	106.01	8	2.95E+05	2	2		39682
K1C18	105.72	11	2.97E+07	4	10		48058
RRS1	105.09	10	1.87E+06	2	9		41193
RAB6A	103.94	21	5.47E+06	2	8	Deamidation (NQ)	23593
ARF5	102.46	17	1.38E+07	2	15		20530
ARF3	102.46	17	1.38E+07	2	15		20601
ARF1	102.46	17	1.38E+07	2	15		20697
VAPA	102.46	16	2.66E+05	3	8		27893
DHCR7	101.95	6	5.44E+06	2	4		54489
LIMD1	100.34	4	9.80E+04	2	2		72190
RL13	99.02	14	1.13E+06	3	5		24261
ANKL2	98.44	4	3.90E+05	3	4	Carbamidomethylation; Deamidation (NQ)	104114
HNRPQ	98.09	4	3.13E+05	2	3		69603

K2C8	97.33	12	5.08E+05	2	12		53704
PIMT	97.32	7	8.68E+05	1	1	Carbamidomethylation	24636
DHRS7	96.2	13	4.51E+06	2	7	Carbamidomethylation	38299
RHG01	95.92	8	1.21E+06	3	6		50436
PHLP	95.81	10	1.38E+06	3	6		34282
SRPRB	95.79	10	8.41E+05	2	3		29702
COPD	95.17	6	1.72E+06	3	4	Carbamidomethylation	57210
PICAL	95.1	3	3.04E+05	1	3		70755
ASPH	93.93	5	1.14E+06	3	4		85863
SC22B	93.31	11	4.04E+06	2	3		24593
KAP2	92.98	5	1.06E+06	2	3		45518
ST134	92.62	11	8.64E+05	2	3		27407
F10A1	92.62	7	8.64E+05	2	3		41332
NB5R1	92.55	12	6.50E+06	2	8	Carbamidomethylation	34095
RBMS1	92.41	8	6.85E+05	3	5	Carbamidomethylation	44505
STIM1	91.15	7	1.52E+06	4	6		77423
EFHD2	91.06	9	3.47E+05	2	2		26697
XRCC6	90.88	6	2.12E+05	2	4		69843
SSRA	90.86	15	5.52E+06	3	5		32235
PGRC1	90.29	21	4.65E+05	1	7	Carbamidomethylation	21671
UBA1	90.27	3	4.68E+05	2	2		117849
MTX3	90.04	6	3.10E+05	2	2	Carbamidomethylation	35093
DESP	89.49	1	1.36E+05	2	2		331774
RAB9A	89.29	16	4.74E+05	1	6		22838
SSRG	88	8	1.15E+06	2	2		21080
UB2J1	87.81	9	9.03E+05	2	3		35199
RL8	86.17	13	1.93E+06	3	5		28025
1433E	86.15	8	2.27E+05	1	2	Carbamidomethylation	29174
EMD	85.94	13	2.05E+06	3	4		28994
SYAP1	85.67	4	6.62E+05	1	3		39933
STAU1	85.56	5	9.72E+05	2	2		63182
HMOX2	85.26	10	4.75E+06	2	5		36033
SH3G1	84.84	9	6.74E+05	3	3	Carbamidomethylation	41490
HSPB1	83.68	17	7.36E+06	2	3	Deamidation (NQ)	22783
TBB4B	83.55	6	5.03E+05	1	2		49831
NUP53	82.82	6	1.28E+06	1	2		34774
RL31	82.26	18	4.73E+05	2	2		14463
RTN4	81.3	2	2.99E+06	2	5	Carbamidomethylation	129931
TX264	81.27	8	7.91E+05	2	3	Carbamidomethylation	34189
TCPB	80.88	3	2.16E+05	1	1		57488

PABP1	80.34	3	8.45E+04	1	1	Carbamidomethylation	70671
PABP4	80.34	2	8.45E+04	1	1	Carbamidomethylation	70783
RM34	80.33	24	2.17E+06	2	5		10165
CALD1	79.97	3	5.35E+05	2	3		93231
PGRC2	78.76	10	1.88E+05	1	5	Carbamidomethylation	23818
TM109	78.35	9	1.71E+06	3	9		26210
RAB3B	78.25	10	2.51E+05	1	8	Deamidation (NQ)	24758
RAB3D	78.25	10	2.51E+05	1	8	Deamidation (NQ)	24267
RAB3A	78.25	10	2.51E+05	1	8	Deamidation (NQ)	24984
RAB3C	78.25	10	2.51E+05	1	8	Deamidation (NQ)	25952
ZYX	78.07	5	7.59E+04	2	4		61277
EI24	77.38	6	1.16E+06	2	2	Carbamidomethylation	38965
IF2B3	77.01	3	2.60E+05	1	2		63705
RCN1	76.94	4	6.46E+05	1	2		38890
S38A2	76.73	3	1.26E+05	1	2		56026
ANXA1	76.69	4	1.90E+05	1	1		38714
PREB	76.36	4	6.44E+05	1	1		45468
PROF1	75.94	21	5.90E+05	2	3		15054
RL34	75.85	22	1.42E+07	4	9		13293
HMX3	74.94	4	0.00E+00	1	1		37825
SNX4	74.72	3	1.57E+05	1	1		51909
SAR1A	73.98	11	8.38E+06	2	6		22367
EP15R	73.41	5	3.82E+05	2	2		94255
COPG1	71.97	3	1.27E+05	2	2		97718
STBD1	71.68	5	9.23E+05	2	2		39007
HNRPR	71.49	4	2.57E+05	2	2		70943
KPYM	71.34	7	2.29E+06	2	4	Carbamidomethylation	57937
MK67I	71.25	4	1.35E+05	1	1		34222
CND3	69.97	1	1.27E+05	1	1		114334
CP51A	69.15	3	6.02E+05	1	4		56806
NP1L4	68.7	9	3.25E+05	2	2		42823
TFCP2	68.62	3	4.38E+04	1	2	Carbamidomethylation	57256
PRDX4	68.24	7	3.50E+05	1	2		30540
RL26	67	10	1.32E+06	3	3		17258
RL26L	67	10	1.32E+06	3	3		17256
1433T	66.93	8	0.00E+00	1	2	Carbamidomethylation	27764
S38A1	66.2	2	7.27E+05	1	2		54048
CRCM1	66.13	4	3.72E+05	1	1		32668
RL22	65.99	10	2.50E+05	1	1		14787
LDHA	65.58	9	5.61E+05	2	4	Carbamidomethylation	36689

DHB12	64.97	5	5.25E+05	1	2		34324
AT1A2	64.79	2	1.50E+05	1	1		112265
AT1A3	64.79	2	1.50E+05	1	1		111748
AT1A1	64.79	2	1.50E+05	1	1		112896
PRS7	64.66	6	1.08E+06	2	4		48634
FKBP8	64.57	4	3.39E+05	1	1		44562
LDHB	64.48	4	9.38E+04	1	1		36639
MBOA7	63.54	7	6.89E+05	2	4	Carbamidomethylation	52765
JPH1	63.11	2	1.07E+06	1	2		71686
RL14	61.66	6	7.54E+05	1	1		23432
DBNL	61.17	7	1.36E+06	2	2		48207
NBR1	61.03	1	2.57E+05	1	1		107413
PGAM2	58.63	6	3.70E+05	1	2		28766
PGAM1	58.63	6	3.70E+05	1	2		28804
PGAM4	58.63	6	3.70E+05	1	2		28777
MACOI	58.43	2	4.75E+05	1	1		76178
PLST	57.95	6	8.84E+05	2	3	Carbamidomethylation	70811
CDKAL	55.9	2	5.01E+05	1	2		65112
PDCD5	55.7	9	3.87E+05	1	1		14285
HS90B	55.45	2	3.66E+05	1	1		83264
HS902	55.45	3	3.66E+05	1	1		39365
HS90A	55.45	2	3.66E+05	1	1		84660
H90B2	55.45	3	3.66E+05	1	1		44349
RABL3	54.99	18	2.59E+05	2	3		26423
RS7	54.65	12	3.70E+05	2	3		22127
SYMC	54.59	1	3.02E+05	1	1		101116
SQSTM	53.88	6	1.36E+06	1	3		47687
NUP98	53.48	1	1.89E+05	1	2		197578
AAAT	53.36	2	3.86E+05	1	2		56598
IF4H	52.86	12	9.72E+05	1	5		27385
RAB21	52.71	5	4.80E+05	1	2		24348
GOGA5	52.48	3	2.39E+05	1	1		83024
SC24B	52.19	1	9.83E+04	1	1		137417
OSBL8	51.94	1	2.36E+05	1	1		101196
BET1	51.41	9	2.45E+06	1	3		13289
LNP	51.3	3	7.61E+05	1	2		47740
ACATN	51.23	2	1.00E+05	1	1		60909
EIF3G	51.02	4	0.00E+00	1	1		35611
ITM2B	50.52	9	6.69E+05	1	2		30338
FIBB	50.19	3	1.19E+04	1	3	Deamidation (NQ)	55928

PEX19	49.64	7	1.46E+05	1	2		32807
AT2C2	49.03	1	1.28E+05	1	1		103187
MMGT1	49.03	11	1.00E+06	1	2		14686
AT131	48.94	1	2.37E+05	1	1		132955
2A5D	48.58	2	4.12E+05	1	1		69992
CSN8	48.01	7	0.00E+00	1	1		23226
F177A	47.4	6	0.00E+00	1	1		23757
BASI	47.24	2	1.89E+05	1	1		42200
NDC1	46.43	2	0.00E+00	1	1		76305
TOP1	46.38	1	2.28E+05	1	1		90726
APOL2	46.3	3	2.21E+04	1	1		37092
SERA	45.56	2	9.14E+04	1	1		56651
NCPR	43.89	3	1.98E+05	2	2		76690
TMX2	43.46	4	4.36E+05	1	2		34038
ALG9	43.4	2	4.17E+05	1	2		69864
SEC62	43.33	3	4.85E+04	1	2		45862
IF2B2	43.11	3	1.68E+05	1	1	Carbamidomethylation	66121
KC1A	42.49	3	7.42E+04	1	1		38915
KC1AL	42.49	3	7.42E+04	1	1		39086
RALA	42.29	6	4.22E+05	1	1		23567
RBM28	41.27	2	1.44E+05	1	1		85738
CDV3	40.91	3	3.28E+05	1	1		27335
ARM10	40.77	3	2.43E+05	1	1		37540
RL36	40.53	10	2.60E+07	1	5	Carbamidomethylation	12254
EDF1	40.44	7	4.75E+05	1	1		16369
DDX27	40.27	2	8.37E+04	1	1	Carbamidomethylation	89835
TMX3	39.82	2	3.86E+05	1	1		51872
COPB2	39.49	2	1.87E+05	1	1		102487
PERQ2	39.29	2	1.23E+05	1	2		150070
P121B	39.11	2	5.41E+06	1	1		83015
P121C	39.11	1	5.41E+06	1	1		125059
P121A	39.11	1	5.41E+06	1	1		127720
IST1	37.71	2	1.60E+05	1	1		39751
IF4G2	37.07	1	2.46E+05	1	1		102362
SYAC	36.35	1	4.98E+04	1	1		106810
NSDHL	36.33	3	6.10E+04	1	1		41900
MFS10	36.22	3	1.34E+05	1	1		48339
TTF2	36.16	1	6.31E+03	1	1		129588
CBPD	35.9	1	1.43E+05	1	1		152931
NOP2	35.77	2	0.00E+00	1	1	Carbamidomethylation	89302

ATLA3	35.72	3	1.61E+05	1	1		60542
MPRI	35.13	1	2.20E+05	1	2	Carbamidomethylation	274373
NB5R3	35.07	6	5.05E+05	1	1		34235
SC61B	35.02	16	3.29E+04	1	1		9974
SCD5	34.72	4	1.03E+05	1	1		37610
CA123	34.44	8	5.26E+05	1	1		18048
NOG1	33.66	4	2.29E+05	1	1		73965
ABCAD	32.08	0	4.13E+05	1	1		576166
HPDL	31.8	3	6.12E+04	1	2	di-Glycine	39386
AT2A2	31.74	1	3.25E+05	1	2		114757
NUDC	31.03	3	2.04E+05	1	1		38243
RANG	30.97	4	6.08E+04	1	1		23310
HACD3	30.27	6	5.94E+05	1	5		43160
CCD66	30.25	1	0.00E+00	1	1	Deamidation (NQ)	109411
TM131	30.09	1	3.78E+05	1	1		205137
RS16	30	7	2.14E+05	1	1		16445
RENR	29.35	2	3.05E+05	1	1		39008
F117B	29.21	5	0.00E+00	1	1	Oxidation (M)	61968
RYR1	28.94	0	7.37E+05	1	1	Oxidation (M)	565184
P5I11	28.73	5	2.27E+04	1	2		21054
CNKR3	28.1	3	0.00E+00	1	1		61904
C2D1A	27.82	2	0.00E+00	1	1		104062
RTN3	27.69	1	0.00E+00	1	1		112611
SMC5	27.37	1	1.45E+08	1	1	Oxidation (M)	128806
KINH	27.29	1	4.90E+05	1	1		109685
TNC18	27.07	0	4.23E+04	1	1		314520
FIBA	26.26	1	4.20E+05	1	1		94973
NMT1	26.22	3	1.73E+05	1	1		56806
RL3	26.02	2	4.05E+05	1	1		46109
CHD5	26	0	0.00E+00	1	1		223048
CHD3	26	0	0.00E+00	1	1		226590
FBSL	25.86	1	0.00E+00	1	1		110907
SPCS2	25.66	3	2.81E+06	1	2		25003
COHA1	25.32	2	1.67E+06	1	1	Deamidation (NQ)	150419

[a]Peptide spectrum match score
[b]Percentage of the full open reading frame sequenced
[c]Area of a peptide feature calculated by PEAKs
[d]Number of unique fragments identified for the gene
[e]Number of precursor spectrum matches matched to the supporting peptides for the protein
[f]Post-translational modifications identified in the peptide fragments
[g]Monoisotopic mass of the peptide

Appendix 3. Summary table showing cadidate SPCA2C interacting proteins identified using BioID MS analysis in PEAKS (after exclusion of negative control hits and common proteomics contaminants).

Gene name	-10lgP	Coverage (%)	Area	#Unique	#Spec	PTM	Avg. Mass
ITB1	180.73	13	8.85E+06	9	25	Carbamidomethylation; Deamidation (NQ)	88415
STX5	175.23	20	1.46E+07	7	17	Carbamidomethylation	39673
TMX1	154.62	22	8.32E+07	7	33	Carbamidomethylation	31791
NUPL2	136.22	14	4.27E+06	5	9	Carbamidomethylation	44872
VAS1	129.88	7	8.16E+05	2	4		52026
CLGN	121.24	7	2.64E+06	3	5		70039
DHRS7	96.2	13	4.51E+06	2	7	Carbamidomethylation	38299
RHG01	95.92	8	1.21E+06	3	6		50436
ASPH	93.93	5	1.14E+06	3	4		85863
SC22B	93.31	11	4.04E+06	2	3		24593
ST134	92.62	11	8.64E+05	2	3		27407
F10A1	92.62	7	8.64E+05	2	3		41332
NB5R1	92.55	12	6.50E+06	2	8	Carbamidomethylation	34095
SSRA	90.86	15	5.52E+06	3	5		32235
MTX3	90.04	6	3.10E+05	2	2	Carbamidomethylation	35093
RAB9A	89.29	16	4.74E+05	1	6		22838
UB2J1	87.81	9	9.03E+05	2	3		35199
HMOX2	85.26	10	4.75E+06	2	5		36033
NUP53	82.82	6	1.28E+06	1	2		34774
RM34	80.33	24	2.17E+06	2	5		10165
TM109	78.35	9	1.71E+06	3	9		26210
EI24	77.38	6	1.16E+06	2	2	Carbamidomethylation	38965
RCN1	76.94	4	6.46E+05	1	2		38890
HMX3	74.94	4	0.00E+00	1	1		37825
CP51A	69.15	3	6.02E+05	1	4		56806
CRCM1	66.13	4	3.72E+05	1	1		32668
MBOA7	63.54	7	6.89E+05	2	4	Carbamidomethylation	52765
MACOI	58.43	2	4.75E+05	1	1		76178
HS902	55.45	3	3.66E+05	1	1		39365
H90B2	55.45	3	3.66E+05	1	1		44349
BET1	51.41	9	2.45E+06	1	3		13289

LNP	51.3	3	7.61E+05	1	2		47740
ACATN	51.23	2	1.00E+05	1	1		60909
ITM2B	50.52	9	6.69E+05	1	2		30338
FIBB	50.19	3	1.19E+04	1	3	Deamidation (NQ)	55928
PEX19	49.64	7	1.46E+05	1	2		32807
AT2C2	49.03	1	1.28E+05	1	1		103187
MMGT1	49.03	11	1.00E+06	1	2		14686
CSN8	48.01	7	0.00E+00	1	1		23226
F177A	47.4	6	0.00E+00	1	1		23757
APOL2	46.3	3	2.21E+04	1	1		37092
NCPR	43.89	3	1.98E+05	2	2		76690
TMX2	43.46	4	4.36E+05	1	2		34038
ALG9	43.4	2	4.17E+05	1	2		69864
SEC62	43.33	3	4.85E+04	1	2		45862
RALA	42.29	6	4.22E+05	1	1		23567
ARM10	40.77	3	2.43E+05	1	1		37540
TMX3	39.82	2	3.86E+05	1	1		51872
P121B	39.11	2	5.41E+06	1	1		83015
IST1	37.71	2	1.60E+05	1	1		39751
MFS10	36.22	3	1.34E+05	1	1		48339
CBPD	35.9	1	1.43E+05	1	1		152931
ATLA3	35.72	3	1.61E+05	1	1		60542
NB5R3	35.07	6	5.05E+05	1	1		34235
SCD5	34.72	4	1.03E+05	1	1		37610
CA123	34.44	8	5.26E+05	1	1		18048
ABCAD	32.08	0	4.13E+05	1	1		576166
HPDL	31.8	3	6.12E+04	1	2	di-Glycine	39386
CCD66	30.25	1	0.00E+00	1	1	Deamidation (NQ)	109411
TM131	30.09	1	3.78E+05	1	1		205137
RENR	29.35	2	3.05E+05	1	1		39008
F117B	29.21	5	0.00E+00	1	1	Oxidation (M)	61968
RYR1	28.94	0	7.37E+05	1	1	Oxidation (M)	565184
P5I11	28.73	5	2.27E+04	1	2		21054
CNKR3	28.1	3	0.00E+00	1	1		61904
SMC5	27.37	1	1.45E+08	1	1	Oxidation (M)	128806
TNC18	27.07	0	4.23E+04	1	1		314520
FIBA	26.26	1	4.20E+05	1	1		94973

FBSL	25.86	1	0.00E+00	1	1		110907
SPCS2	25.66	3	2.81E+06	1	2		25003
COHA1	25.32	2	1.67E+06	1	1	Deamidation (NQ)	150419

[a]Peptide spectrum match score
[b]Percentage of the full open reading frame sequenced
[c]Area of a peptide feature calculated by PEAKs
[d]Number of unique fragments identified for the gene
[e]Number of precursor spectrum matches matched to the supporting peptides for the protein
[f]Post-translational modifications identified in the peptide fragments
[g]Monoisotopic mass of the peptide

Appendix 4. Table indicating the Ca^{2+} associated protein interaction candidates that appeared after excluding negative control and common contaminant/ background proteins.

Gene	-10lgP[a]	Description	Function[a]
VAS1	129.88	V-type proton ATPase subunit S1 OS=Homo sapiens GN=ATP6AP1 PE=1 SV=2	Involved in membrane trafficking and Ca^{2+}-dependent membrane fusion.
CLGN	121.24	Calmegin OS=Homo sapiens GN=CLGN PE=1 SV=1	Required for normal male fertility. Binds calcium ions.
ASPH	93.93	Aspartyl/asparaginyl beta-hydroxylase OS=Homo sapiens GN=ASPH PE=1 SV=3	Isoform 8: membrane-bound Ca^{2+}-sensing protein, which is a structural component of the ER-plasma membrane junctions. Isoform 8 regulates the activity of Ca(+2) released-activated Ca(+2) (CRAC) channels in T-cells.
NB5R1	92.55	NADH-cytochrome b5 reductase 1 OS=Homo sapiens GN=CYB5R1 PE=1 SV=1	Among its related pathways are Response to elevated platelet cytosolic Ca2+ and PAK Pathway.
TM109	78.35	Transmembrane protein 109 OS=Homo sapiens GN=TMEM109 PE=1 SV=1	May mediate cellular response to DNA damage by protecting against ultraviolet C-induced cell death. Can form voltage-gated calcium and potassium channels in vitro
RCN1	76.94	Reticulocalbin-1 OS=Homo sapiens GN=RCN1 PE=1 SV=1	May regulate calcium-dependent activities in the endoplasmic reticulum lumen or post-ER compartment.
CRCM1	66.13	Calcium release-activated calcium channel protein 1 OS=Homo sapiens GN=ORAI1 PE=1 SV=2	The protein encoded by this gene is a membrane calcium channel subunit that is activated by the calcium sensor STIM1 when calcium stores are depleted.
AT2C2	49.03	Calcium-transporting ATPase type 2C member 2 OS=Homo sapiens GN=ATP2C2 PE=1 SV=2	This magnesium-dependent enzyme catalyzes the hydrolysis of ATP coupled with the transport of calcium.
RYR1	28.94	Ryanodine receptor 1 OS=Homo sapiens GN=RYR1 PE=1 SV=3	Calcium channel that mediates the release of Ca^{2+} from the sarcoplasmic reticulum into the cytoplasm

[a]-10logP score from PEAKS MS analysis

[b]Funcion determined based on Uniprot or Genecard function.

Curriculum Vitae

Melissa Fenech

Education

PhD	University of Western Ontario, Physiology and Pharmacology "The role of pancreas specific Secretory Pathway Calcium Atpase 2C in Calcium Homeostasis"	In progress
BMSc	University of Western Ontario, Physiology and Pharmacology Honours Specialization in Medical Sciences	May, 2014

Awards and Honours

American Pancreatic Association Young Investigators Award	September, 2018
Canada Graduate Scholarships – Michael Smith Foreign Study Supplements (CGS-MSFSS)	August, 2018
Natural Sciences and Engineering Research Council (NSERC) – Alexander Graham Bell Canada Graduate Scholarship-Doctorial (CGS D)	March, 2017
Queen Elizabeth II Graduate Scholarship in Science and Technology (QEII-GSST)	June, 2016 and June, 2017
Ontario Graduate Scholarship (OGS)	June, 2016
American Pancreatic Association Young Investigators Award	September, 2015
Paediatric Graduate Studentship	May, 2016
Dean's Honour List in Hounours Specialization Medical Sciences, University of Western Ontario	May, 2014 May, 2013 May, 2012 May, 2011

Teaching Experience

Teaching Assistant September, 2014 – May,2015
Physiology and Pharmacology, University of Western Ontario September, 2015 – May, 2016
Physiology 3130 Laboratory Course

Course Co-coordinator September, 2016
Physiology and Pharmacology, Univeristy of Western Ontario September, 2017
September, 2018
Physiology 9550 Molecular Techniques

Publications

- **Fenech, M**., Sullivan, C. M., Ferreira, L. T., Mehmood, R., MacDonald, W. A., Stathopulos, P. B., & Pin, C. L. (2016). Atp2c2 Is Transcribed from a Unique Transcriptional Start Site in Mouse Pancreatic Acinar Cells. *Journal of Cellular Physiology*. http://doi.org/10.1002/jcp.25391

- Pin, C and **Fenech, M.** (2017) Development of the Pancreas. Pancreapedia: Exocrine Pancreas Knowledge Base, DOI: 10.3998/panc.2017.09

- **Fenech, M.**, Carter, M., Stathopulos, P., Pin, C.(2019). The Secretory Pathway Calcium Atpase 2C is involved in multiple Calcium pathways. *BBA-MCR.*

Presentations

- **Melissa Fenech**, Mckenzie Carter, Peter Stathopulos, Christopher Pin. Pancreas-specific isoform of Secretory Pathway Calcium ATPase 2 Affects SOCE and SICE through interactions with ORAI1. Univeristy of Michigan Annual Pancreatic Disease Retreat, University of Michigan, Ann Arbour, MI: poster presentation — June, 2018
- **Melissa Fenech**, Mckenzie Carter, Christopher Pin. Pancreas-specific Secretory Pathway Calcium ATPase 2 Affects Calcium Influx and ER Calcium Stores Through Store-Operated and Store-Independent Calcium Entry. Developmental Biology — June, 2018

Research Day, University of Western Ontario, London, ON: Oral presentation.

- **Melissa Fenech**, Mckenzie Carter, Peter Stathopulos, Christopher Pin. Pancreas-specific isoform of Secretory Pathway Calcium ATPase 2 Affects SOCE and SICE through interactions with ORAI1. Paediatric Research Day, Victoria Hospital, London, ON: poster presentation — May, 2018
- **Melissa Fenech**, Peter Stathopulos, Christopher Pin. The pancreas-specific isoform of SPCA2 affects Store Operated Ca^{2+} Entry. Physiology and Pharmacology Research Day, Univeristy of Western Ontario, London, ON: poster presentation — October, 2017
- **Melissa Fenech**, Peter Stathopulos, Christopher Pin. The pancreas-specific isoform of SPCA2 affects Store Operated Ca^{2+} Entry. Canadian Student Health Research Forum, Winnipeg, MB: poster presentation. — April, 2017
- **Melissa Fenech**, Peter Stathopulos, Christopher Pin. The pancreas-specific isoform of SPCA2 affects Store Operated Ca^{2+} Entry. Pediatric Research Day, Children's Hospital, London, ON: Oral presentation. — March, 2017
- **Melissa Fenech**, Peter Stathopulos, Christopher Pin. The pancreas-specific isoform of SPCA2 affects Store Operated Ca^{2+} Entry. London Health Research Day, Western University, London, ON: Oral presentation. — March, 2017
- **Melissa Fenech**, Peter Stathopulos, Christopher Pin. The pancreas-specific isoform of SPCA2 affects Store Operated Ca^{2+} Entry. American Pancreatic Association Annual Conference, Boston, MA: poster presentation (Poster of distinction, top 10 abstracts submitted). — November, 2016
- **Melissa** Fenech and Christopher Pin. Pancreas-Specific Secretory Pathway Ca^{2+}-Atpase 2 affects GPCR-mediated Ca^{2+} signaling. American Pancreatic Association Annual Meeting, San Diageo, CA: poster presentation. — November, 2015